CANADIAN THESES ON MICROFICHE

I.S.B.N.

THESES CANADIENNES SUR MICROFICHE

National Library of Canada
Collections Development Branch

Canadian Theses on
Microfiche Service

Ottawa, Canada
K1A 0N4

Bibliothèque nationale du Canada
Direction du développement des collections

Service des thèses canadiennes
sur microfiche

NOTICE

The quality of this microfiche is heavily dependent upon the quality of the original thesis submitted for microfilming. Every effort has been made to ensure the highest quality of reproduction possible.

If pages are missing, contact the university which granted the degree.

Some pages may have indistinct print especially if the original pages were typed with a poor typewriter ribbon or if the university sent us a poor photocopy.

Previously copyrighted materials (journal articles, published tests, etc.) are not filmed.

Reproduction in full or in part of this film is governed by the Canadian Copyright Act, R.S.C. 1970, c. C-30. Please read the authorization forms which accompany this thesis.

THIS DISSERTATION
HAS BEEN MICROFILMED
EXACTLY AS RECEIVED

AVIS

La qualité de cette microfiche dépend grandement de la qualité de la thèse soumise au microfilmage. Nous avons tout fait pour assurer une qualité supérieure de reproduction.

S'il manque des pages, veuillez communiquer avec l'université qui a conféré le grade.

La qualité d'impression de certaines pages peut laisser à désirer, surtout si les pages originales ont été dactylographiées à l'aide d'un ruban usé ou si l'université nous a fait parvenir une photocopie de mauvaise qualité.

Les documents qui font déjà l'objet d'un droit d'auteur (articles de revue, examens publiés, etc.) ne sont pas microfilmés.

La reproduction, même partielle, de ce microfilm est soumise à la Loi canadienne sur le droit d'auteur, SRC 1970, c. C-30. Veuillez prendre connaissance des formules d'autorisation qui accompagnent cette thèse.

LA THÈSE A ÉTÉ
MICROFILMÉE TELLE QUE
NOUS L'AVONS REÇUE

NL-339 (r. 82/08)

Canada

269

0-315-12580-2

National Library
of Canada

Bibliothèque nationale
du Canada

Canadian Theses Division

Division des thèses canadiennes

Ottawa, Canada
K1A 0N4

60491

PERMISSION TO MICROFILM — AUTORISATION DE MICROFILMER

- Please print or type — Écrire en lettres moulées ou dactylographier

Full Name of Author — Nom complet de l'auteur

ONG SEE YEN

Date of Birth — Date de naissance NOV. 13, 1958	Country of Birth — Lieu de naissance MALAYSIA

Permanent Address — Résidence fixe

2 JALAN KOTA
KUALA TRENGGANU
TRENGGANU, MALAYSIA

Title of Thesis — Titre de la thèse

EFFECT OF TYPE OF WEB REINFORCEMENT ON DEEP BEAMS

University — Université

UNIVERSITY OF ALBERTA

Degree for which thesis was presented — Grade pour lequel cette thèse fut présentée

MASTER OF SCIENCE IN CIVIL ENGINEERING

Year this degree conferred — Année d'obtention de ce grade 1982	Name of Supervisor — Nom du directeur de thèse J. G. MACGREGOR

Permission is hereby granted to the NATIONAL LIBRARY OF CANADA to microfilm this thesis and to lend or sell copies of the film.

The author reserves other publication rights, and neither the thesis nor extensive extracts from it may be printed or otherwise reproduced without the author's written permission.

L'autorisation est, par la présente, accordée à la BIBLIOTHÈQUE NATIONALE DU CANADA de microfilmer cette thèse et de prêter ou de vendre des exemplaires du film.

L'auteur se réserve les autres droits de publication; ni la thèse ni de longs extraits de celle-ci ne doivent être imprimés ou autrement reproduits sans l'autorisation écrite de l'auteur.

Date AUGUST 17, 1982	Signature

NL-91 (4/77)

THE UNIVERSITY OF ALBERTA

EFFECT OF TYPE OF WEB REINFORCEMENT ON DEEP BEAMS

by

Ⓒ ONG, SEE YEN

A THESIS
SUBMITTED TO THE FACULTY OF GRADUATE STUDIES AND RESEARCH
IN PARTIAL FULFILMENT OF THE REQUIREMENTS FOR THE DEGREE
OF MASTER OF SCIENCE
IN
CIVIL ENGINEERING

DEPARTMENT OF CIVIL ENGINEERING

EDMONTON, ALBERTA
FALL, 1982

THE UNIVERSITY OF ALBERTA

RELEASE FORM

NAME OF AUTHOR ONG SEE YEN

TITLE OF THESIS *EFFECT OF TYPE OF WEB REINFORCEMENT ON DEEP BEAMS*

DEGREE FOR WHICH THESIS WAS PRESENTED MASTER OF SCIENCE

YEAR THIS DEGREE GRANTED FALL, 1982

Permission is hereby granted to THE UNIVERSITY OF ALBERTA LIBRARY to reproduce single copies of this thesis and to lend or sell such copies for private, scholarly or scientific research purposes only.

The author reserves other publication rights, and neither the thesis nor extensive extracts from it may be printed or otherwise reproduced without the author's written permission.

(SIGNED) Ong See Yen

PERMANENT ADDRESS:

2 JALAN KOTA
KUALA TRENGGANU
TRENGGANU, MALAYSIA

DATED AUGUST 16, 1982

THE UNIVERSITY OF ALBERTA

FACULTY OF GRADUATE STUDIES AND RESEARCH

The undersigned certify that they have read, and recommend to the Faculty of Graduate Studies and Research, for acceptance, a thesis entitled *EFFECT OF TYPE OF WEB REINFORCEMENT ON DEEP BEAMS* submitted by ONG SEE YEN in partial fulfilment of the requirements for the degree of MASTER OF SCIENCE in CIVIL ENGINEERING.

....

Supervisor

....

........Kennedy.....

Date...AUGUST 16, 1982...........

IN MEMORY OF MY MOTHER

Abstract

The effect of type of web reinforcement on deep beams is investigated in this thesis. Four two-span continuous deep beams with a clear shear span to effective depth ratio, *x/d*, of 1.43 were tested. The types of web reinforcement tested were horizontal, vertical and orthogonal web reinforcements. For comparision, one beam without any web reinforcement was tested. The overall length of the specimens was 4400 mm. The beams were loaded at the middle of each span with concentrated loads applied through column stubs built integrally with the beams. The beams were supported in a similar manner. The loads, support reactions, midspan deflections, support settlements and strains in the flexural reinforcement, web reinforcement and concrete were measured during the test. Crack propagation was recorded using photographs taken at regular intervals.

On the basis of the limited test results, horizontal web reinforcement was found to have no influence on the ultimate shear strength of the beams tested. Vertical web reinforcement was very effective in increasing the ultimate shear strength. The vertical web reinforcement can be assumed to yield at the failure load. All the beams failed in shear, and sliding along a critical inclined crack was the major cause of failure. Before failure, a high amount of arch action had developed. Very poor correlation with the test results was obtained using the ACI Code equation for the ultimate shear capacity of deep beams. The behaviour of

the beams was generally elastic at first inclined cracking load and was inelastic at loads near the failure load.

Acknowledgements

The author wishes to express his gratitute to Professor J. G. MacGregor for his encouragement and patient guidance throughout the course of this thesis.

Thanks are also due to the technical staff at the I. F. Morrison Structural Laboratory for their assistance in the fabrication and testing of the specimens, D. M. Rogowsky for his occasional advice on the subject and T. A. Casey for his assistance in using the computer.

The financial support provided by the National Science and Engineering Research Council through Grant No. A1673 is greatly appreciated.

Table of Contents

Chapter Page

Abstract v

Acknowledgements vii

Table of Contents viii

List of Tables xi

List of Figures xii

List of Notations xvii

1. INTRODUCTION 1

 1.1 General 1

 1.2 Objective 2

 1.3 Scope 2

2. LITERATURE REVIEW 4

 2.1 Introduction 4

 2.2 Shear Transfer Mechanisms 4

  2.2.1 Concrete Shear Stress 5

  2.2.2 Interface Shear Transfer 5

   2.2.2.1 Interface Shear Transfer of Uncracked Concrete With Reinforcement Crossing Shear Plane ...6

   2.2.2.2 Interface Shear Transfer of Initially Cracked Concrete With Reinforcement Crossing Shear Plane ...7

  2.2.3 Dowel Action 10

  2.2.4 Arch Action 11

  2.2.5 Web Reinforcement 14

 2.3 Factors Affecting Behaviour of Deep Beams 15

  2.3.1 M/(V.d) or a/d Ratio 15

  2.3.2 Method of Load Application 15

2.3.3 Nature of Loading 17

2.3.4 Type of Web Reinforcement 17

2.3.5 Detailing of Longitudinal Reinforcement 19

2.4 Design Approximations 19

2.4.1 de Paiva and Siess 20

2.4.2 Kong and Robins 22

2.4.3 Ramakrishnan and Ananthanarayana 24

2.4.4 1977 ACI Building Code (ACI 318-77) 26

2.4.5 ACI-ASCE Committee 426 28

2.4.6 Comité Europeén du Béton (CEB) 31

3. EXPERIMENTAL PROGRAM 46

3.1 Introduction 46

3.2 Specimen Geometry 46

3.3 Material Used 49

3.3.1 Concrete 49

3.3.2 Reinforcing Steel 49

3.3.3 Base Plates 50

3.4 Curing Of Specimens 50

3.5 Specimen Instrumentation 51

3.6 Test Setup 52

3.7 Testing Procedures 53

4. BEHAVIOUR OF BEAMS IN TESTS 70

4.1 Load-Deflection Behaviour 70

4.1.1 Load and Midspan Deflection Relationship 70

4.1.2 Load and Support Settlement Relationships ...73

4.2 Development of Cracking 74

4.3 Modes of Failure 80

4.4 Steel and Concrete Strains 82
4.4.1 Strains in Flexural Reinforcement 82
4.4.2 Strains in Vertical Web Reinforcement 85
4.4.3 Strains in Horizontal Web Reinforcement 86
4.4.4 Strains in Concrete 88
4.5 Retest Results 89
4.5.1 Load and Midspan Deflection Relationships ...89
4.5.2 Load and Support Settlement Relationships ...90
4.5.3 Loads and Reactions 91
4.6 Shear Stresses at First Inclined Cracking 91
4.7 Ultimate Shear Stress 99
5. SUMMARY AND CONCLUSIONS 139
5.1 Behaviour 139
5.2 Strength 141
BIBLIOGRAPHY 143
Appendix A - Plots of Jack Load versus Midspan Deflection of Beams No. 2, 3 and 4 153
Appendix B - Plots of Jack Load versus Support Settlement of Beams No. 2, 3 and 4 160
Appendix C - Plots of Jack Load versus Midspan Deflection of Beams No. 1, 2, 3 and 4 from the Retest 164
Appendix D - Plots of Jack Load versus Support Settlement of Beams No. 1, 2, 3 and 4 from the Retest 173
Appendix E - Jack Loads and Support Reactions of Beams No. 1, 2, 3 and 4 from the Retest 178

List of Tables

Table Page

3.1 Compressive Strength of Test Cylinders, in MPa 55

3.2 Properties of Reinforcing Bars 56

4.1 Cracking and Ultimate Loads 107

4.2 Jack Loads and Support Reactions of Beam No. 1 108

4.3 Jack Loads and Support Reactions of Beam No. 2 109

4.4 Jack Loads and Support Reactions of Beam No. 3 110

4.5 Jack Loads and Support Reactions of Beam No. 4 111

4.6 Comparision of Actual and Computed Shear Stresses at Inclined Cracking 112

4.7 Actual Ultimate Shear Stresses in the Original Test and Retest 113

4.8 Comparision of Actual Ultimate Shear Stresses from the Original Test With Computed Ultimate Shear Stresses 114

E.1 Jack Loads and Support Reactions of Beams No. 1 from the Retest 179

E.2 Jack Loads and Support Reactions of Beams No. 2 from the Retest 180

E.3 Jack Loads and Support Reactions of Beams No. 3 from the Retest 181

E.4 Jack Loads and Support Reactions of Beams No. 4 from the Retest 182

List of Figures

Figure Page

2.1 Forces Acting on a Diagonal Crack of a Reinforced Concrete Member 34

2.2 Push-Off Test Specimen 35

2.3 "Truss" Formed After Diagonal Tension Cracking (Mattock and Hawkins, 1972) 36

2.4 Shear-Friction Analogy (ACI-ASCE Committee 426, 1973) 37

2.5 Arch Action in a Simply Supported Beam 38

2.6 Variation in Shear Capacity With *a/d* for Rectangular Beams (Bresler and MacGregor, 1967) 39

2.7 Reserve Shear Capacity of Deep Beams (ACI-ASCE Committee 426, 1973) 40

2.8 Method of Load Application 41

2.9 Principal Stress Trajectories of the Uncracked State of Deep Beams (Leonhardt, 1966) 42

2.10 Inclination of Shear Cracks in Deep Beams (Crist, 1971) 43

2.11 Diagonally Reinforced Coupling Beam (Paulay, 1971) 44

2.12 Effect of Inclined Cracking on Steel and Concrete Strains (de Paiva and Siess, 1965) 45

3.1 External Dimensions of Deep Beams 57

3.2 Flexural Reinforcement Used in Deep Beams 58

3.3 Arrangement of Web Reinforcement in Beam No. 2 59

3.4 Arrangement of Web Reinforcement in Beam No. 3 60

3.5 Arrangement of Web Reinforcement in Beam No. 4 61

3.6 Stress-Strain Plot of Reinforcing Steel 62

Figure Page

3.7 Location of Instrumentation of Concrete Strains in a Typical Beam 63

3.8 Location of Instrumentation of Steel Strains in Beam No. 1 64

3.9 Location of Instrumentation of Steel Strains in Beam No. 2 65

3.10 Location of Instrumentation of Steel Strains in Beam No. 3 66

3.11 Location of Instrumentation of Steel Strains in Beam No. 4 67

3.12 Test Setup 68

3.13 External Stirrups Used in Retest 69

4.1 Plot of Jack Load versus North Midspan Deflection of Beam No. 1 115

4.2 Plot of Jack Load versus South Midspan Deflection of Beam No. 1 116

4.3 Plot of Jack Load versus Support Settlement of Beam No. 1 117

4.4 First Inclined Cracking Pattern of Beam No. 1 (Load Step 8) 118

4.5 First Inclined Cracking Pattern of Beam No. 2 (Load Step 6) 119

4.6 First Inclined Cracking Pattern of Beam No. 3 (Load Step 8) 120

4.7 First Inclined Cracking Pattern of Beam No. 4 (Load Step 9) 121

4.8 Comparision of Actual and Elastic Shearing Force and Bending Moment Diagrams of Beam No. 1 at First Inclined Cracking (Load Step 8) 122

4.9 Comparision of Actual and Elastic Shearing Force and Bending Moment Diagrams of Beam No. 2 at First Inclined Cracking (Load Step 6) 123

Figure Page

4.10 Comparision of Actual and Elastic Shearing Force and Bending Moment Diagrams of Beam No. 3 at First Inclined Cracking (Load Step 8) 124

4.11 Comparision of Actual and Elastic Shearing Force and Bending Moment Diagrams of Beam No. 4 at First Inclined Cracking (Load Step 9) 125

4.12 Failure Cracking Pattern of Beam No. 1 126

4.13 Failure Cracking Pattern of Beam No. 2 127

4.14 Failure Cracking Pattern of Beam No. 3 128

4.15 Failure Cracking Pattern of Beam No. 4 129

4.16 Comparision of Actual and Elastic Shearing Force and Bending Moment Diagrams of Beam No. 1 at Last Load Step Prior to Failure (Load Step 11) 130

4.17 Comparision of Actual and Elastic Shearing Force and Bending Moment Diagrams of Beam No. 2 at Last Load Step Prior to Failure (Load Step 13) 131

4.18 Comparision of Actual and Elastic Shearing Force and Bending Moment Diagrams of Beam No. 3 at Last Load Step Prior to Failure (Load Step 11) 132

4.19 Comparision of Actual and Elastic Shearing Force and Bending Moment Diagrams of Beam No. 4 at Last Load Step Prior to Failure (Load Step 18) 133

4.20 Typical Steel Strain Distribution in the Negative Moment Flexural Reinforcement, North Span of Beam No. 4 134

4.21 Typical Steel Strain Distribution in the Positive Moment Flexural Reinforcement, North Span of Beam No. 4 135

4.22 Typical Plot of Jack Load versus Steel Strain in a Vertical Stirrup 136

4.23 Steel Strain Distribution of Vertical Stirrups Crossing Major Inclined Cracks

Figure Page

in Beam No. 2 137

4.24 Typical Steel Strain Distribution in a Horizontal Stirrup 138

A.1 Plot of Jack Load versus North Midspan Deflection of Beams No. 2 154

A.2 Plot of Jack Load versus South Midspan Deflection of Beams No. 2 155

A.3 Plot of Jack Load versus North Midspan Deflection of Beams No. 3 156

A.4 Plot of Jack Load versus South Midspan Deflection of Beams No. 3 157

A.5 Plot of Jack Load versus North Midspan Deflection of Beams No. 4 158

A.6 Plot of Jack Load versus South Midspan Deflection of Beams No. 4 159

B.1 Plot of Jack Load versus Support Settlement of Beam No. 2 161

B.2 Plot of Jack Load versus Support Settlement of Beam No. 3 162

B.3 Plot of Jack Load versus Support Settlement of Beam No. 4 163

C.1 Plot of Jack Load versus North Midspan Deflection of Beam No. 1 from the Retest 165

C.2 Plot of Jack Load versus South Midspan Deflection of Beam No. 1 from the Retest 166

C.3 Plot of Jack Load versus North Midspan Deflection of Beam No. 2 from the Retest 167

C.4 Plot of Jack Load versus South Midspan Deflection of Beam No. 2 from the Retest 168

C.5 Plot of Jack Load versus North Midspan Deflection of Beam No. 3 from the Retest 169

C.6 Plot of Jack Load versus South Midspan Deflection of Beam No. 3 from the Retest 170

C.7 Plot of Jack Load versus North Midspan

Figure Page

Deflection of Beam No. 4 from the Retest 171

C.8 Plot of Jack Load versus South Midspan Deflection of Beam No. 4 from the Retest 172

D.1 Plot of Jack Load versus Support Settlement of Beam No. 1 from the Retest 174

D.2 Plot of Jack Load versus Support Settlement of Beam No. 2 from the Retest 175

D.3 Plot of Jack Load versus Support Settlement of Beam No. 3 from the Retest 176

D.4 Plot of Jack Load versus Support Settlement of Beam No. 4 from the Retest 177

List of Notations

A : area of shear plane;

$A*$: ratio of interior support reaction to the sum of the jack loads;

As : area of flexural tension reinforcement;

Av : area of web reinforcement perpendicular to main flexural tension reinforcement;

Avh : area of web reinforcement parallel to main flexural tension reinforcement;

a : length of shear span from the center of a load point to the center of a support;

b : width of beam;

bw : thickness of web;

C : compression force;

d : effective depth of beam;

Fv : component of the axial force in the reinforcing bar opposing the shear parallel to the shear plane;

$f'c$: compressive strength of concrete;

ft : tensile strength of concrete cylinders;

fu : ultimate strength in reinforcing steel;

fy : yield strength of reinforcement;

H : total depth of beam;

L : center to center span;

Lc : width of loading column;

Ls : width of interior support;

ln : clear span distance measured face-to-face of supports;

ls : distance from the point of zero shear to the center of support;

M : moment at the critical section considered;

N : force normal to shear plane;

N-E : north exterior shear span;

N-I : north interior shear span;

N-M : negative moment span;

N-P : north positive moment span;

$P1$: north jack load;

$P2$: south jack load;

$P''s$: shear strength, according to Eqn. 2.5;

Pc : ultimate load in shear, according to Eqn. 2.7;

Pcr : first inclined cracking load;

Pf : flexural cracking load;

Pu[N] : north jack load at failure;

$Qult$: ultimate shear strength, according to Eqn. 2.6;

R : support reaction;

$R1$: north end support reaction;

$R2$: interior support reaction;

$R3$: south end support reaction;

S-E : south exterior shear span;

S-I : south interior shear span;

S-P : south positive moment span;

S_1 : spacing of web reinforcement perpendicular to main flexural tension reinforcement;

S_2 : spacing of web reinforcement parallel to main flexural tension reinforcement;

sh : spacing of horizontal web reinforcement, according to Eqn. 2.15;

T : tension force;

V : shear at the critical section considered;

Va : shear transferred across inclined crack by interface shear transfer;

Vaa : shear transferred by arch action;

Vc : shear carried by concrete;

Vcr : average shear at first inclined cracking;

Vd : shear transferred by dowel forces;

Vh : shear carried by horizontal web reinforcement;

Vn : total shear capacity;

V[N] : shear in the north interior span;

V[S] : shear in the south interior span;

Vs : shear carried by web reinforcement;

Vu : shear at ultimate load;

Vv : shear carried by vertical web reinforcement;

v'cz : ultimate shear stress carried by concrete, according to Eqn. 4.8;

v"n : ultimate shear stress, according to Eqns. 4.7 and 2.9;

v'n : ultimate shear stress, according to Eqns. 2.10 and 2.14;

vuz : total ultimate shear stress;

vb : basic shear stress, according to Eqn. 2.11;

vc : shear stress carried by concrete;

vcr : first inclined cracking shear stress;

vcz : cracking shear stress, according to Eqn. 4.6;

vn : total shear stress, according to Eqns. 2.8 and 2.9;

vs : shear stress carried by web reinforcement;

vu : ultimate shear stress;

vx : inclined cracking shear stress, according to Eqn. 4.3;

x : clear shear span between load blocks;

Δmax : maximum differential settlement;

ϵu : ultimate strain in reinforcing steel;

θ : angle of inclination of shear cracks;

ρ : longitudinal reinforcement ratio based on beam width [$As/(b.d)$];

ρw : longitudinal reinforcement ratio based on web thickness [$As/(bw.d)$];

τxy : shear stress in the shear plane at the center of a strut at failure;

μ : coefficient of friction.

1. INTRODUCTION

1.1 General

Deep beams are usually classified as members where the depth is comparable to the span and the thickness is small relative to the span or depth. There is no definite boundary as to what constitutes a deep beam. Deep beams occur far less frequently than beams with high span-depth ratios, but can be commonly found in structures in the form of transfer girders, shear walls, coupling beams, pile caps and walls of tanks. These members are primarily loaded in the plane of the member and can be characterized by a state of plane stress.

In the design of deep beams, shear is a highly dominant factor. The flexure theory applicable to ordinary slender beams cannot be applied to deep beams. The internal stresses in deep beams are affected by the normal pressures on the top and bottom faces of the beam caused by external loads and reactions. These effects cannot be neglected in the design and analysis of deep beams. The bending stress distribution across a transverse section deviates from the straight line distribution assumed in ordinary slender beams. Transverse sections which are plane before bending do not remain plane after bending. Even more important, when cracking develops, the beam converts to a tied arch and tends to fail in a mode associated with the failure of a tied arch.

1.2 Objective

Extensive research has been carried out on the effect of types of web reinforcement on the behaviour and strength of deep beams but the results obtained were far from conclusive. The aim of this investigation is to shed some light on the problem. Emphasis is on the shear characteristic of two span continuous deep beams with a clear shear span to effective depth ratio, *x/d*, of 1.43. Beams of a realistic model size without web reinforcement, with vertical web reinforcement only, with horizontal web reinforcement only and with orthogonal web reinforcement are studied. This is part of a broader study at the University of Alberta where the major variables involved are the span-depth ratio and the types and amount of web reinforcement. The study is ultimately aimed at revising the design provisions for deep beams in building codes.

1.3 Scope

Chapter 2 discusses the general behaviour and strength of deep reinforced concrete beams. In this chapter, the basic mechanisms of shear transfer are presented. An outline of the factors affecting the behaviour of deep beams is given and several design approximations on the ultimate strength of deep beams are reviewed. The experimental program is described in Chapter 3. The properties of the material used in the test are shown in the form of tables and graphs in this chapter. The test results are presented and discussed in Chapter 4. Several equations for predicting the cracking and ultimate shear strength of deep beams are compared to test data. The summary and conclusions of this investigation are listed in Chapter 5. Appendices A to E present additional test results in tabular and graphical forms.

2. LITERATURE REVIEW

2.1 Introduction

Most research on deep beams has concerned their shear strength. This chapter discusses the basic mechanisms of shear transfer with special emphasis on the shear characteristics of deep beams. Factors affecting the behaviour of deep beams are presented. Several design approximations are reviewed.

2.2 Shear Transfer Mechanisms

In reinforced concrete members, shear can be transmitted by the mechanisms illustrated in Fig. 2.1:

a) concrete shear stress,V_c

b) interface shear transfer,V_a

c) dowel action,V_d

d) arch action,V_{aa}

e) web reinforcement,V_s

These mechanisms of shear transfer can influence the behaviour and mode of failure of reinforced concrete members. The applied shear is resisted by one or a combination of these forces.

2.2.1 Concrete Shear Stress

Shear transfer by concrete shear stress is the simplest method of shear transfer but is still not fully understood. This mechanism of shear transfer occurs in uncracked members or in uncracked sections of cracked members.

Shear forces were once thought to be carried only in the compression zones of cracked members. With further investigations contradicting the idea, the contribution of uncracked sections to the shear strength of a cracked member remains uncertain, even to this day. It has been proposed that the contribution, *Vc*, shown in Fig. 2.1 and the compression force, *C*, together enhance the arch action (see section 2.2.4) of deep beams. Taylor (1968) concludes that the compression zone contribution of the shear force is from 20-40% in a member without stirrups.

2.2.2 Interface Shear Transfer

Interface shear transfer refers to the transmission of shear across a plane where slip may occur. This mechanism of shear transfer has also been called aggregate interlock, shear friction or tangential shear transfer.

The mechanism of interface shear transfer can occur across a plane located in monolithic concrete or across an existing crack or interface.

2.2.2.1 Interface Shear Transfer of Uncracked Concrete With Reinforcement Crossing Shear Plane

A large number of push-off tests have been performed to study shear transfer across monolithic concrete shear planes. Fig. 2.2 shows a typical example of such a test specimen. The loads shown cause shear on the shear plane. This, in turn, causes principal tensile and compressive stresses.

As the applied load is increased, the principal tensile stress of the concrete is increased. When the principal tensile stress equals the tensile strength of the concrete, a series of short, parallel diagonal tension cracks forms resulting in a series of diagonal struts as shown in Fig. 2.3. With shear acting, these diagonal struts tend to rotate, causing a relative displacement of the concrete on either side of the shear plane. This relative displacement produces tensile stresses in the transverse reinforcement crossing the shear plane. A truss is thus formed by the transverse reinforcement and the compression between the diagonal cracks, as shown in Fig. 2.3. Failure will occur when the diagonal struts crush under axial and shearing forces. In this truss mechanism, not all the shear is transferred by interface shear transfer; some shear is transferred by dowel action (see section 2.2.3) of the transverse reinforcement.

In his tests with push-off specimens similar to that shown in Fig. 2.2, Mattock (1974) used closed #3 bar stirrups arranged parallel to one another or orthogonally at various angles to the shear plane for transverse reinforcement. Without including the effect of normal stress acting across the shear plane, he concluded that the ultimate shear stress, νu, is given by:

$$\nu u = \frac{Fv}{A} + K.\ \tau xy \qquad (2.1)$$

where Fv = the component of the axial force in the reinforcing bar opposing the shear parallel to the shear plane,

A = the area of the shear plane,

K = a coefficient,

τxy = the shear stress in the shear plane at the center of a strut at failure.

2.2.2.2 Interface Shear Transfer of Initially Cracked Concrete With Reinforcement Crossing Shear Plane

Shear can only be transmitted in an initially cracked specimen if there is a clamping force on the shear plane. Clamping force can be provided through lateral confinement or through transverse reinforcement crossing the shear plane.

When an initially cracked specimen is loaded in shear, slip will occur along the shear plane. Due to the rough and irregular nature of the cracked surfaces, the cracks open up, stressing the transverse reinforcement in tension. The tension force in the transverse reinforcement is balanced by a compressive force on the concrete across the crack (Fig. 2.4). The compressive force can be viewed as a normal force causing frictional resistance to sliding between the two cracked surfaces. In an under-reinforced shear plane, the separation of the cracked surfaces is sufficient to yield the transverse reinforcement. For transverse reinforcement approximately normal to the cracked surfaces, the ultimate shear, Vu, can be written as:

$$Vu = \mu . As . fy \qquad (2.2)$$

where μ = the equivalent coefficient of friction,
As = the total area of the transverse reinforcement,
fy = the yield stress of the transverse reinforcement.

Shear transfer by dowel action of the transverse reinforcement is significant but is neglected in Eqn. 2.2. To compensate for that, the ACI Code (1977) proposed a high value of 1.4 for μ be used for a crack in monolithic concrete. To account for the presence of a normal force, N, across the cracked shear plane, Eqn. 2.2 can be modified as:

$$Vu = \mu (As . fy + N) \qquad (2.3)$$

where *N* is positive in compression and negative in tension (Mattock et.al., 1975).

For a heavily reinforced shear plane or when sufficient externally applied compressive force is provided, the shear resistance due to friction and dowel action may exceed the shear causing failure in an initially uncracked specimen having the same physical characteristics. When this happens, the cracks lock and the behaviour and strength are similar to those for an initially uncracked specimen (Mattock and Hawkins, 1972).

Fenwick and Paulay (1968) investigated the effect of crack width and concrete strength on the shear transfer capacity of initially cracked specimen. Precracked unreinforced push-off specimens were used. In the first series of tests, concrete strength was kept constant at 32 MPa and the width of the preformed crack was varied from 0.06 mm to 0.38 mm. The crack widths were adjusted by applying a normal force across the crack. In the second series of tests,the width of the preformed crack was kept at 0.19 mm and the concrete strength varied from 19 MPa to 56 MPa. The results showed a significant reduction of shear transfer across the interface for an increase in crack width and for a decrease in concrete strength. The relationship between load and slip could be best expressed as functions of the inverse of the crack width and the square root of the compressive strength of concrete. Unfortunately, in actual beams, shear occurs simultaneously with increasing crack width and not with constant crack width.

To simulate the conditions in an actual beam, Taylor (1970) tested concrete blocks in a special test rig that maintained a constant ratio between the displacement normal to a crack, ΔN, and the shear displacement parallel to a crack, ΔS. His findings showed ultimate shear stress and the ultimate displacement to decrease with increasing $\Delta N/\Delta S$. The shear transfer strength was found to be linearly related to the concrete strength and is also a function of the roughness of the fracture surface.

2.2.3 Dowel Action

Dowel action is due to the reinforcing bars being able to carry forces perpendicular to the longitudinal axis of the bar. When reinforcing bars cross a crack, the bars act as a dowel connecting adjacent crack edges. Shearing displacement along the crack will be resisted. Splitting along the reinforcement frequently occurs due to the tensile force induced in the surrounding concrete and the wedging action of the bars. Splitting reduces the stiffness of the concrete and therefore the dowel forces.

Many studies have been carried out on the effect of dowel action in reinforced concrete beams but no general theory has evolved. Results obtained from simplified models may not represent the actual condition in a cracked reinforced concrete beam. Some investigations (Swamy and Andripoulos, 1974) suggest an interdependence between shear transfer by interface shear transfer and dowel action, making it difficult to assess each contribution quantitatively. Failure to recognize shear transfer by interface shear transfer can lead to over-estimation of dowel forces. Dowel action has been found to be a function of: tensile strength of concrete; bar diameter; number and spacing of bars; amount and spacing of web reinforcement; and interface shear transfer (Krefeld and Thurston, 1966, Baumann, 1968, Taylor, 1969, Dulacska, 1972 and Swamy and Andripoulos, 1974). To consider all the variables involved in the contribution of dowel action seems impractical.

Shear transfer by dowel action is relatively less dominant than other mechanisms of shear transfer but it can affect the failure mechanism of certain structural elements. Dowel action which causes splitting cracks along the tension reinforcement during inclined cracking in beams induces wider inclined cracks. Shear transfer by interface shear transfer decreases with increase in crack width, as reported earlier. This can lead to failure of the structure.

2.2.4 Arch Action

Shear transfer by arch action, unlike other mechanisms of shear transfer, is not a transmission of tangential force from one plane to another. Arch action, however, permits a direct transfer of a concentrated force to a reaction thereby reducing the contribution of other mechanisms of shear transfer.

In a simply supported beam shown in Fig. 2.5 loaded at the third points with concentrated loads, the arch is composed of two inclined concrete compression struts outside the inclined cracks, a concrete compression crown between the concentrated loads and a tension tie at the base of the arch. The inclined struts or arch ribs are frequently formed by an inclined crack on the inside followed by a second inclined crack on the outside almost parallel to the first inclined crack. The tension tie is usually provided by longitudinal reinforcement. In a short beam like the one shown in Fig. 2.5, web reinforcement and compression steel are not necesary. Adequate anchorage of the longitudinal rebars is required to develop this truss-like tied-arch mechanism. Failure by improper anchorage is due to the high tensile stress in the longitudinal rebars which, in short shear spans, is constant throughout the length of the shear span. Provisions for anchorage can be provided by welding steel plates to the ends of the bars or by hooking the bars. Leonhardt (1966) prefers hooks lying in the horizontal plane because the splitting action of the hooks can be compensated by vertical compression in the concrete near the bearing area. Bearing failure can also occur as a result of high compressive stresses in the support and loading regions. Assuming anchorage and bearing failures are prevented, de Paiva and Siess (1965) reported flexural failure and shear failure as the primary failure modes of a tied arch. Flexural failure occurs by crushing of the concrete rib at the crown or by rupture of the tension tie. Flexural failure is usually accompanied by extensive inelastic deformations. Shear failure occurs by the destruction of the arch ribs that form between the load point and support. Little or no inelastic deformation occurs during shear failure.

Manuel (1974) predicted the shear capacity of deep beams by the crushing strength of the arch ribs. Based on the assumption that the thickness of the arch rib equals the thickness of the web, b_w, and the width of the arch rib measured in the horizontal direction equals the width of the support or load point, L_s, it can be shown that:

$$V_u = \frac{0.85 f'_c . L_s . b_w}{[1 + (a/d)^2]} \qquad (2.4)$$

where a = length of shear span from the center of the load point to the center of the support,

d = effective depth of beam,

f'_c = compressive strength of concrete.

The arch action mechanism increases as the a/d ratio decreases. For deep beams with a/d ratio of less than 2.5, shear transfer by arch action is highly significant. For members with lower a/d ratios, arch action becomes the dominant shear transfer mechanism.

2.2.5 Web Reinforcement

The contribution of web reinforcement to the shear strength can be direct or indirect. Part of the shear force is directly resisted by tensile stress in the web steel, thereby reducing the contribution of other forms of shear transfer. The loads supported in this manner have been customarily assumed to be transmitted to the reactions by means of a truss made up of the web reinforcement and main reinforcement acting as tension members and concrete struts acting as compression members.

Web reinforcement can also enhance other mechanisms of shear transfer. When inclined cracks form across any web reinforcement, the web reinforcement restricts the widening of the cracks. This helps to maintain the shear transferred by interface shear transfer and arch action. In addition to the main reinforcement, web reinforcement also helps in developing dowel action, although its contribution is small compared to that of the main reinforcement. More importantly, however, web reinforcement supports the longitudinal reinforcement, reducing or delaying the decrease in dowel shear.

The role of web reinforcement, especially vertical stirrups, changes from that of carrying shear by direct tension to that of serving as interface shear transfer reinforcement as the slenderness ratios of beams are decreased. Particularly for deep beams, web reinforcement prevents a sliding failure along the inclined crack. The present ACI Code equations for web reinforcement in deep beams assume interface shear transfer as the sole means of shear transfer by web reinforcement (ACI-ASCE Committee 426, 1973).

2.3 Factors Affecting Behaviour of Deep Beams

2.3.1 M/(V.d) or a/d Ratio

The effect of the moment to shear ratio, $M/(V.d)$, or the center to center shear span to effective depth ratio, a/d, in the case of concentrated loads on shear strength can be summarized through Fig. 2.6 and Fig. 2.7. For low a/d ratios, the capacity of the beams are dictated by the shear strength rather than the flexural strength. For a beam with a/d less than about 2.5, the shear strength of the beam increases significantly as a/d decreases. The extra shear capacity beyond inclined cracking, or reserve shear capacity in beams without web reinforcement, holds only for beams loaded and supported on opposite sides so that compressive struts can develop as shown in Fig. 2.5 (see section 2.3.2).

2.3.2 Method of Load Application

A deep beam with the applied loads and reactions acting directly on the beam, either on opposite sides, top and bottom, of the beam or on the same side is classified as directly loaded. When the loads and reactions are applied through other structural members framing into the sides of the beam, the beam is classified as indirectly loaded (Fig. 2.8).

For directly loaded deep beams with the loads applied so that a compression strut can form, the shear capacity can be increased beyond that causing inclined cracking. This reserve shear capacity results from arch action. The development of the arch can be visualized through principal stress trajactories shown in Fig. 2.9 for a uniform load.

When the loads are applied on the tension side of the beam, arch action cannot develop. Therefore, no increase in shear capacity can be expected. Designs for beams loaded in this way should be the same as for ordinary slender beams (ACI Committee 318, 1977). If hanger reinforcement is provided to lift the loads up to the compression face, the behaviour approaches that of a beam loaded on the top face.

Structural members framing into the sides of a deep beam tend to distribute the load through the depth of the beam. Limited amounts of arch action can be attained. Consequently, the ultimate shear capacity is less than that of a beam loaded directly on the compression side. Smith and Fereig (1974) found that deep beams without web reinforcement loaded indirectly had ultimate strengths of 1/2 to 2/3 of beams loaded directly on the compression side.

2.3.3 Nature of Loading

Wind and earthquake loadings may cause reversal of shear in deep beams. Under wind loading, the main requirement is that a member develop its design ultimate strength. However, under an earthquake loading, the shear capacity of the member should be sustained while the member undergoes several cycles of reversed inelastic deformation.

When a member is subjected to reversal of loading, inclined cracks develop across the cracking caused by the preceeding loading. Tests performed by Paulay (1971) showed that before yielding of the web reinforcement, this cross cracking does not destroy the integrity of the member but may reduce its stiffness considerably. If the longitudinal or web reinforcement yielded, however, the shear strength was reduced. Uncertainty still exists regarding the effect of load reversal on the ultimate shear strength (ACI-ASCE Committee 426, 1973).

2.3.4 Type of Web Reinforcement

For deep beams with $M/(V.d)$ or a/d ratio between 0 and 2.5, web reinforcement perpendicular to the longitudinal axis becomes less effective (Crist, 1971). As the clear span to effective depth ratio, l_n/d, of a uniformly loaded beam decreases, the angle of inclination of the shear cracks, θ, increases beyond the 45° commonly assumed for ordinary reinforced concrete beams, as shown in Fig. 2.10. This effect is also evident for deep beams loaded with concentrated loads. As the angle of inclination of the shear cracks increases, web reinforcement parallel to the longitudinal axis of the deep beam will become more perpendicular to the crack. Therefore, for low *M/(V.d)* or *a/d* ratios, this type of web reinforcement has been reported as being more effective in resisting shear (Crist, 1971). As *a/d* approaches zero, this web reinforcement would be expected to resist shear by the concept of interface shear transfer (Hofbeck et.al., 1969 and Mattock and Hawkins, 1972). Other investigators have reported that horizontal web reinforcement is ineffective in deep beams (Smith and Ferigh, 1974).

Inclined web reinforcement was found to be most effective for deep beams with clear shear span to effective depth ratios, *x/d*, ranging from 0.23 to 0.70 (Kong et.al., 1972) even though the ACI Code does not recognized its value in deep beams.

In the case of shear walls coupled by short, deep coupling beams, Paulay and Binney (1974) proved that coupling beams with reinforcement made up of diagonal bundles of bars as shown in Fig. 2.11 are superior to conventionally reinforced coupling beams with respect to seismic type of loading. Such beams possess excellent ductility and the energy absorption properties which are essential under seismic load condition.

2.3.5 Detailing of Longitudinal Reinforcement

Inclined cracking in deep beams may extend the full length of the shear span, as shown in Fig. 2.5, intercepting the main reinforcement at the base of the crack. This tends to increase the stress in the flexural tension reinforcement where it crosses the crack. This stress becomes a function of the moment at a section through the top of the crack. As a result, the stress is much higher than indicated by the moment diagram and the beam can fail by anchorage failure. Adequate anchorage is necessary and can be provided by well restrained hooks, welded transverse bars, or steel anchor plates welded to the ends of the bars. The increase in stress in the flexural tension reinforcement is greatest in beams without web reinforcement and least in beams with effective web reinforcement.

The Comité Europeén du Béton or CEB (1970) recommends that main reinforcement in deep beams be distributed over a certain depth instead of being concentrated at the extreme tension zone. Besides acting as flexural reinforcement, distributed main reinforcement acts to widen the diagonal compression strut, increasing its capacity.

2.4 Design Approximations

Many methods are available for predicting the shear capacity of deep beams. This section will outline the methods of de Paiva and Siess (1965), Kong and Robins

(1972), Ramakrishnan and Ananthanarayana (1968), ACI 318-77 (1977), ACI-ASCE Committee 426 (1977) and CEB (1970).

2.4.1 de Paiva and Siess

de Paiva and Siess (1965) tested simply supported beams with center to center span length to effective depth ratios, *L/d*, of 4,3 and 2 and *a/d* ratios ranging from 0.67 to 1.33. The beams were loaded directly with concentrated loads at the third points on the compression side. The major variables were the amount of tension reinforcement, the concrete strength, the amount of web reinforcement and the span-depth ratio. All the beams tested had well developed inclined cracks at failure and behaved essentially as tied arches. After inclined cracking, the strain in the tension reinforcement was nearly uniform along the beam and the concrete strains tended to concentrate near the midspan over the ends of the inclined cracks, as shown in Fig. 2.12(a). For comparision, the strain distributions expected in normal reinforced concrete beams are shown in Fig. 2.12(b).

The authors reported that an increase in concrete strength increased the ultimate shear strength and in some cases changed the failure mode of the beams. The mode of failure also tended to change from flexure to shear with an increase in the amount of tension reinforcement. The presence of up to 1.42% of inclined or vertical web reinforcement had little or no effect on the development of the inclined cracks and the ultimate strength but tended to reduce the deflection at ultimate load. For beams with *a/d* ratios less than 3, shear capacity beyond cracking load increased significantly as *a/d* decreased. Based on their test results and those from other investigators, the following empirical formula was suggested to calculate the ultimate shear strength of deep beams.

$$P''s = 0.8b.H[1 - 0.6(\frac{x}{H})][200 + 0.188f'c + 21{,}300pt] \quad (2.5)$$

valid only for $0 \leq x/H \leq 1.0$

where $P''s$ = the computed shear strength, in psi,

$pt = As(1 + \sin\alpha)/(b.H)$,

As = the area of tension reinforcement, in inches^2,

α = the angle of inclination of bent-up reinforcement to the axis of the beam,

b = the width of the beam, in inches,

H = the total depth of the beam, in inches,

x = the clear shear-span distance between load blocks, in inches,

$f'c$ = the compressive strength of concrete, in psi.

The last term in parenthesis was developed by Laupa, Siess and Newmark (1959). The quantity $As(1 + \sin\alpha)$ refers to the total steel area, including compression reinforcement, crossing a vertical section between the load point and support. When both horizontal and inclined web reinforcements are used, *p*t must be evaluated for each part separately. The effectiveness of inclined web reinforcement increases with α and is maximum when $\alpha = 62.7°$. Vertical web reinforcement is ineffective in Eqn. 2.5.

2.4.2 Kong and Robins

Kong et al. (1972) investigated the effect of web reinforcement in normal and lightweight concrete beams. All the beams were simply supported with two point loads and have L/d ratios ranging from 1 to 3 and x/d ratios ranging from 0.23 to 0.70. The types of web reinforcement tested included vertical stirrups, horizontal stirrups, orthogonal stirrups and inclined stirrups. Of the different types of web reinforcement tested, inclined stirrups were found to be the most effective in increasing the ultimate shear strength for the L/d and x/d ratios studied. Beams with ineffective web reinforcement failed at low loads as a result of propagation of diagonal cracks. Inclined stirrups were reported to have effectively arrested the growth of diagonal cracks in the deeper beams. Such beams failed by vertical splitting above a support followed by crushing near the bearing block. Once sufficient inclined stirrups were provided, no increase in the shear strength resulted from additional steel. This suggests an optimum amount of inclined web reinforcement. The only other effective web reinforcement in the range of L/d and x/d studied was closely spaced horizontal stirrups anchored near the bottom of the beam.

The following formula was proposed to predict the ultimate shear strength of the beam.

$$Qult = C_1[1 - 0.35(\frac{x}{H})]ft.b.H. + C_2\sum^{n} A[\frac{y}{H}]\sin^2\alpha \qquad (2.6)$$

where $Qult$ = the ultimate shear strength, in newtons,

C_1 = a coefficient equal to 1.4 for normal weight concrete and 1.0 for light weight concrete,

C_2 = a coefficient equal to 130 MPa for plain round bars and 300 MPa for deformed bars,

ft = the cylinder tensile strength, in MPa,

A = the area of an individual web bar, including the main longitudinal bars, in mm^2,

y = the depth, in mm, measured from the top of the beam, at which an individual bar intersects the line joining the inside edge of the bearing block at the support to the outside edge of the bearing plate at the loading point,

α = the angle between the bar being considered and the line described in the definition of y ($90° \geq \alpha \geq 0°$),

n = the total number of web bars, including main longitudinal bars that cross the line described in the definition of y.

Although C_1 and C_2 are empirical coefficients determined by least-square analysis of 135 tests, the above formula is based on an assumed diagonal tension failure model. The first term in Eqn. 2.6 represents the concrete contribution to the ultimate shear strength. The second term represents the additional strength due to the web and main reinforcements. This term assumes that the effectiveness of a bar varies linearly from zero at the top to a maximum at the bottom. Bars perpendicular to a crack are most effective.

Eqn. 2.6 applies only for static loads and is restricted to beams with x/d ratios ranging from 0.23 to 0.70. For uniformly distributed loads, x/H should be taken as $L/(4H)$.

2.4.3 Ramakrishnan and Ananthanarayana

Ramakrishnan and Ananthanarayana (1968) conducted tests to investigate the behaviour and ultimate shear strength of reinforced concrete deep beams. Twenty six simply supported beams having different span-depth ratios were subjected to one and two-point concentrated loads and distributed loads. Tension reinforcement was kept as low as possible and no web reinforcement was provided. The major variables were the span-depth ratio and the type of loading.

Diagonal tension failure was the predominant mode of failure. This failure was similar to the splitting of a cylinder under diametral compression. Some beams failed by a diagonal compression mode and were noted to have slightly higher strengths than those failing by the diagonal tension mode. Due to the uncertainty of the conditions causing the diagonal compression mode of failure, the authors estimated the ultimate shear strength of deep beams based on the diagonal tension mode only.

Adopting Brock's (1964) prediction of the ultimate strength of reinforced concrete beams based on the basis of the splitting strength of concrete, an equation was developed to compute the ultimate shear strength of deep beams.

$$Pc = 2K.ft.b.H \tag{2.7}$$

where Pc = the computed ultimate load in shear,
K = the splitting coefficient,
ft = the splitting strength of concrete.

K depends on the shape of the specimen and for all practical purposes, is taken equal to a reasonable lower bound value of 1.12.

Eqn. 2.7 was found to apply for both concentrated and uniformly loaded beams loaded on the compression side. The effect of the longitudinal reinforcement in preventing splitting has been neglected. The formula disregards the influence of web reinforcement on the ultimate strength.

2.4.4 1977 ACI Building Code (ACI 318-77)

The shear design expressions for deep beams adopted by ACI 318-77 (1977) are based on the work of Crist (1971). Members with l_n/d less than 5 and loaded directly on the compression side are classified in the ACI Code as deep members for shear. Adequate anchorage is assumed to be provided although the Code does not definitely require adequate anchorage.

The shear capacity of a deep beam without web reinforcement is given by the expression:

$$V_c = \left[3.5 - 2.5\left(\frac{M_u}{V_u . d}\right)\right]\left[1.9\sqrt{f'_c} + 2500\,\rho_w\left(\frac{V_u . d}{M_u}\right)\right]b.d \qquad (2.8)$$

$$\leq 6\sqrt{f'_c}.b.d$$

where V_c = the shear strength carried by the concrete, in lbs,

M_u = the moment at the critical section,

V_u = shear force at the critical section,

f'_c = the compressive strength of concrete, in psi,

ρ_w = the longitudinal reinforcement ratio based on the web thickness.

The critical section is defined as a section located at a distance $0.15(l_n)$ from the face of the support for uniformly loaded beams and $0.50(x)$ but not more than d from the face of the support for beams loaded with concentrated loads. The first term in the parenthesis is the magnification factor due to the reserve shear capacity of deep beams without web reinforcement (see section 2.3.1) but shall not be taken more than 2.5.

For beams with web reinforcement, the ACI Code assumes that the total shear capacity, Vn, can be taken as the addition of the contribution of Vc and the shear capacity of the web reinforcement, Vs. Recognizing that the inclination of diagonal cracking in deep beams may be steeper than 45°, both vertical and horizontal stirrups are required by the ACI Code. Based on the interface shear transfer concept developed by Crist (1971), the shear strength provided by web reinforcement is given by:

$$Vs = \left[\frac{Av}{s_1}\left(\frac{1 + ln/d}{12}\right) + \frac{Avh}{s_2}\left(\frac{11 - ln/d}{12}\right) \right] fy.d \qquad (2.9)$$

where Av and s_1 = the respective area and spacing of web reinforcement perpendicular to flexural tension reinforcement,

Avh and s_2 = the respective area and spacing of web reinforcement parallel to flexural tension reinforcement.

The first and second terms in the inner parentheses represent the cosine and sine of the crack angle respectively. Inclined web reinforcement is disregarded in

Eqn. 2.9.

In the ACI Code, when l_n/d is less than 2, V_u shall not exceed $8\sqrt{f'_c}.b.d$ and when l_n/d is between 2 and 5, V_u shall not exceed $(2/3)(10 + l_n/d)\sqrt{f'_c}.b.d$.

2.4.5 ACI-ASCE Committee 426

The ACI-ASCE Committee 426 (1977) suggested revisions for the design provisions for deep beams to overcome two shortcomings of the ACI 318-77.

1. In ACI 318-77, the critical section for beams loaded with concentrated loads is $0.50(x)$ from the face of the support. However, in the case of a continuous deep beam, the point of contraflexure is very close to $0.50(x)$ and as a result, V_c reaches the maximum limit. For such a case, the maximum increase in shear stress is not in good agreement with test data (MacGregor and Gergely, 1977). In the suggested revisions, the slope of the thrust line joining the load and support is referred to, rather than the $M/(V.d)$ ratio.

2. The expression for the shear carried by web reinforcement in ACI 318-77 assumes shear transfer by interface shear transfer only. A serious discontinuity exists as the slenderness ratio passes from just greater than 5 to just less than 5. In the suggested revisions, modifications are made to reflect both interface shear transfer and normal stirrup action in the web reinforcement, thus eliminating the discontinuity.

The ACI-ASCE Committee 426 defined a deep beam, with respect to shear, as "one in which a significant portion of the shear force is transferred directly from the loads to the support by a compression strut action". The beam should be loaded on the compression side and have an a/d ratio less than 2. For deep beams without web reinforcement supporting concentrated loads, the shear stress carried by the concrete, v_c, is given by:

$$v_c = (2d/a)v_b \tag{2.10}$$

$$\text{and } v_b \le v_c \le 0.2f'_c \text{ or } 800 \text{ psi.}$$

v_b is the basic shear stress carried by the concrete in a slender beam and is given by:

$$v_b = (0.8 + 120\rho_w)\lambda\sqrt{f'_c} \tag{2.11}$$

$$\text{and } \lambda\sqrt{f'_c} \le v_b \le 2.3\lambda\sqrt{f'_c}, \text{ in psi.}$$

where λ = 1.0 for normal weight concrete
= 0.75 for 'all-lightweight' concrete
= 0.85 for 'sand-lightweight' concrete

a is the distance from a principal load to the reaction at the end of the beam under consideration; a should be taken as the center to center distance but not more than 1.15 times the clear distance. A principal load is defined as a concentrated load which causes 50 percent or more of the shear at the support of that shear span.

For deep beams with web reinforcement, the total shear capacity, Vn, is taken as:

$$Vn = Vc + Vv + Vh \tag{2.12}$$

Vv is the shear force carried by the vertical stirrups,

$$Vv = \frac{Av.fy(a - d/2)}{s_1} \tag{2.13}$$

$$\text{and } 0 \le Vv \le (Av.fy.d)/s_1$$

Vh is the shear force carried by the horizontal stirrups,

$$Vh = \frac{Avh.fy(3d/2 - a)}{s_2} \tag{2.14}$$

$$\text{and } 0 \le Vh \le (Avh.fy.d)/s_2$$

For deep beams loaded with uniform loads, Vn, Vv, and Vh in the above equations can be computed by replacing a with $2(ls)/3$; ls should be taken as the distance from the point of zero shear to the center of the support but not more than 1.15 times the clear distance from the point of zero shear to the face of the support.

The shear force due to web reinforcement, $Vv + Vh$, should not exceed $8b.d.\lambda\sqrt{f'c}$ and the total shear force, Vn, should not exceed $0.2b.d.f'c$ nor $800b.d$ (lb). The upper limit for V_n was set based on the interface shear transfer mechanism developed by Mattock (1972,1974).

The first term in paranthesis in Eqn 2.10 is a magnification factor to account for the increase in shear capacity for beams with *a/d* decreasing from 2. In Eqn. 2.13, the vertical stirrups are not effective until *a/d* exceeds 0.5 and will be fully effective when *a/d* = 1.5. Eqn. 2.14 was derived by Crist (1971):

$$V_h = \frac{A_{vh}.f_y.d}{s_h} \sin^2\theta \tan\phi \qquad (2.15)$$

where s_h = the spacing of the horizontal web reinforcement,
$\tan\phi$ = the coefficient of friction,
θ = the angle of the critical inclined crack.

When $\tan\phi$ is set to unity and for *a/d* between 0 and 1, $\sin^2\theta$ is approximately $(1.5 - a/d) \leq 1.0$. With these substitutions, Eqn. 2.15 equals Eqn. 2.14.

2.4.6 Comité Europeén du Béton (CEB)

The CEB (1970) defines deep beams as straight beams, generally of constant cross-section with a slenderness ratio, *L/H*, of less than 2.0 for simply supported beams and 2.5 for continuous beams. The length, *L*, is taken to be the distance between the centerline of supports but not more than 1.15 times the clear distance.

The area of the principal longitudinal reinforcement should be calculated from the ultimate bending moment the same manner as for a normal beam subjected to an equal moment except that the lever arm, z, being taken as:

for simply supported beams

$$\begin{aligned} z &= 0.2(L + 2H) \text{ for } 1 \le L/H < 2 \\ &= 0.60L \text{ for } L/H < 1 \end{aligned} \tag{2.16}$$

for continuous beams

$$\begin{aligned} z &= 0.2(L + 1.5H) \text{ for } 1 \le L/H < 2.5 \\ &= 0.50L \text{ for } L/H < 1 \end{aligned} \tag{2.17}$$

For $L/H < 1$, z is independent of H and for $1 \le L/H < 2$ or $1 \le L/H < 2.5$, z increases with H but is smaller than in normal slender beams.

The principal longitudinal reinforcement for simply supported beams should be uniformly distributed over a depth equal to $(0.25H - 0.05L)$ measured from the soffit of the beam. The principal longitudinal reinforcement should extend, without curtailment, from one support to another. For continuous beams, the CEB suggests that one half of the negative moment flexural tension reinforcement over the support should extend over the full length of the adjacent spans. The other half may be stopped a distance of $0.4H$ from the face of the support. The longitudinal tension reinforcement at the support should be distributed within two horizontal bands consisting of:

1. The upper band which extends to a depth of $0.2H$ measured from the top of the beam in which horizontal reinforcement with an area equal to $0.5(L/H - 1)$ of the total area is provided.
2. The lower band which extends from $0.2H$ to $0.8H$ below the top in which the remainder of the negative moment reinforcement is placed.

Whenever the depth exceeds the span ($H > L$), H should be replaced by L in the above rules.

Adequate anchorage should be provided for the principal longitudinal reinforcement so as to develop at least 80 percent of the maximum force. Leonhardt (1966) recommended the use of horizontal hooks in place of vertical hooks to avoid promoting cracking in the anchorage zone. Small diameter bars can also be used to limit the width and development of cracks under service loads and to facilitate anchorage at the supports. For beams loaded directly on the compression side, a light mesh of orthogonal reinforcement, consisting of vertical stirrups and horizontal bars placed near each face and surrounding the extreme vertical bars will generally be sufficient for web reinforcement. This web reinforcement would primarily serve to control cracks.

The CEB limits the total shear force to the lesser of $0.1b.H.f'c$ or $0.1b.L.f'c$.

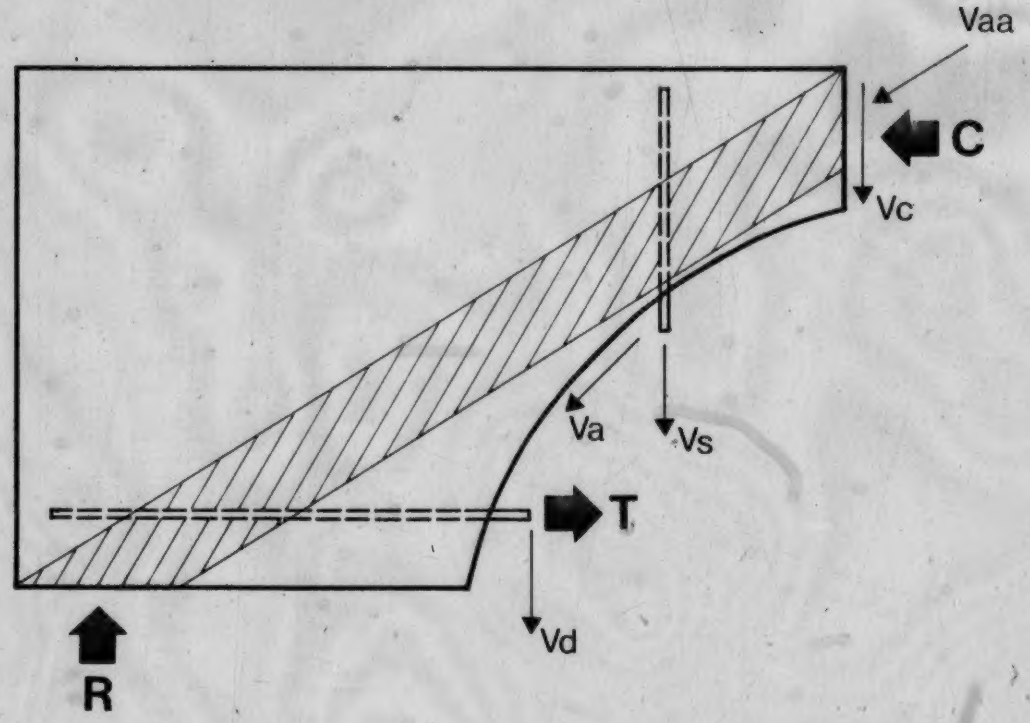
Vaa
C
Vc
Va
Vs
T
Vd
R

Figure 2.1 Forces Acting on a Diagonal Crack of a Reinforced Concrete Member

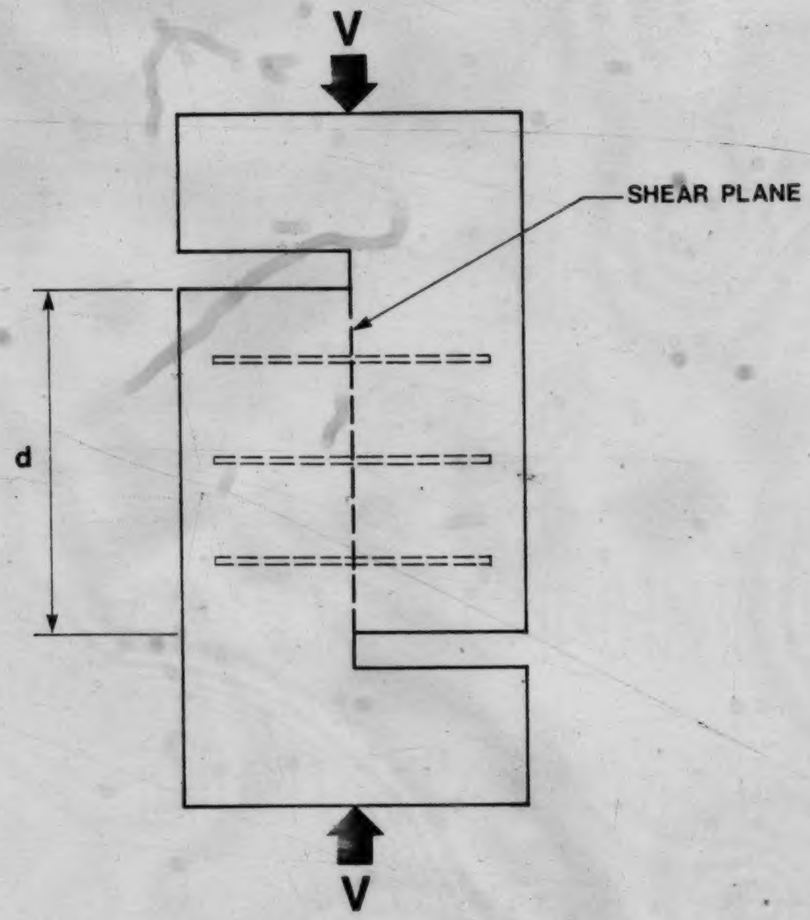
V
SHEAR PLANE
d
V

Figure 2.2 Push-Off Test Specimen

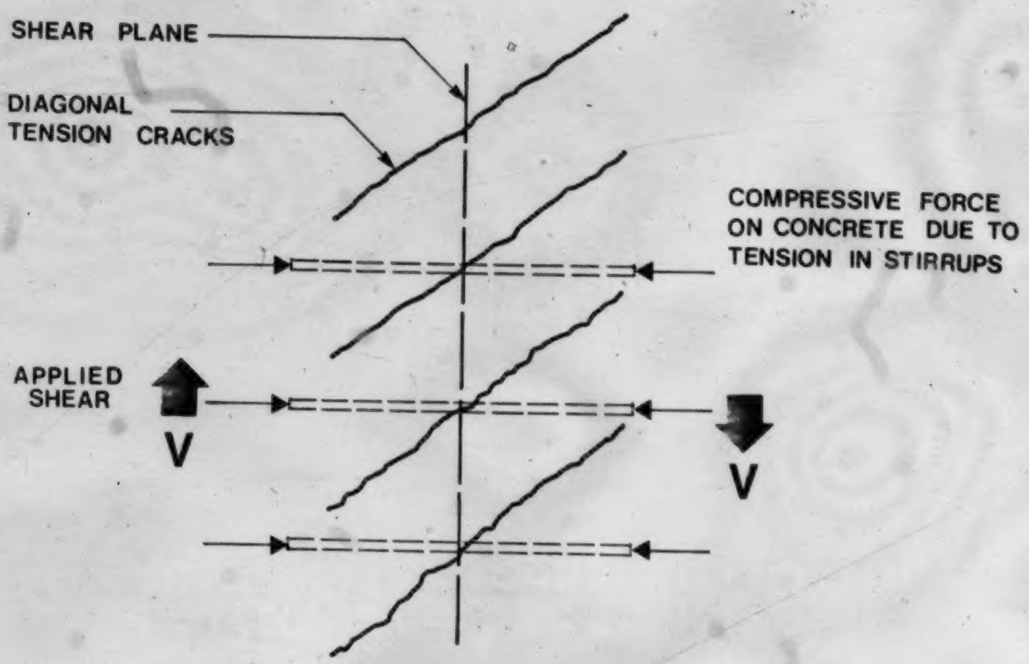
SHEAR PLANE
DIAGONAL TENSION CRACKS
COMPRESSIVE FORCE ON CONCRETE DUE TO TENSION IN STIRRUPS
APPLIED SHEAR
V
V

Figure 2.3 "Truss" Formed After Diagonal Tension Cracking (Mattock and Hawkins, 1972)

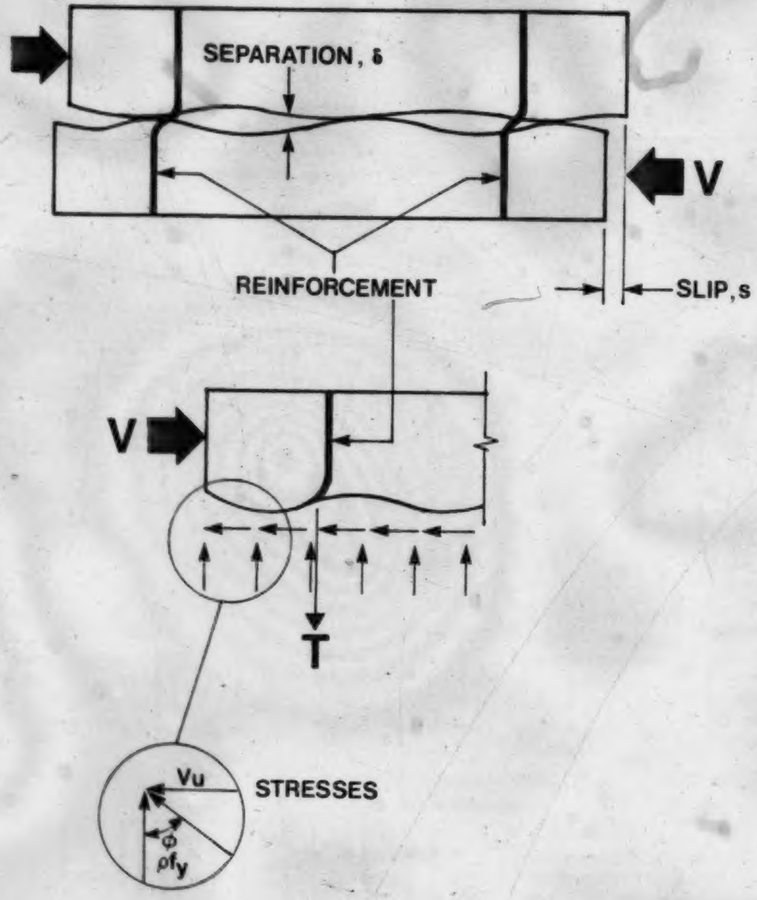
SEPARATION, δ
V
REINFORCEMENT
SLIP, s
V
T
Vu
STRESSES
Φ
ρfy

Figure 2.4 Shear-Friction Analogy (ACI-ASCE Committee 426, 1973)

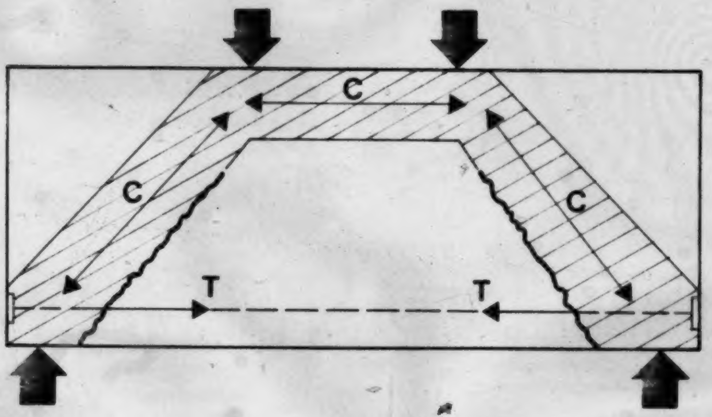

Figure 2.5 Arch Action in a Simply Supported Beam

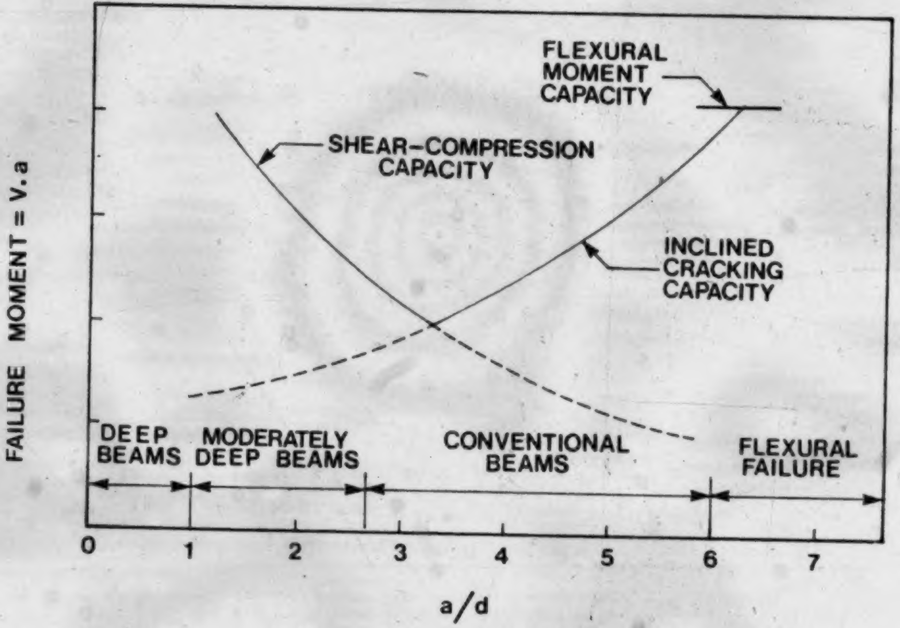

Figure 2.6 Variation in Shear Capacity With *a/d* for Rectangular Beams (Bresler and MacGregor, 1967)

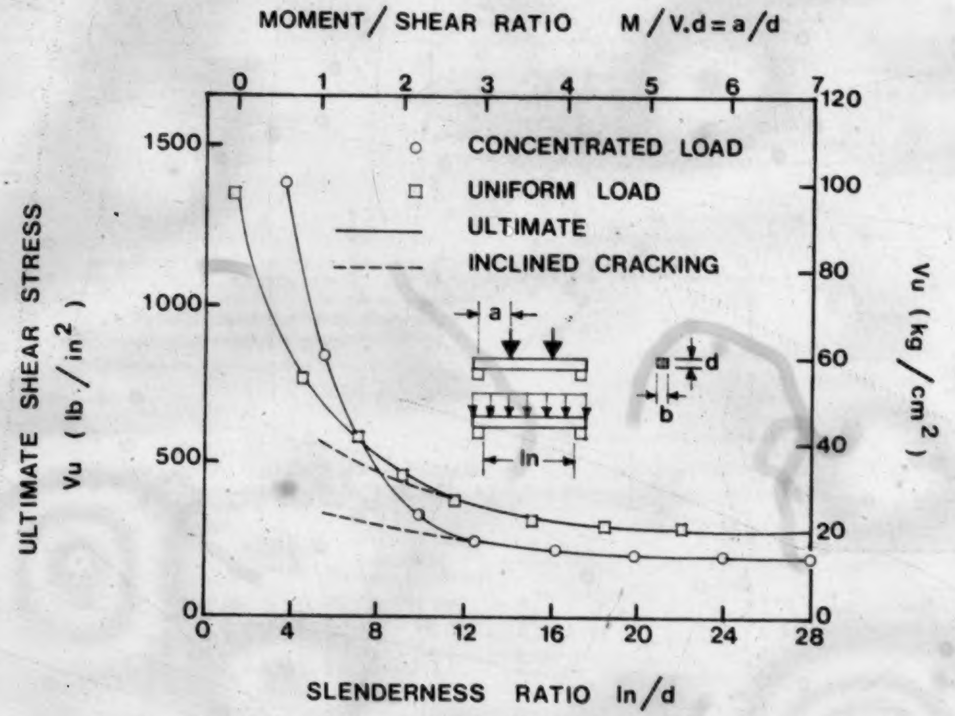

Figure 2.7 Reserve Shear Capacity of Deep Beams (ACI-ASCE Committee 426, 1973)

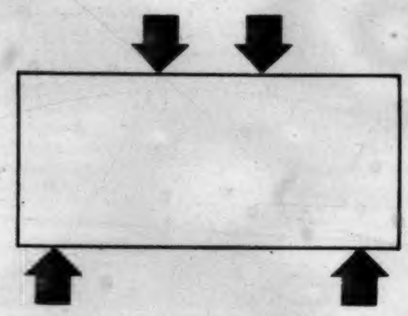

a) DEEP BEAM DIRECTLY LOADED ON THE COMPRESSION SIDE

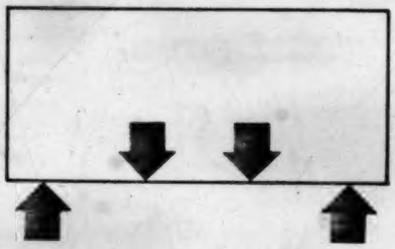

b) DEEP BEAM DIRECTLY LOADED ON THE TENSION SIDE

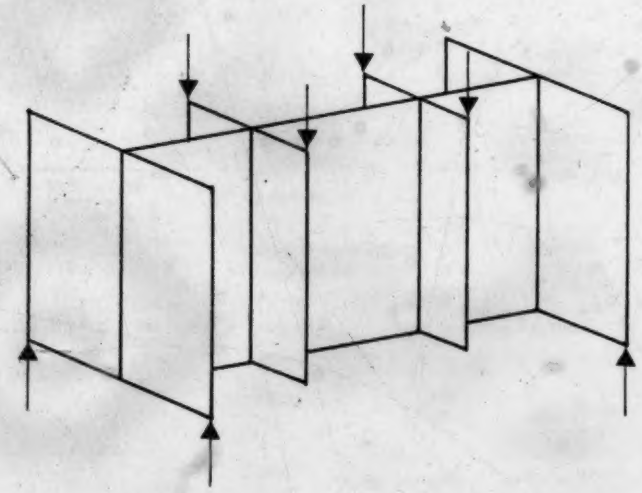

c) INDIRECTLY LOADED DEEP BEAM

Figure 2.8 Method of Load Application

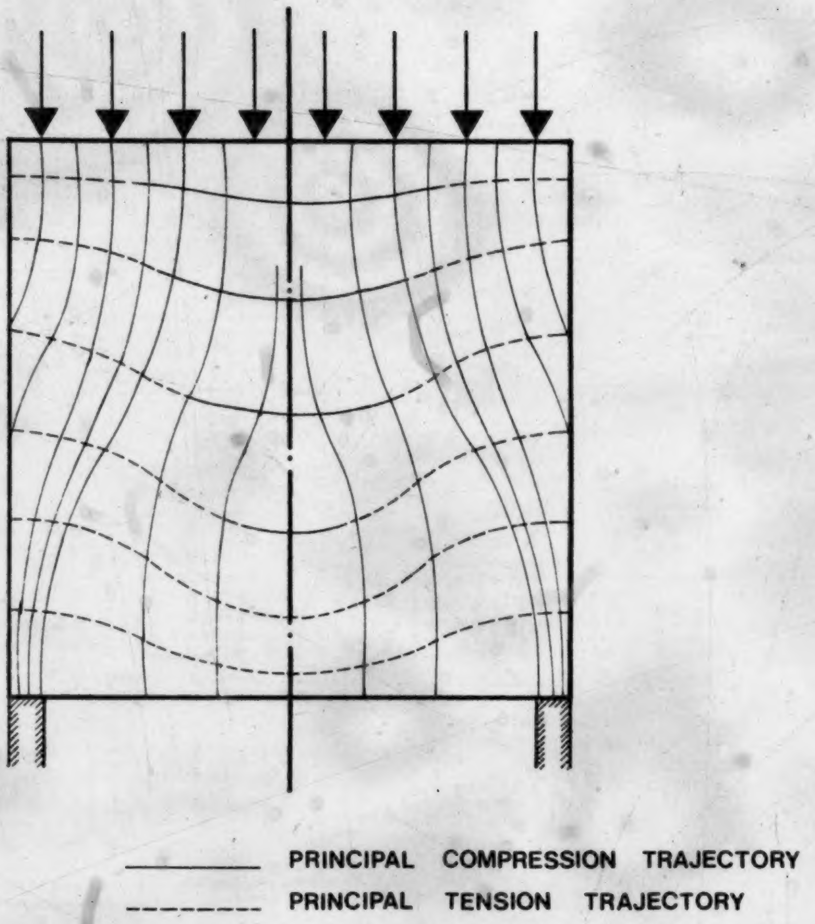
PRINCIPAL COMPRESSION TRAJECTORY
PRINCIPAL TENSION TRAJECTORY

Figure 2.9 Principal Stress Trajectories of the Uncracked State of Deep Beams (Leonhardt, 1966)

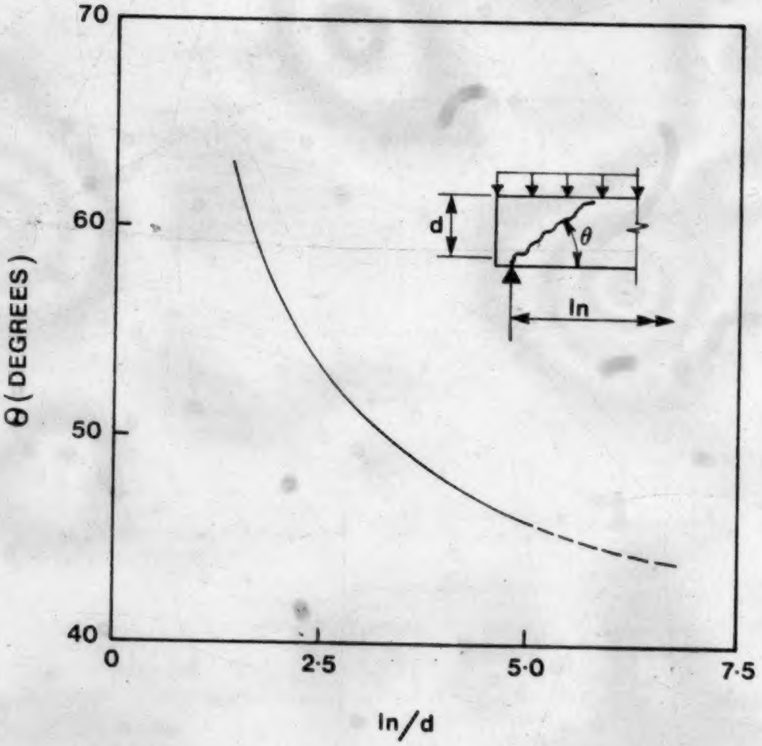

Figure 2.10 Inclination of Shear Cracks in Deep Beams (Crist, 1971)

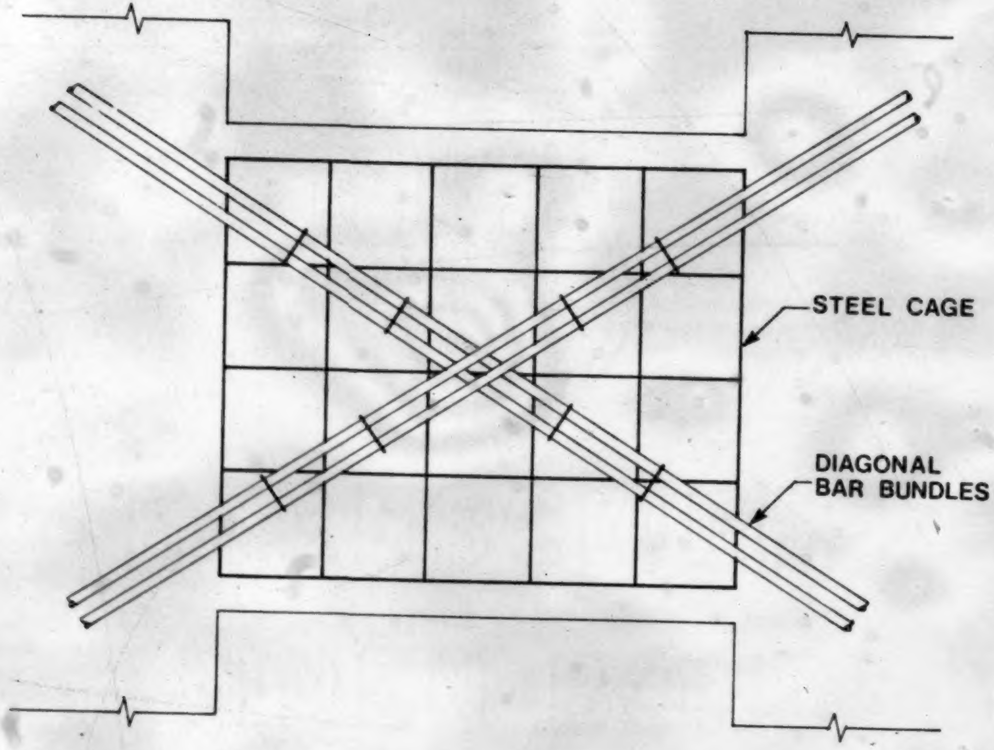
STEEL CAGE
DIAGONAL BAR BUNDLES

Figure 2.11 Diagonally Reinforced Coupling Beam (Paulay, 1971)

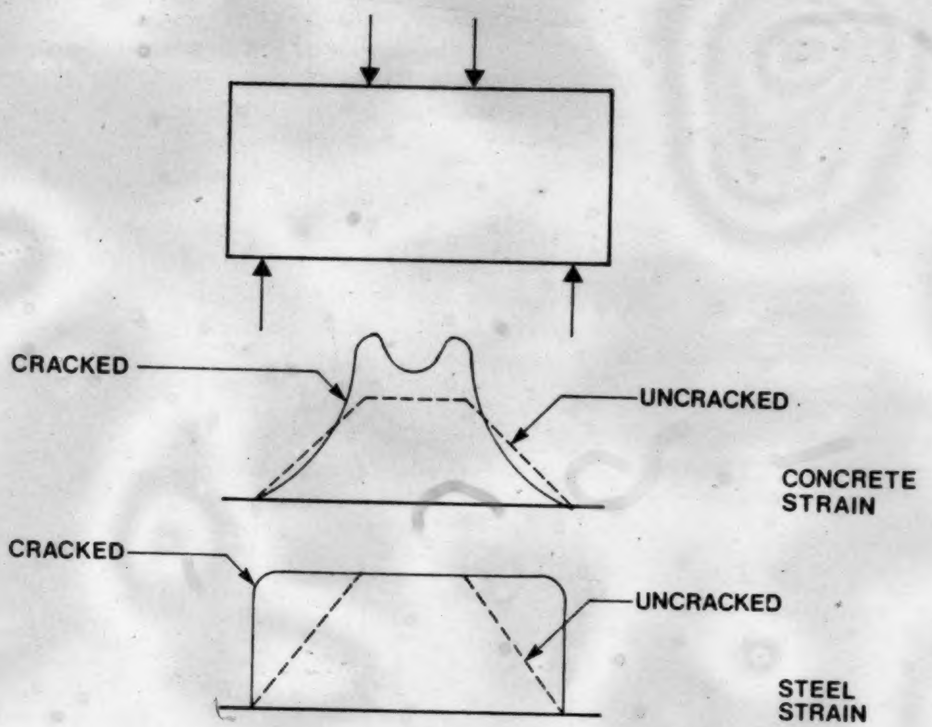
CRACKED
UNCRACKED
CONCRETE STRAIN
CRACKED
UNCRACKED
STEEL STRAIN

(a) DEEP BEAMS

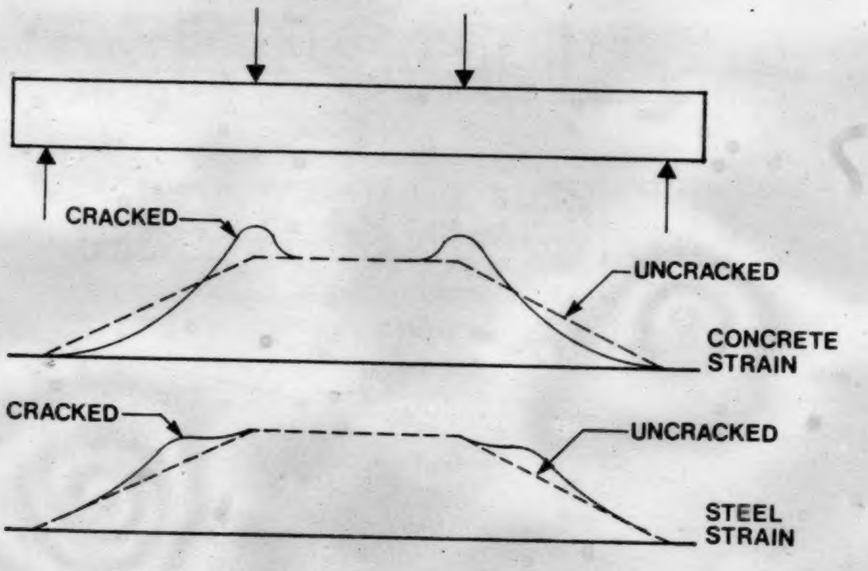
CRACKED
UNCRACKED
CONCRETE STRAIN
CRACKED
UNCRACKED
STEEL STRAIN

(b) CONVENTIONAL BEAMS

Figure 2.12 Effect of Inclined Cracking on Steel and Concrete Strains (de Paiva and Siess, 1965)

3. EXPERIMENTAL PROGRAM

3.1 Introduction

To study the effects of vertical and horizontal web reinforcements on the shear strength of continuous deep beams, four two-span continuous deep beams were built and tested. The external dimensions of all the specimens were the same. The beams differed from each other mainly in the type of web reinforcement present. Loads were applied at the midspan of the beams through hydraulic jacks. A special loading frame was constructed for this purpose. Loads and reactions were measured using load cells, deflection and support settlements were measured using dial gages and strains were measured using mechanical demec gages.

3.2 Specimen Geometry

The external dimensions of the specimens are shown in Fig. 3.1. All the beams had a uniform thickness of 200 mm. The overall length of the two-span beams was 4400 mm with a height of 600 mm. All the beams were supported with two spans of 2100 mm center to center of supports. All loading and supporting columns had lengths of 300 mm. The width of the loading columns were 300 mm. The end and center supporting columns had widths of 200 mm and 400 mm respectively.

All the beams were reinforced for positive and negative moments using 15M and 10M reinforcing bars. The stress-strain characteristics of these bars were established and are presented in the later section. The positive moment reinforcement consisted of four 15M and two 10M bars placed in three layers. These bars were continuous through both spans and into the end supporting columns. Anchorage was provided by bending the ends of the bars into vertical standard hooks. For negative moment reinforcement, six 15M bars were placed in three layers. Two bars in the uppermost layer were extended the full length of the beam. Another two bars in the middle layer were extended 1625 mm on either side from the centerline of the beam. The remaining two bars in the lowermost layer were extended 600 mm from either side of the centerline. The arrangement of these flexural reinforcements are shown in Fig. 3.2(a). The effective depths of the beam under the load points and over the center support were 525 mm, as shown in Fig. 3.2. The clear shear span to effective depth ratio, x/d, was 1.43.

The loading and supporting columns were reinforced with 15M vertical bars. Six 600 mm long bars were used in each of the loading columns. These bars terminated 300 mm above the bottom face of the beam. Each end supporting column was reinforced with four bars. Their lengths were 900 mm, extending the full height of the beam to provide support for the top reinforcement. In the center supporting column, eight 600 mm long bars were used. These bars terminated

230 mm below the top face of the beam. Ties spaced at 130 mm apart were formed from 6 mm plain round bars.

The four specimens were designed to differ from each other only by the type of web reinforcement present. Six mm diameter deformed bars were used as web reinforcement. Beam No. 1 had no web reinforcement. Beam No. 2 had closed vertical stirrups only. Beam No. 3 had single-legged horizontal stirrups placed alternately on the faces of the beam and no vertical stirrups. Beam No. 4 was a combination of Beam No. 2 and Beam No. 3 and therefore, had both vertical and horizontal stirrups. All beams are symmetrical about their centerlines. The arrangement of the web reinforcement in Beams No. 2, 3 and 4 are shown in Fig. 3.3, 3.4 and 3.5 respectively.

Steel base plates were provided at the ends of the loading and supporting columns to transmit loads to the load cells. and supporting columns. The loading column base plates were 50 mm thick. Base plates at the end supporting columns were 20 mm thick and those at the center supporting column were 70 mm thick. To fit into the casting form, the sizes of these plates were milled slightly smaller than the sizes of their respective columns. The ends of the column reinforcement in contact with the base plates were tack welded to the plates to ensure load transfer to the bars by bearing.

3.3 Material Used

3.3.1 Concrete

The concrete used was made from normal Portland cement, sand and gravel. The fineness modulus of the sand was 2.75. The maximum aggregate size of the gravel was 3/8 in. (9.5 mm). For a design strength of 30 MPa at 28 days, the water-cement ratio and sand-cement ratio were 0.55 and 2.5 respectively. For each beam, three batches of concrete were mixed and placed. Three cylinders were cast for each batch giving a total of nine cylinders per beam. All the cylinders were tested in compression in a Baldwin Testing Machine. The properties of the cylinders are tabulated in Table 3.1. For an unknown reason, the compressive strength, $f'c$, of the concrete in Beam No. 2 was exceptionally low (14.5 MPa). The concrete strengths, $f'c$, ranged from 30.4 MPa to 37.2 MPa for the other beams.

3.3.2 Reinforcing Steel

The 15M and 10M reinforcing bars were ordered from a local supplier. These bars were specified to have a minimum yield strength of 400 MPa. All bars of the same size came from the same heat. The 6 mm diameter deformed bars were originally imported from Sweden. The properties of the reinforcement determined from tension tests are tabulated in Table 3.2. Since the yield strengths of the 15M and 10M bars were very close to each other, an average value of 470 MPa was used for both bar sizes. The yield strength of the 6 mm deformed bars was 500 MPa. Stress-strain diagrams for the reinforcement are shown in Fig. 3.6. The cross-sectional areas of the 6 mm, 10M and 15M bars were taken as 31.5 mm², 96.4 mm² and 191.4 mm² respectively.

3.3.3 Base Plates

Base plates had a specified minimum yield strength of 36 ksi (248 MPa). The base plates for the supporting columns were tack welded to the column steel before the reinforcing cages were fabricated.

3.4 Curing Of Specimens

A 3/4 in. (19 mm) plywood form was used to cast all the specimens. Standard cylinders moulds were used to cast the test cylinders. Forty eight hours after casting, the form was removed and the cylinder moulds stripped. All the specimens and cylinders were cured the same way. Moist burlap was wrapped around the specimen and the cylinders. A large piece of waterproof plastic sheet was then used to cover the specimens to keep the atmosphere inside the plastic cover moist. Regular wetting was needed to prevent the burlap from drying. After two weeks, the plastic cover and the burlap were removed. The specimens and the cylinders were then cured at normal room humidity until they were tested. The average period from the time of casting to the time of testing was about 150 days.

3.5 Specimen Instrumentation

Load cells, dial gages and mechanical demec gages were used for instrumenting the beams during testing.

A 600,000 lb (2670 KN) capacity load cell was used to measure the center reaction and 400,000 lb (1780 KN) capacity load cells were used at the end supporting columns and the loading columns. Loading was applied through a pair of 400,000 lb (1780 KN) capacity hydraulic jacks. These load cells could be read to the nearest 2000 lbs (9 KN).

Dial gages placed at the midspans and at the middle of the bases of the supporting columns recorded the midspan deflections and the support settlements respectively. The dial gages were graduated in 0.0001 inch (0.0025 mm).

Concrete strains were measured using a 2 inch (51 mm) mechanical demec gage. Demec points arranged in 45 degree rosettes were attached to one face of every beam. Fig. 3.7 shows the location of the rosettes on one span in a typical beam. In each specimen, three of the shear spans had only three rosettes, the fourth had eleven rosettes as shown. Measurements from the four pairs of demec points from a rosette can be used to calculate four estimates of the pair of principal strains. Assuming no crack passes through the rosette and the strain measurements were taken accurately, the four pairs of principal strains should be identical. The

2 inch gage length demec gage could be read to the nearest 0.00005 strain.

Reinforcing steel strains were measured using a 5 inch (127 mm) mechanical demec gage. Before the specimens were cast, 6 mm rods were brazed at 5 inches apart along certain rebars. Rubber hoses of about 12 mm diameter were then sleeved onto these rods. After the concrete was cast and hardened, the rubber hoses were removed. Demec points were then attached to the tip of the rods. Steel strains were measured on one span of each beam since both spans were expected to behave similarly. Fig. 3.8 to 3.11 show the location of these demec points in a Beams No. 1 to 4 respectively. The 5 inch demec gage was accurate to within 0.00002 strain.

3.6 Test Setup

A special loading frame was constructed for testing. The test setup can be seen in Fig. 3.12. Lateral braces were provided to prevent the beam from deflecting laterally during loading. The end supporting columns of the specimen were supported on rollers. Except in the case of Beam No. 1, the load cell for the center supporting column rested on a 510 x 510 x 85 mm steel plate which was plastered to a 850 x 850 x 150 mm concrete pedestal cast onto the floor. In place of the concrete pedestal, the center support of Beam No. 1 was supported on a 610 mm diameter x 130 mm thick steel plate plastered onto the floor. The concrete pedestal was constructed after observing excessively high settlement in the center supporting column due in part to the delamination of the topping from the load bed floor under this column.

3.7 Testing Procedures

Loading for all beams was applied in increments of 30 KN until 300 KN. After 300 KN, the load increments continued at 30 KN for Beams No. 1 and 2 but were reduced to 25 KN for Beams No. 3 and 4. The readings from the load cells and dial gages were recorded at every 30 KN until failure for Beams No. 1 and 2. For Beams No. 3 and 4, load cells and dial gages were recorded at every 30 KN until 300 KN after which readings were taken every 25 KN until failure. Due to the vast amount of reading required for concrete and steel strains, strain readings were taken at every other load step. At loads near failure, the load in the north jack was continuously monitored to observe the load at which failure occurred.

Since the strain readings were highly time consuming, the failure load could not be reached in a single day. Unloading of the specimen was necessary at the end of the day to prevent the specimen from creeping under load. The midspan deflection was recorded regularly during the unloading stage. Upon reloading, load cell and dial gage readings were taken at 60 KN intervals starting from zero load as a check on the previous behaviour of the specimen. All readings continued in the manner described above for loads greater than the highest load reached the previous day.

Cracking of the specimen were recorded using photographs taken at regular intervals.

After failure of one span of a beam, the failed span was clamped together with external stirrups as shown in Fig. 3.13. The beam was retested in the same manner as when it was first tested except that strain readings on the steel and concrete were not taken.

Table 3.1 Compressive Strength of Test Cylinders, in MPa

Beam	Batch 1			Batch 2			Batch 3			Average
No.	cyl.1	cyl.2	cyl.3	cyl.1	cyl.2	cyl.3	cyl.1	cyl.2	cyl.3	*f*'c (MPa)
1	29.2	29.7	28.2	30.4	31.1	28.0	32.2	31.5	33.2	30.4
2	15.1	15.1	14.7	14.5	15.6	14.3	13.0	13.6	14.8	14.5
3	33.7	33.2	33.7	33.2	30.2	33.4	32.3	31.3	31.8	32.5
4	35.6	35.6	35.1	38.7	40.0	36.7	38.2	37.8	37.3	37.2

Table 3.2 Properties of Reinforcing Bars

Bar type	Nominal bar diameter(mm)	Area* (mm^2)	fy (MPa)	fu (MPa)	ϵu (%)
15M	16.0	191.4	469.2	786.2	9.3
10M	11.3	96.4	472.1	747.0	10.0
6mm	6.0	31.5	500.0	702.0	13.4

* : based on weight, length and density

fu = ultimate stress

ϵu = ultimate strain

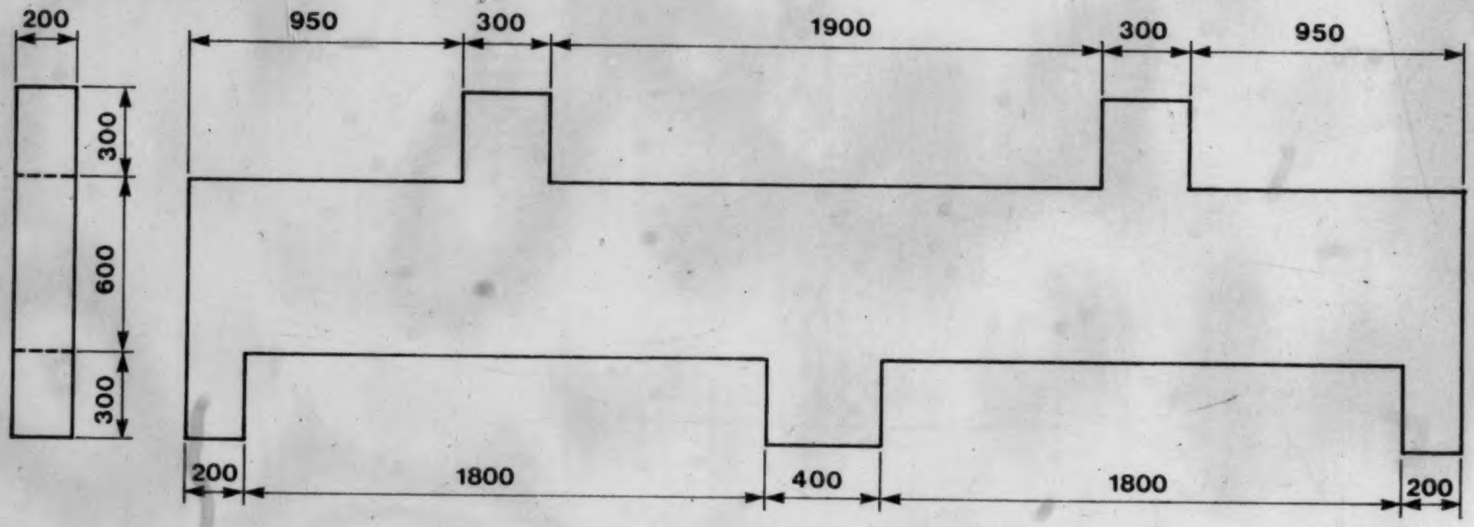
200
300
600
300
950
300
1900
300
950
200
1800
400
1800
200

All dimensions in mm

Figure 3.1 External Dimensions of Deep Beams

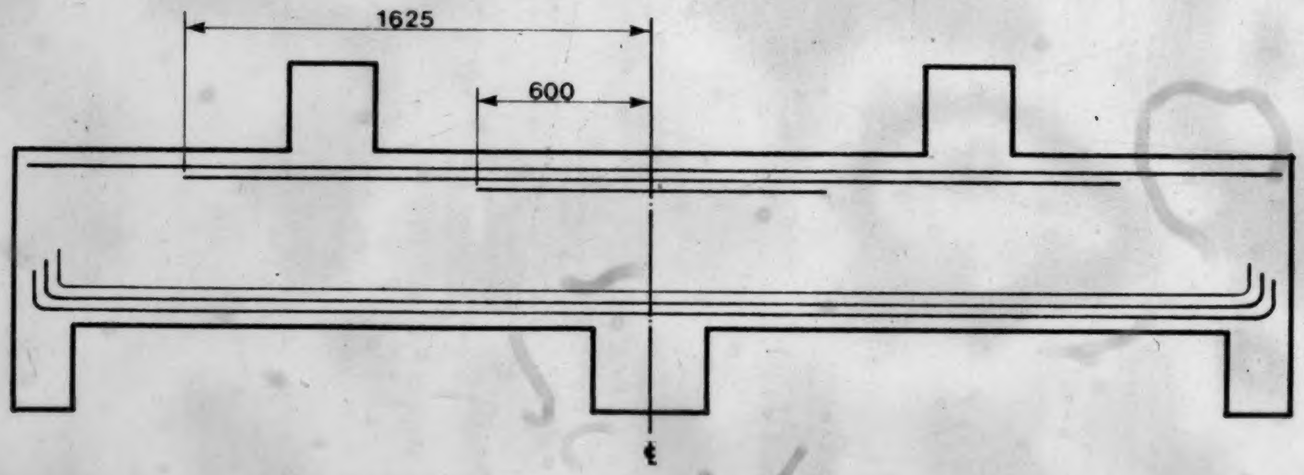

(a) ARRANGEMENT OF FLEXURAL REINFORCEMENT

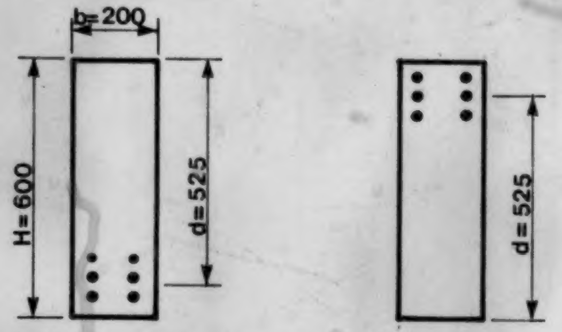
b=200
H=600
d=525
d=525

All dimensions in mm

AT POSITIVE MOMENT REGIONS AT NEGATIVE MOMENT REGIONS

(b) CROSS SECTION DIMENSIONS OF TEST SPECIMENS

Figure 3.2 Flexural Reinforcement Used in Deep Beams

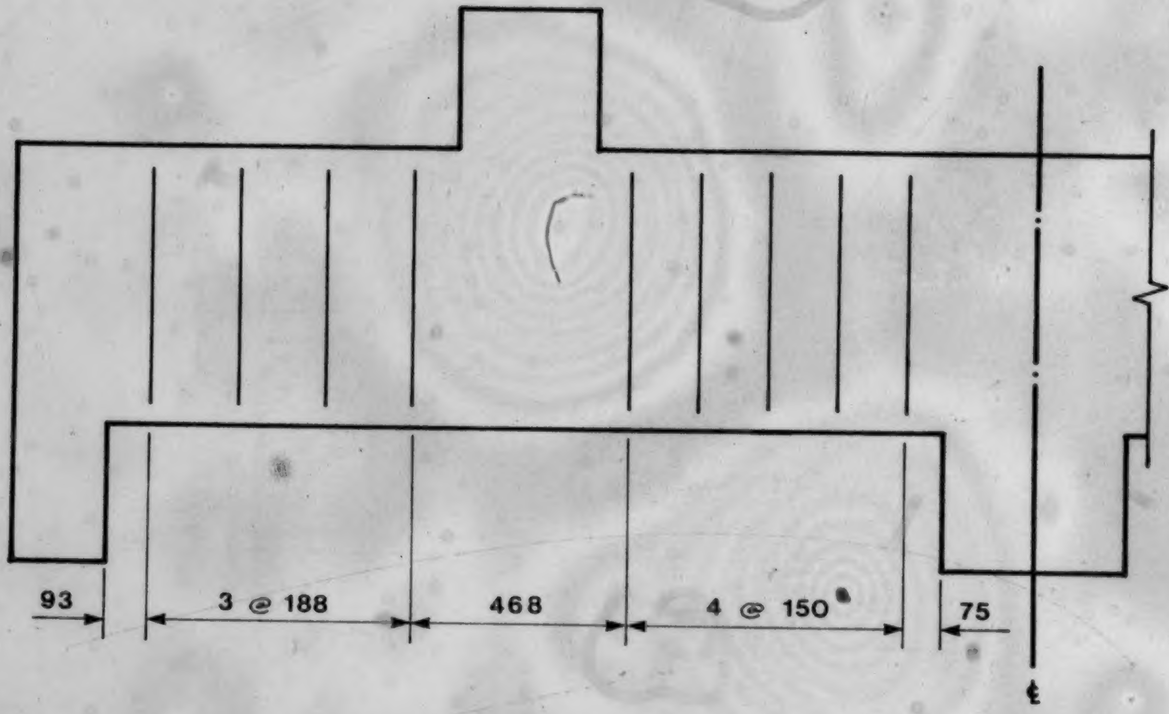
93
3 @ 188
468
4 @ 150
75
℄

All dimensions in mm

Figure 3.3 Arrangement of Web Reinforcement in Beam No. 2

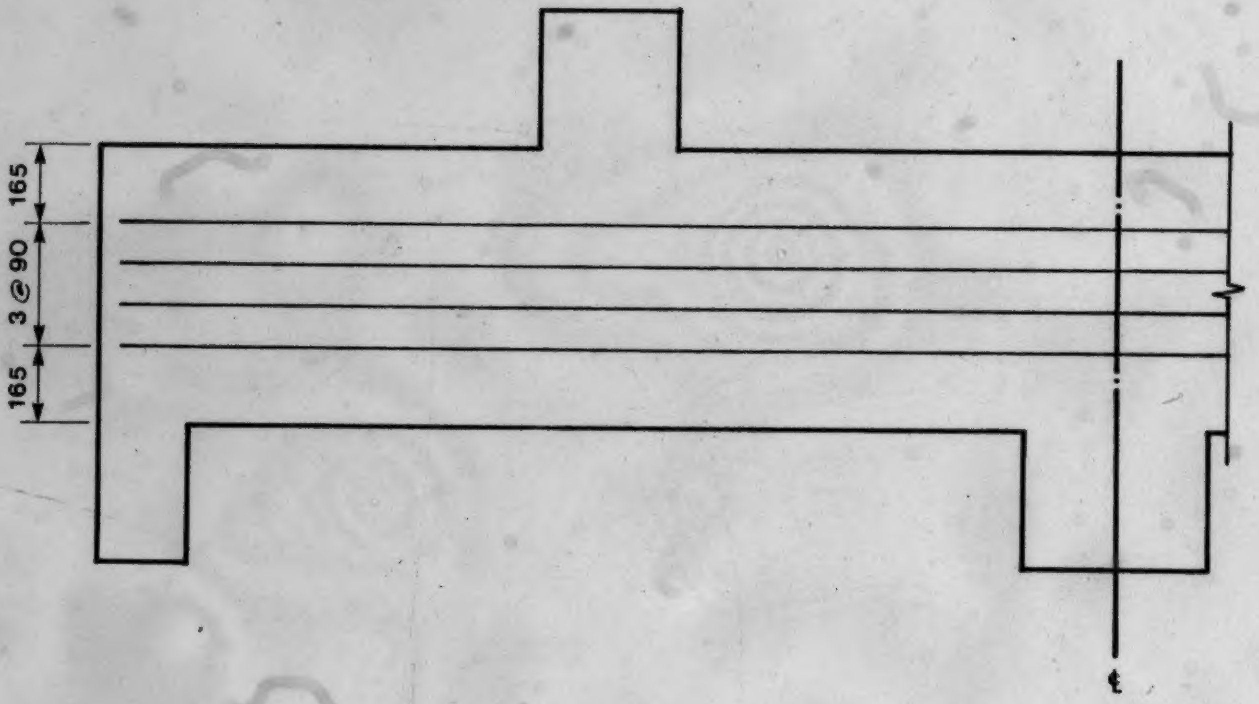

All dimensions in mm

Figure 3.4 Arrangement of Web Reinforcement in Beam No. 3

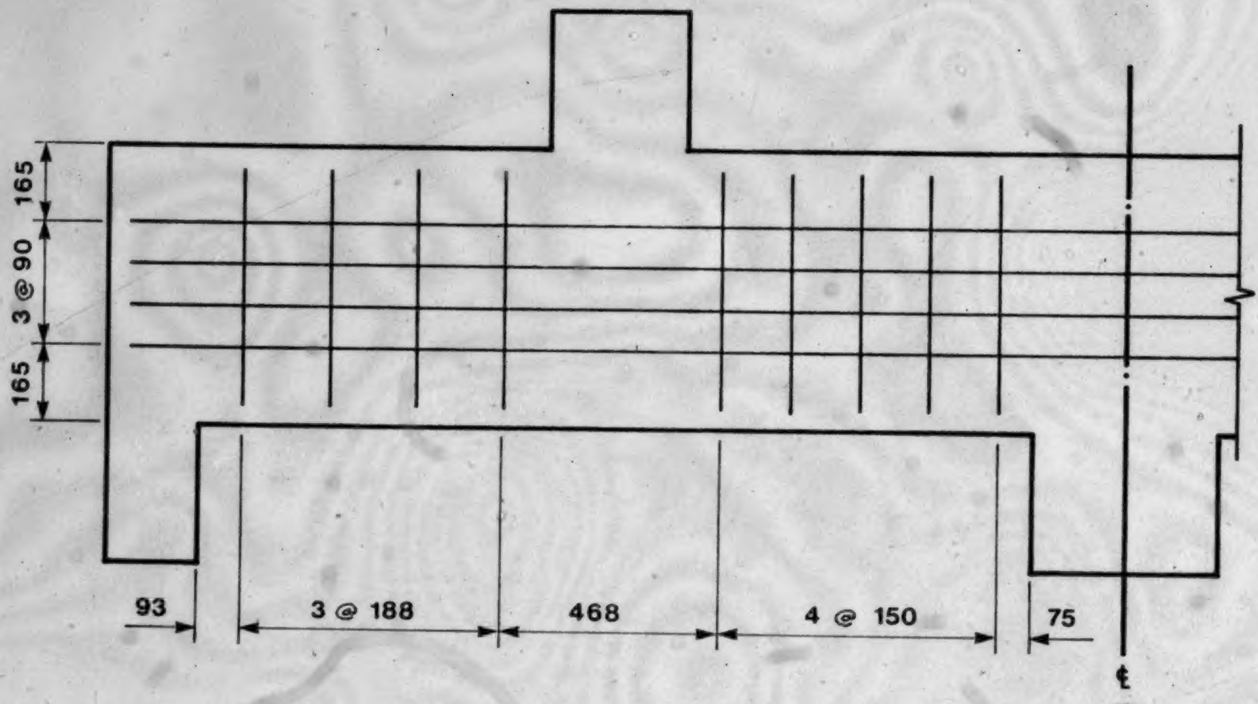
165
3 @ 90
165
93
3 @ 188
468
4 @ 150
75
℄

All dimensions in mm

Figure 3.5 Arrangement of Web Reinforcement in Beam No. 4

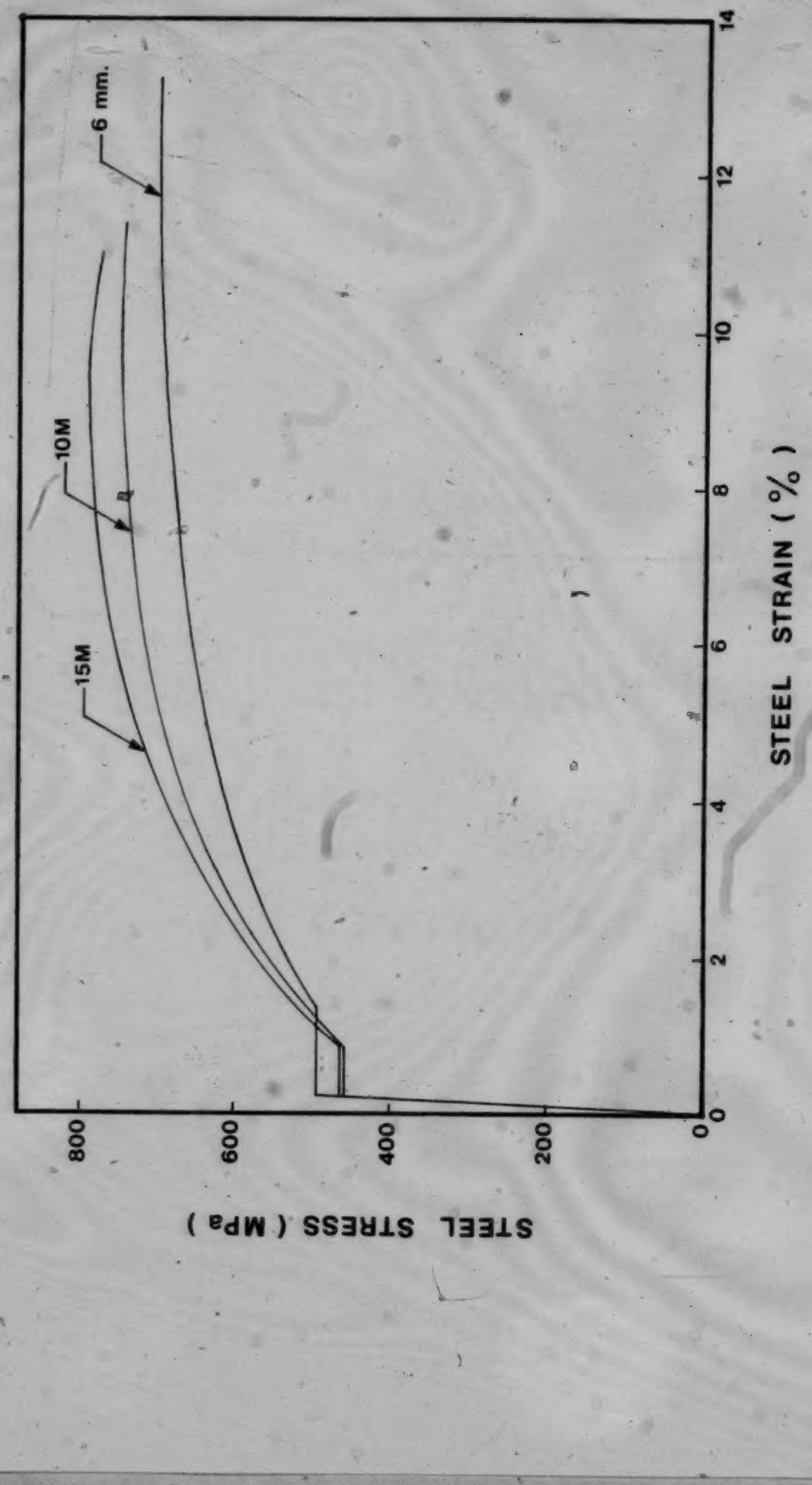

Figure 3.6 Stress-Strain Plot of Reinforcing Steel

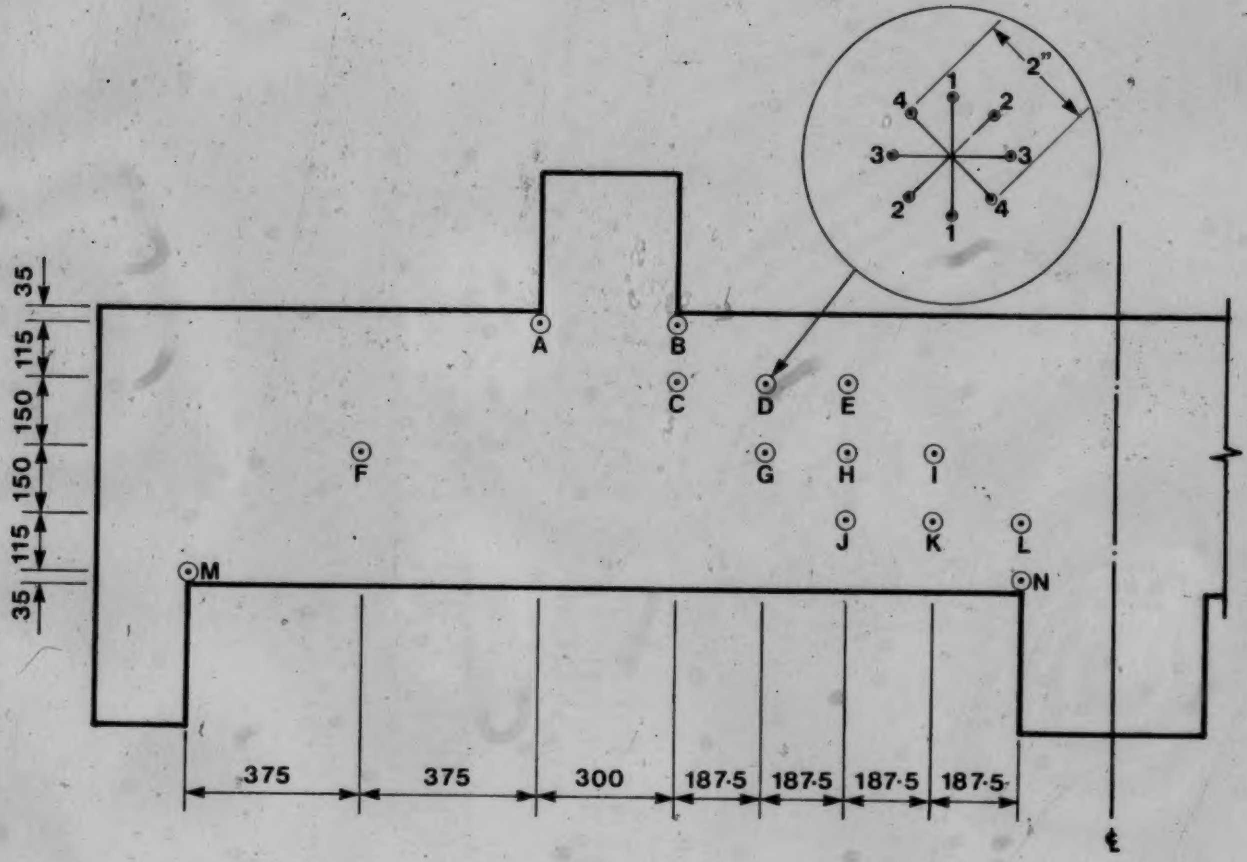
35
115
150
150
115
35
A
B
C
D
E
F
G
H
I
J
K
L
M
N
1
2
3
4
2"
375
375
300
187·5
187·5
187·5
187·5
℄

All dimensions in mm

Figure 3.7 Location of Instrumentation of Concrete Strains in a Typical Beam

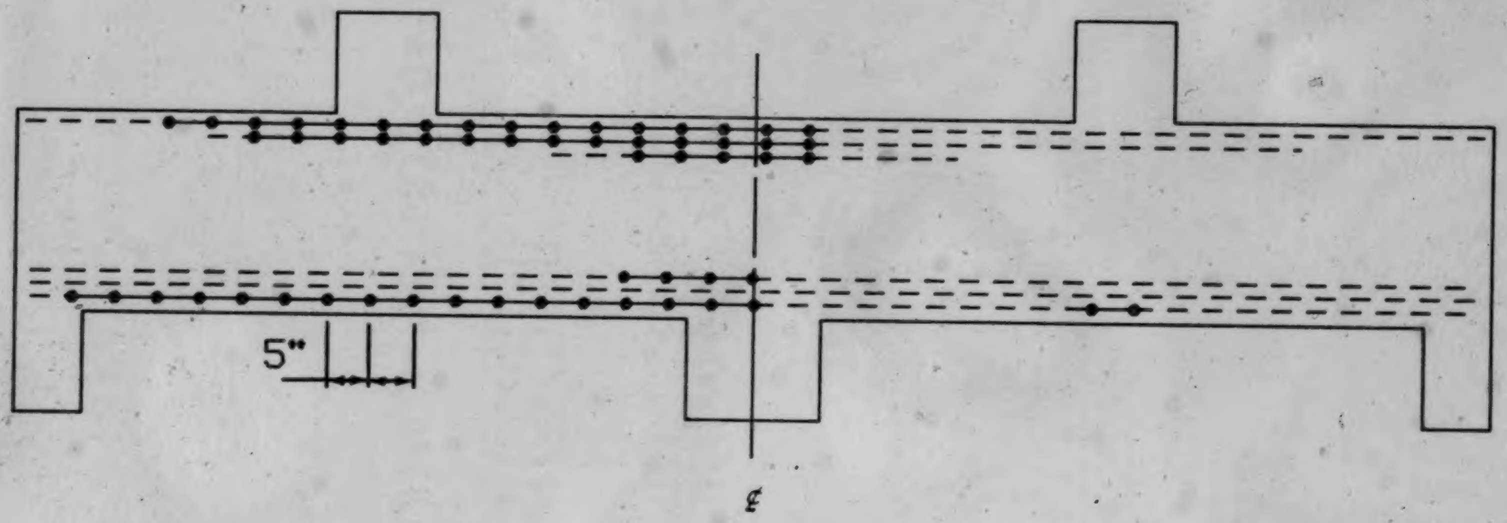

Figure 3.8 Location of Instrumentation of Steel Strains in Beam No. 1

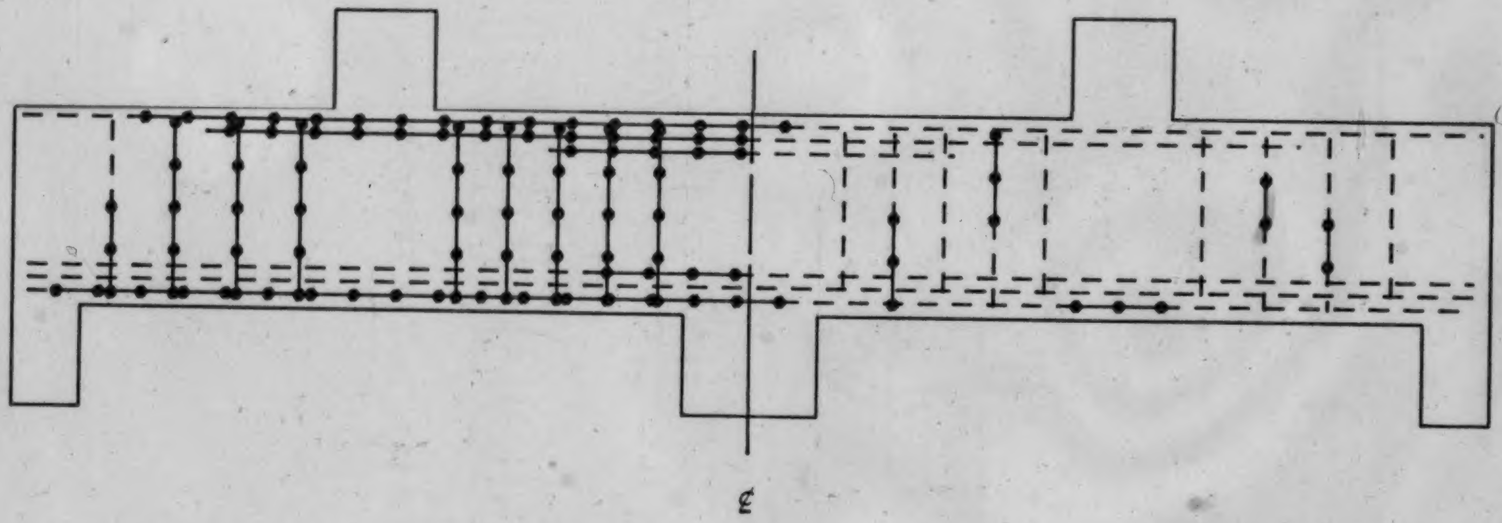

Figure 3.9 Location of Instrumentation of Steel Strains in Beam No. 2

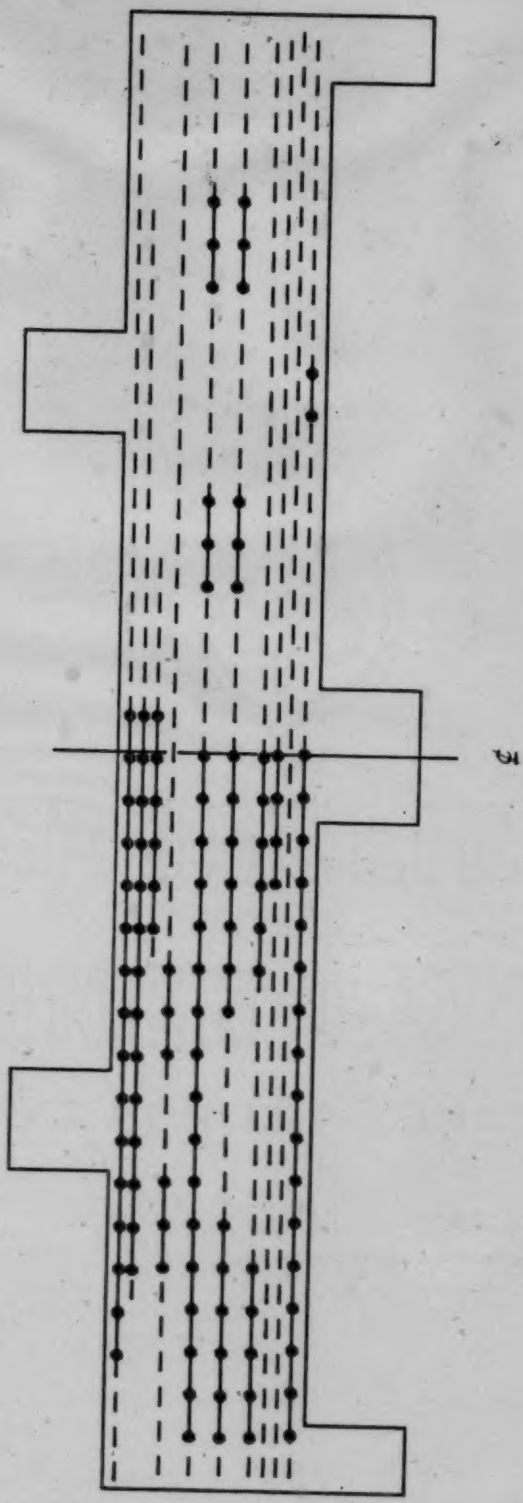

Figure 3.10 Location of Instrumentation of Steel Strains in Beam No. 3

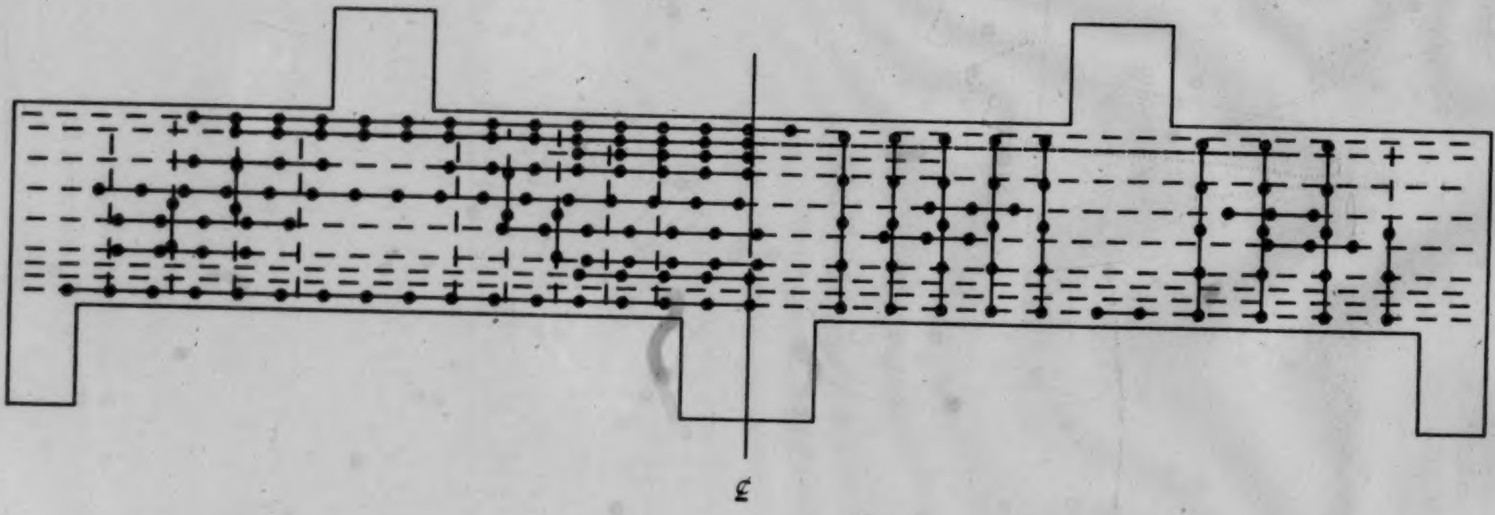

Figure 3.11 Location of Instrumentation of Steel Strains in Beam No. 4

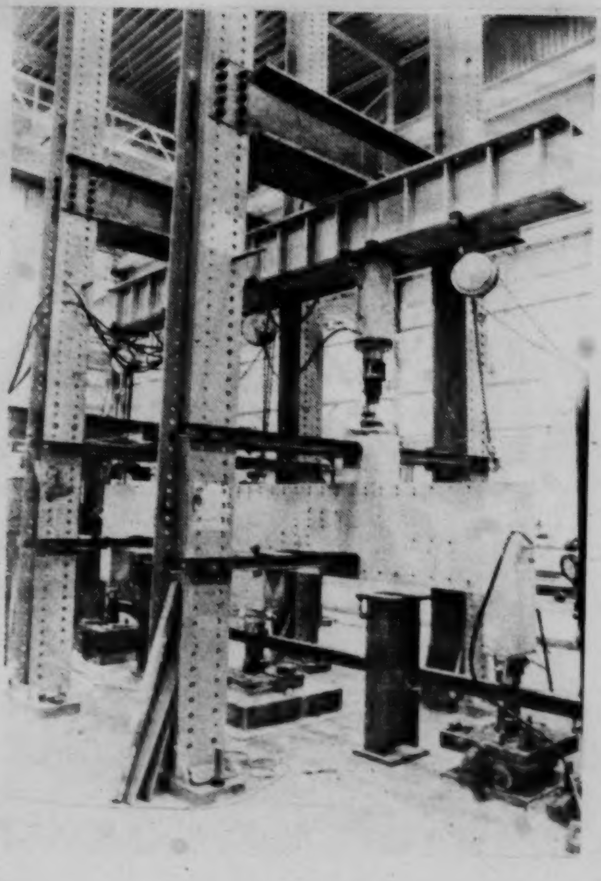

Figure 3.12 Test Setup

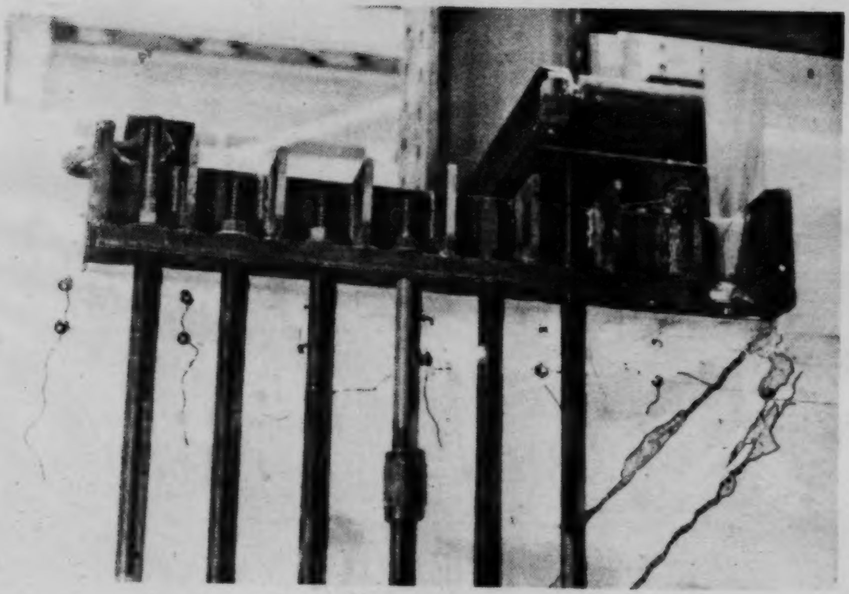

Figure 3.13 External Stirrups Used in Retest

4. BEHAVIOUR OF BEAMS IN TESTS

4.1 Load-Deflection Behaviour

4.1.1 Load and Midspan Deflection Relationship

The jack load versus midspan deflection relationships for Beam No. 1 are shown in Figs. 4.1 and 4.2. Beam No. 1 was chosen because its load-deflection curves represent typical load-deflection characteristics of the beams tested. The relationships between jack load and midspan deflection of Beams No. 2, 3, and 4 are shown in Figs. A.1 to A.6 in Appendix A. The jack load referred to here represents the average of the north and the south jack loads. The midspan deflections referred to here have been corrected by substracting the support settlements from the total measured deflections (see section 4.1.2).

In Fig. 4.1, two major stages in behaviour were observed. The load-deflection behaviour was approximately linear until point A. After point A, the rate of deflection increased as shown by the decrease in the slope of the curve. This type of behaviour was similar in both the north and the south spans of Beam No. 1, as observed in Figs. 4.1 and 4.2.

The jack loads corresponding to point A in Figs. 4.1 and 4.2 are slightly lower than the first inclined cracking load, P_{cr}, of Beam No. 1. The jack load corresponding to point A is about 210 KN at both the north and the south spans. The flexural cracking load, *Pf*, of the positive moment spans in Beam No. 1 was 116 KN. The first inclined cracking load of Beam No. 1 occurred in the north interior and the south exterior shear spans at an average jack load of 239 KN. Inclined cracking reduced the stiffness of the beam rendering it more susceptible to high deflection. The crack separation after inclined cracking also contributed to the midspan deflection. Flexural cracking did not seem to reduce the stiffness of Beam No. 1. Behaviour after first inclined cracking was approximately linear. This beam failed in the south interior shear span at a jack load of 362 KN. The midspan deflection at the failure load was not measured. The cracking and ultimate loads for all the beams are tabulated in Table 4.1. The flexural and first inclined cracking loads referred to here represent the average of the north and south jack loads while the ultimate load represents only the north jack load. Ultimate loads will be discussed in section 4.7.

The load-midspan deflection behaviour of Beams No. 3 and 4, shown in Figs. A.3 to A.6, is similar to that shown for Beam No. 1. Jack load corresponding to point A in Figs. A.3 and A.4 is about 209 KN and the first inclined cracking load of Beam No. 3 was 239 KN. The flexural cracking load of the positive moment spans in Beam No. 3 was 150 KN. Flexural cracking appeared to reduce the stiffness of Beam No. 3 slightly. This beam had horizontal stirrups.

In Beam No. 4, the first inclined cracking load was 266 KN and the jack load corresponding to point A in Figs. A.5 and A.6 is about 208 KN. The increase in the rate of deflection after point A can be explained by the reduction in stiffness of Beam No. 4 due to the extension of major flexural cracks. The flexural cracking load of the positive moment spans in Beam No. 4 was 158 KN. Flexural cracking also reduced the stiffness of Beam No. 4 slightly. This beam had horizontal and vertical stirrups. The load-deflection curves for Beam No. 2, shown in Figs. A.1 and A.2, showed a change in slope after a load of 90 KN which corresponds to the flexural cracking load of the positive moment spans. This beam had vertical stirrups. The first inclined cracking load of Beam No. 2 was 180 KN.

Beam No. 4 showed the lowest deflection and Beam No. 2 showed the highest deflection for equal applied jack load. Comparing Beams No. 1, 3 and 4, Beam No. 1 had the highest deflection at a specific jack load. This shows that the presence of web reinforcement had the effect of reducing the midspan deflection. Vertical and horizontal web reinforcements appeared to be more effective than horizontal web reinforcement alone in deflection control. It is true that the concrete strength of Beams No. 1, 3 and 4 were different but the small difference had only minimal effect on the midspan deflection. On the other hand, the concrete strength of Beam No. 2 was less than half that of Beam No. 1. This large difference in concrete strength offset the effect of vertical web reinforcement in Beam No. 2 and resulted in the high midspan deflection.

4.1.2 Load and Support Settlement Relationships

The relationships between jack load and support settlement of Beam No. 1 are shown in Fig. 4.3. The values plotted are of the interior support settlement and the average of the end supports settlements. Jack load versus support settlement of the other beams are shown in Figs. B.1 to B.3 in Appendix B.

Differential settlement was experienced by all the beams. The settlement at the interior support was always higher than the settlements at the end supports. Therefore, it would be expected that the negative moment over the interior support be reduced, as shall be discussed in a later section. Beam No. 1 was tested before the concrete pedestal (see section 3.6) was placed. Comparing the interior support settlement of Beam No. 1 with that of Beams No. 3 and 4 indicate that the placement of the concrete pedestal under the interior support helped to reduce the interior support settlement considerably. The high settlement at the interior support in the case of Beam No. 2 was caused by improper seating of the interior supporting column load cell. The main cause of differential settlement between the interior and the end supports was the shortening of the interior supporting column load cell. During the tests, that load cell experienced very high loads.

The ratio of the maximum differential settlement to the center to center span length, $\Delta max/L$, ranged from about 1/1875 for Beam No. 2 to about 1/13100 for Beam No. 4.

4.2 Development of Cracking

When the beams were first loaded, flexural cracks appeared near the maximum positive and maximum negative moment regions. Flexural cracks in the positive moment region propagated from the bottom face towards and beyond the mid-depth of the beam. These cracks tended to develop along lines joining the loading column to the bottom face of the beam. The loads corresponding to these cracks in Beams No. 1 to 4 are tabulated in Table 4.1. In the negative moment region, the cracks propagated downwards from the top face of the beam along lines joining the interior support to the top face. These cracks occurred after the positive moment flexural cracks, not before as would be expected from elastic theory. This can be explained by the shift in the moment diagram due to settlement of the interior support discussed later in this section. The flexural cracking loads of the negative moment span of Beams No. 1 to 4 are shown in Table 4.1. The flexural cracks propagated rapidly but after the formation of the first inclined cracks, the propagation slowed to a much reduced rate.

Formation of the first inclined cracks was sudden. Figs. 4.4 to 4.7 show the crack patterns of Beams No. 1 to 4 respectively at first inclined cracking. The inclined cracks are shown with heavier lines in these figures. In all the beams, the inclined cracks were contained within the shear span. The inclined cracks did not initiate from the bottom face or top face of the beam but from a region near mid-depth. The inclined cracks, shown in Figs. 4.4 to 4.7, are not fully developed inclined cracks. A fully developed inclined crack is defined as an inclined crack which has propagated towards the load point or the support and has intersected the flexural reinforcing steel.

Tables 4.2 to 4.5 show the jack loads and the support reactions of Beams No. 1 to 4 respectively from the onset of loading to the load just prior to failure. $P1$ and $P2$ are the north and south jack loads respectively, as shown in Figs. 4.4 to 4.7. $R1$, $R2$ and $R3$ are the north end support, interior support and south end support reactions respectively. $A*$ is a coefficient equal to the ratio of the interior support reaction to the sum of the jack loads, $R2/(P1 + P2)$. The shear in the north interior shear span, $V[N]$, is shown in column 8 of Tables 4.1 to 4.4 and is computed from $(P1 - R1)$. Similarly, the shear in the south interior span, $V[N]$, shown in column 9, is computed from $(P2 - R3)$.

In Beam No. 1, first inclined cracking occurred just before Load Step 8 with an average jack load of 239 KN. The cracks started in the north interior and the south exterior shear spans (Fig. 4.4). With further loads, at Load Step 10 with an average jack load of 299 KN, more inclined cracks appeared in all the spans except the south interior shear span. The cracks which had formed previously had propagated towards the bottom face of the beam and intersected the positive moment flexural reinforcing steel. At Load Step 11, with an average jack load of 330 KN, inclined cracking occurred in the south interior shear span. This crack was accompanied by a loud cracking noise.

In Beam No. 2, first inclined cracking occurred just before Load Step 6 with an average jack load of 180 KN. Inclined cracks appeared in the north exterior and the south interior shear spans (Fig. 4.5). Both cracks were initiated by flexural cracks. Under the same jack load, short horizontal cracks appeared at the level of the negative moment flexural reinforcement in the north interior shear span. These secondary cracks propagated horizontally as the loads were increased. At Load Step 8 with an average jack load of 240 KN, inclined cracking had occurred in every span. The secondary cracks appeared to be part of a dowel or a splitting crack.

In Beam. No. 3, first inclined cracking occurred just before Load Step 8 with an average jack load of 239 KN. Inclined cracks first appeared in the north interior and the south interior shear spans (Fig. 4.6). As more loads were applied, the crack in the north interior shear span propagated towards the corners at the faces of the loading and supporting columns. The crack in the south interior span had propagated to the bottom face of the beam. At Load Step 10 with an average jack load of 299 KN, inclined cracking initiated by flexural cracks occurred in the north and the south exterior spans.

In Beam No. 4, a single inclined crack occurred in the north interior shear span just prior to Load Step 9 with an average jack load of 266 KN (Fig. 4.7). Additional inclined cracks developed in the north exterior, south interior and south exterior shear spans at average jack loads of 396, 320 and 369 KN, respectively. By Load Step 14 with an average jack load of 396 KN, all the spans showed extensive inclined cracking.

With the exception of the crack formed in the north interior shear span of Beam No. 3, the first inclined cracks did not follow the thrust lines joining the load points to the supports. As it turned out, the initial inclined cracks were not critical cracks except for the crack in the north interior shear span of Beam No. 3. A critical crack is defined as a crack which has a direct bearing on the failure of the beam (Kong and Singh, 1972). Inclined cracks that formed after the first inclined cracks followed the thrust lines joining the load points to the supports. These tended to be critical cracks.

Figs. 4.8 to 4.11 show the actual shearing force and bending moment diagrams of Beams No. 1 to 4 at first inclined cracking load. These diagrams were constructed from values taken from Tables 4.2 to 4.5 at the load step corresponding to first inclined cracking. For comparision, shearing force and bending moment diagrams based on an elastic beam theory are shown below the actual diagrams. The elastic shearing force and bending moment diagrams were constructed using a jack load equal to the average of the actual north and south jack loads at first inclined cracking.

From Figs. 4.8, 4.10 and 4.11, the actual shearing force and bending moment diagrams of Beams No. 1, 3 and 4 respectively agree very closely to the elastic shearing force and bending moment diagrams. According to the elastic beam theory, the value of $A*$ is a constant and is equal to 0.66. Comparing this value with the values of $A*$ given in column 7 of Tables 4.1, 4.3 and 4.4 at first inclined cracking load, $A*$ given in Tables 4.1, 4.3 and 4.4 has a value of 0.65. This agrees very well with the elastic value of $A*$. In the case of Beam No. 2, there is considerable difference between the actual and the elastic diagrams, as shown in Fig. 4.9. The actual shearing force ranged from 93% to 114% of the elastic shearing force. In the bending moment diagrams, the actual negative moment was only 76% of the elastic negative moment. The value of $A*$ of Beam No. 2 at first inclined cracking load is only 0.62 compared to the elastic value of 0.66.

In Figs. 4.3, B.2 and B.3, the differential settlement of Beams No. 1, 3 and 4 at first inclined cracking load were 0.44 mm, 0.23 mm and 0.08 mm respectively. These values were compared to the differential settlement of Beam No. 2 at first inclined cracking load which was 0.76 mm (Fig. B.1). The high settlement of the interior support of Beam No. 2 with respect to the end supports reduced the rotation of the part of the beam above the interior support, thereby reducing its negative moment.

In the usual case, the behaviour of the beam after the formation of inclined cracks would be expected to be different from the elastic behaviour before inclined cracking. In the case of Beams No. 1, 3 and 4, shortly after first inclined cracking, the beams still displayed the elastic force distribution. This is probably because the first inclined cracks formed were not fully developed inclined cracks. The deformations due to these non-fully developed inclined cracks were insufficient to cause a change in behaviour of the beams. At loads much higher than the first inclined cracking load, elastic behaviour ceased and the beams followed a tied arch behaviour (see section 4.4). The ratio of the interior support reaction to the sum of the jack loads decreased slightly at high loads.

4.3 Modes of Failure

Figs. 4.12 to 4.15 show the crack patterns of Beams No. 1 to 4, respectively, at failure. The major cracks are marked boldly and crushing is denoted by cross-hatching.

All the beams experienced shear failure. The beams were able to sustain loads higher than the first inclined cracking loads before the final failure. All the beams, except Beam No. 3, failed in the south interior span. Beam No. 3 failed in the north interior span. A fan-like pattern of cracking was observed. The critical inclined cracks formed following the thrust lines joining the load points to the supports. These inclined cracks divided the interior span of the beams into two triangular halves. The major cause of failure was by sliding along the critical inclined cracks. This was evidenced by the difference in height of an initially straight line on the two adjacent sides of the critical crack. A closer examination of the critical inclined cracks indicated there were contacts between the aggregates in some parts of the crack and separation at others. Beam No. 1 experienced some crushing at the lower end of the critical inclined crack. There were no signs of anchorage or bearing failure in any of the beams. The horizontal crack in the north interior span of Beam No. 2 did not seem to be harmful to the beam. Only Beam No. 1 failed with an explosive noise. Other beams failed slowly and some spalling of the concrete was observed.

The actual shearing force and bending moment diagrams of Beams No. 1 to 4 are shown in Figs. 4.16 to 4.19, respectively, for the last load step prior to failure. For comparision, the elastic shearing force and bending moment diagrams are shown below the actual diagrams. The elastic diagrams were constructed using a jack load equalled to the average of the north and the south jack loads prior to failure.

All the beams showed some deviation from the elastic values. The actual shear was consistently higher than the elastic shear in the exterior shear spans. Likewise, the actual positive bending moment was also always higher than the elastic positive bending moment. This value ranged from 107%, in Beam No. 3, to 116%, in Beam No. 2, of the elastic value. On the other hand, the actual shear in the interior shear span was always lower than the elastic shear. This value ranged from 93%, in Beam No. 2, to 97%, in Beam No. 3, of the elastic shear in the interior span. The actual negative moment was also lower than the elastic negative moment. This value ranged from 73%, in Beam No. 2, to 89%, in Beam No. 3, of the elastic negative moment.

Beam No. 2 showed the greatest deviation from the elastic values and Beam No. 3 showed the least. This can be expected of Beam No. 2 since it had already deviated considerably from the elastic values at the first inclined cracking load. From the results obtained, it would be inaccurate to predict the shearing force and bending moment of the test specimens at loads near the failure load using the elastic beam theory. The deviation of the actual shearing force and bending moment diagrams from the elastic shearing force and bending moment diagrams indicated that the behaviour of the beams was inelastic at loads near the failure load.

4.4 Steel and Concrete Strains

4.4.1 Strains in Flexural Reinforcement

Typical examples of steel strains in flexural reinforcement are shown in Figs. 4.20 and 4.21. Fig. 4.20 shows the distribution of steel strains in the uppermost layer of the negative moment flexural reinforcement in Beam No. 4 before and just after first inclined cracking and prior to failure. Fig. 4.21 shows the distribution of steel strains in the lowermost layer of the positive moment flexural reinforcement in Beam No. 4 at loads before and just after first inclined cracking and prior to failure. Steel strains at failure load were not available and had to be extrapolated from plots of jack load versus steel strains.

Before the formation of cracks, the flexural steel strains were small. After flexural cracking occurred, the steel strain distribution along the beam was consistent with the elastic bending moment. The point of contraflexure in the elastic bending moment diagram (Fig. 4.11(b)) is 585 mm from the centerline of the beam. In Beam No. 4, the points of zero strain in the negative and positive moment reinforcement were about 660 mm and 440 mm, respectively, from the centerline at the load step just before first inclined cracking (Load Step 8). Thus, there was tension in both layers of steel at the elastic point of contraflexure. Steel strains in the anchorage region of the positive moment reinforcement showed a near zero strain (Fig. 4.21). This is consistent with the elastic beam theory.

After the formation of the first inclined cracks (Load Step 10), the steel strain distribution differed slightly from the distribution before first inclined cracking. Although the previous literature suggests that a remarkable difference in the steel strain distribution should occur, the inclined cracks at Load Step 10 had not greatly affected the strains in the flexural reinforcement at Load Step 10. The magnitude of the strains were higher. The point of zero strain in the negative moment reinforcement had moved closer to the loading column and the point of zero strain in the positive moment reinforcement had moved towards the interior support. Steel strains in the anchorage region of the negative moment reinforcement remained unchanged but those of the positive moment reinforcement increased. This shows that the steel in the anchorage region experienced tensile stress and the behaviour is indicative of a tied arch behaviour.

At loads prior to failure (Load Step 16), the steel strains showed a significantly different distribution than at previous load steps. The inclined cracks had become fully developed inclined cracks. Marked changes in the steel strains were recorded indicating that arching action had developed. At regions experiencing flexural cracks and when these cracks widened, peak steel strains were registered at wide flexural cracks. The point of zero strain in the negative moment reinforcement moved away from the centerline of the beam, almost to the inner face of the loading column. The point of zero strain in the positive moment reinforcement also moved towards the centerline of the beam and had passed the inner face of the interior support. If the trend continued for the positive moment reinforcement, a point of zero strain would not exist in the bottom flexural reinforcement at the failure load. The entire length would be in tension and bars should not be cut off at the elastic point of contraflexure. Steel strains in the anchorage region of the positive moment reinforcement were much higher than in the previous load steps. At this rate of increase, the steel strains near the end support would be of the same order of magnitude as the strains in the midspan at the failure load.

In the beams tested, the average strain in the positive moment reinforcement was always higher than the average strain in the negative moment reinforcement. This was caused by differential settlement of the interior support. When extrapolated to the failure load, the flexural reinforcement in all the beams was generally found to be elastic. The strain in the flexural reinforcement at yielding was computed to be 2350 x 10^{-6} mm/mm.

4.4.2 Strains in Vertical Web Reinforcement

Fig. 4.22 shows a typical jack load versus steel strain plot of a vertical stirrup crossing a critical inclined crack. The jack load referred here represents the average of the north and the south jack loads. The stirrup for which the plot in Fig. 4.22 represents was located near the middle of the south interior span of Beam No. 2. For vertical stirrups that did not cross a critical inclined crack, the behaviour of the stirrups was essentially the same, although the strains in these stirrups were somewhat lower.

Two stages of behaviour can be observed in Fig. 4.22. Before the jack load of 180 KN, the vertical stirrup experienced very little or no deformation. After 180 KN, the stirrup suddenly deformed at a rapid rate. Deformation continued beyond the strain at yielding, computed to be 2500 x 10^{-6} mm/mm. The jack load of 180 KN corresponds to the first inclined cracking load, *P*cr, of Beam No. 2.

Fig. 4.23 shows the steel strain distribution of vertical stirrups crossing major inclined cracks in Beam No. 2. Before first inclined cracking, most of the stirrups experienced small compressive strains. At first inclined cracking, strains in the stirrups increased and the stirrups were in tension. At the last load step prior to failure, at regions where the inclined cracks widened, peak steel strains were recorded. One of the stirrups had yielded.

The plots of jack load versus steel strain of the vertical stirrups which crossed critical inclined cracks, when extrapolated to the failure load, indicated that the strains in the stirrups near the middle of the shear span exceeded the strain at yielding and strains in the stirrups at the ends of the shear span were slightly below the strain at yielding. This suggests that the critical inclined crack was widest at the middle of the shear span. Higher steel strain in the stirrups at the middle of the shear span, shown in Fig. 4.23, supports this view. As a consequence, interface shear transfer is expected to diminish at that region. As a result, high shearing stresses would be expected at the ends of the shear span.

4.4.3 Strains in Horizontal Web Reinforcement

Fig. 4.24 shows the strain distribution along the second horizontal stirrup from the top face of Beam No. 3 at loads before, at and after first inclined cracking. This distribution is typical of the horizontal stirrups found in Beams No. 3 and 4.

Before first inclined cracking (Load Step 6), strains in the horizontal stirrup were very small. The strain distribution was essentially flat at near zero strain except at regions where flexural cracks have propagated and intersected the stirrup. The highest strain recorded was about 230 x 10^{-6} mm/mm.

At the formation of first inclined cracking (Load Step 8), there were sharp increases in the steel strain at locations where the inclined cracks crossed the horizontal stirrup. This occurred in the interior span, as shown in Fig. 4.24 (see also Fig. 4.6). The steel strains in the exterior span did not differ much from the strains in the previous load step. The maximum steel strain recorded was below the yield point strain.

At the last load step prior to failure (Load Step 11), there were further increases in the steel strains at locations where the cracks crossed the stirrup. The peak value of the strain recorded exceeded the yield point strain. The strain distribution did not seem to follow a specific pattern.

After extrapolating to failure load from plots of jack load versus steel strain of other horizontal stirrups the strains in the stirrups at the interior shear span were above the yield strain where the stirrup crossed critical inclined cracks. The strains in the upper level stirrups were somewhat lower than the strains in the lower level stirrups. The same is true for stirrups in the exterior span except that the magnitudes of the strain were below the yield strain. It should be noted that the location where the critical inclined crack crossed the horizontal stirrups were in the middle part of the shear span.

4.4.4 Strains in Concrete

The results obtained from the principal strains in the concrete were less conclusive. There were very wide variations in the results and in some cases, cracks passed through the strain measuring rosettes. Principal strains could not be computed for such rosettes. Nevertheless, for those rosettes where principal strains could be computed, several observations were made. Before first inclined cracking, strains in the concrete were very small. Principal strain diagrams showed that the direction of the principal compressive strains was along the line joining the load point to the support. Following inclined cracking, there was no noticeable difference in the pattern of the principal strain diagrams except the principal compressive and tensile strains were higher. At loads prior to failure, the principal compressive strains in the interior and the exterior spans at the regions near the faces of the loading and supporting columns were very high; as high as 0.002 mm/mm in the failing span. This magnitude of strain is sufficient to cause crushing, as occurred in Beam No. 1. In the middle of the interior shear span, at mid-depth, rosettes indicated compressive strains in both principal directions. The magnitude of the compressive strain whose direction was roughly perpendicular to the crack was small. No tensile strain existed at that region. Generally, the direction of the principal compressive strains showed a widening of the compressive strut at the middle of the shear span. This resulted in the principal compressive strain at the middle of the shear span being relatively smaller than at the ends of the shear span. The direction of the principal tensile strains were approximately perpendicular to the inclined cracks.

4.5 Retest Results

Following the initial failure, the failed shear spans was clamped together with the device shown in Fig. 3.13 and the beam was again tested to failure. Only loads, deflections and crack extensions were recorded in the retest.

4.5.1 Load and Midspan Deflection Relationships

Jack load versus midspan deflection relationships from the retest results are shown in Figs. C.1 to C.8 in Appendix C. As in section 4.1.1, the midspan deflections did not include the support settlements.

For the spans that failed during the original test, the jack load-midspan deflection plots showed essentially a straight line (Figs. C2, C4, C5 and C8). During the original test, these spans had cracked extensively. No new cracking was observed in those spans during the retest. Therefore, no sudden decrease in stiffness occurred, resulting in a constant increase in midspan deflection with jack load in the spans that did not fail during the original test. In two of the beams (Beams No. 1 and 2), new inclined cracks formed at jack load much higher than the first inclined cracking load. In Fig. C.1, a decrease in the slope of the curve can be seen corresponding to a jack load of about 420 KN. The new inclined crack formed at this load was outside and parallel to the previous inclined crack, giving Beam No. 1 a strut-like appearance. In Fig. C.3, a similar decrease in slope can be seen at a jack load of about 360 KN. No new inclined cracks were observed in Beams No. 3 and 4 during the retest.

4.5.2 Load and Support Settlement Relationships

Jack load versus support settlement relationships from retest results are shown in Figs. D.1 to D.4 in Appendix D.

As in the original test, the settlement at the interior support was always higher than the settlement at the end support. The settlement at the end support was taken to be the average of the north and the south end supports. The ratio of the maximum differential settlement to the span length, $\Delta max/L$, ranged from 1/4350 in Beam No. 1 to about 1/14280 in Beam No. 2. The concrete pedestal placed under the interior support did reduce the differential settlement.

4.5.3 Loads and Reactions

Tables E.1 to E.4 in Appendix E show the jack loads and the support reactions of Beams No. 1 to 4 respectively during the retest. The behaviour of the beams prior to failure was very much the same as in the original test. Comparision of the actual shearing force and bending moment diagrams with the elastic shearing force and bending moment diagrams showed that the actual shear in the exterior span and the positive bending moment ranged from 107%, in Beam No.4, to 114%, in Beams No. 1 and 2, of the elastic values. In the interior span, the actual shear ranged from 93%, in Beams No. 1 and 2, to 97%, in Beam No. 4, of the elastic shear. The actual negative moment ranged from 74%, in Beam No. 1, to 89%, in Beam No. 4, of the elastic negative moment.

4.6 Shear Stresses at First Inclined Cracking

The actual shear stresses in the interior spans of Beams No. 1 to 4 at first inclined cracking, vcr, are shown in column 3 in Table 4.6. The interior span was chosen because it was the span where all the critical cracks occurred. vcr was computed from values taken from Tables 4.2 to 4.6 at the load corresponding to the formation of the first inclined cracks. Since the shear in the north interior shear span, $V[N]$, was very close to that in the south interior shear span, $V[S]$, the average of the two shears, *Vcr*, was used to compute *vcr*.

$$vcr = \frac{Vcr}{b.d} \tag{4.1}$$

The shear at first inclined cracking appeared to be affected by the presence of vertical web reinforcement, the concrete strength and the somewhat random location of the initial cracks. The latter effect cannot be discussed numerically.

The presence of horizontal web reinforcement had negligible effect on the first inclined cracking shear stress. The shear stress in the interior span of Beam No. 1 was very close to the shear stress of Beam No. 3. The difference in concrete strength of both beams was small enough not to have any major effect on the shear stress.

Vertical web reinforcement appeared to increase the first inclined cracking shear stress. Beam No. 4 had both vertical and horizontal web reinforcements. Since horizontal web reinforcement was shown to be ineffective in increasing the first inclined cracking shear stress, Beam No. 4 can be considered to have just vertical stirrups. The first inclined cracking shear stress of Beam No. 4 was about 10% higher than that of Beam No. 1. Part of this increase in the shear stress at cracking of Beam No. 4 could be due to the slightly higher concrete strength but this difference is believed to have a relatively smaller effect on the shear stress compared to the effect due to vertical web reinforcement.

A large decrease in the concrete strength had a very strong influence in reducing the first inclined cracking shear stress. Beam No. 2, with a concrete strength less than half that of Beam No. 1, had a shear stress at first inclined cracking of only 71% of the corresponding shear stress in Beam No. 1. Despite the presence of vertical web reinforcement which should increase the shear stress, the big difference in concrete strength had offset its effect. It would, therefore, be appropriate to include the concrete strength as a major variable in establishing an equation to predict the first inclined cracking shear stress.

de Cossio and Siess (1960) investigated the shear strength of 49 simply supported beams and 24 frames members. Based on their results, an empirical equation was developed to predict the inclined cracking shear stress.

$$vx = 2.14\sqrt{f'c} + 4600\,\rho\,\left(\frac{V.d}{M}\right) \qquad (4.2)$$

where vx = the inclined cracking shear stress at the critical section, in psi,

d = the effective depth of the beam, in inches,

$f'c$ = the concrete strength, as determined from 6 x 12-in cylinders, in psi,

ρ = tensile steel ratio, $As/(b.d)$,

As = the area of tension reinforcement, in inches^2,
b = the width of the beam, in inches,
V = shear at the critical section where vx is computed,
M = moment at the critical section where vx is computed.

Eqn. 4.2 applies only to beams without axial load. Good corelation was obtained between the predicted results from the equation and the results of simply supported beams with concentrated loads by taking the critical section at the middle of the shear span. For uniformly loaded simply supported beams and for uniformly loaded frames in the positive moment region, the same degree of accuracy was obtained by taking the critical section at a distance of $0.15l'$ towards the midspan from the point of zero moment. l' was defined as the span length from the center to center of supports in simply supported beams and as the distance between the points of contraflexure in frames. In the case of frames failing in the negative moment region, the critical section was taken at a distance d from the face of the column. This approach, however, gave extremely conservative results.

The inclined cracking shear stress computed from Eqn. 4.2 can be used to compare with the actual inclined cracking shear stress after a few modifications. Eqn. 4.2 was developed primarily based on results from simply supported beams. For a simply supported beam with concentrated loads, the $V.d/M$ ratio, where V and M are the shear and moment at the middle of the shear span (at $0.5a$), can be replaced by an equivalent effective depth to shear span ratio, $d/(0.5a)$. Thus the second term in Eqn. 4.2 would become $9200\,\rho\,(d/a)$. In the case of a continuous beam, in the interior span, $V.d/M$ varies from a minimum for a critical section at the face of the support to infinity for a critical section at the point of contraflexure. Therefore, it would be inappropriate to use $V.d/M$ for cases involving points of contraflexure. In the exterior span of a continuous beam, $V.d/M$ can be substituted by an equivalent d/a ratio without the problem of points of contraflexure. For an interior span the slope of the compression thrust line is approximately d/a. When an equivalent d/a ratio was substituted for the $V.d/M$ ratio in Eqn. 4.2 and applied to the interior span, very good agreement was obtained between the actual and the predicted inclined shear stresses if the term $9200\,\rho\,(d/a)$ was changed to $11500\,\rho\,(d/a)$. Eqn. 4.3 was modified as shown:

$$vx = 2.14\sqrt{f'c} + 11500\,\rho\left(\frac{d}{a}\right) \qquad (4.3)$$

where a = the center to center shear span, in inches.

The computed shear stresses from Eqn. 4.3 for Beams No. 1 to 4 were converted from psi units to MPa units and are shown in column 4 of Table 4.6. Ratios of the actual to the computed cracking shear stresses are shown in column 5. Eqn. 4.2 or Eqn. 4.3 is a function of the square root of the concrete strength. The effect of the web reinforcement was not taken into account.

The actual inclined shear stresess were also compared with the shear stress equation given in section 11.3 of the ACI 318-77 (1977). The equation, shown below as Eqn. 4.4, was developed by ACI-ASCE Committee 326 (1962) and is an empirical equation to predict the flexure-shear cracking load of reinforced concrete beams without web reinforcement. It represents the lower bound for 194 beams tested.

$$v_c = 1.9\sqrt{f'c} + 2500\,\rho w\left(\frac{V.d}{M}\right) \qquad (4.4)$$

$$\leq 3.5\sqrt{f'c}$$

where v_c = shear stress carried by the concrete, in psi.

As in the case with the de Cossio and Siess equation, the $V.d/M$ ratio was substituted by an equivalent d/a ratio. For deep beams subjected to concentrated loads, the ACI specifies the critical section to be taken at $0.5x$ but not more than d from the face of the support. Therefore, instead of d/a, an equivalent effective depth to clear shear span ratio, d/x, would be more appropriate in this case. For a critical section taken at $0.5x$ from the face of the support and with $V.d/M$ substituted by an equivalent d/x ratio, Eqn. 4.4 becomes:

$$
\begin{aligned}
v_c &= 1.9\sqrt{f'_c} + 2500\,\rho_w\left(\frac{d}{0.25L_c+0.5x+0.25L_s}\right) \qquad (4.5)\\
&\le 3.5\sqrt{f'_c}
\end{aligned}
$$

where L_c = the width of the loading column,

L_s = the width of the interior support.

The factor ($0.25L_c+0.5x+0.25L_s$) is in effect equal to $0.5a$. In accordance to the ACI-ASCE Committee 426 (1977), ($0.25L_c+0.5x+0.25L_s$) should not be taken more than $(1.15/2)x$ (see section 2.4.5). ACI 318-77 limits the ratio $V.d/M$ to no more than 1.0. This was done to prevent the use of M near points of inflexion. Since in Eqn. 4.5, M was replaced, this limitation was ignored.

Results of Eqn. 4.5, converted from psi units to MPa units, are shown in column 6 of Table 4.6. Ratios of the actual to the computed cracking shear stresses are shown on column 7. The results showed little scatter but are extremely conservative.

The ACI equation has the same form as the de Cossio and Siess equation. It is also a function of the square root of the concrete strength.

Zsutty (1968) pointed out that Eqn. 4.4 has serious imperfections as a predictor of the true behaviour of the available shear test results. First, the equation empirically represents two separate types of beam behaviour; beam action and arch action. Beam action involves a more or less constant internal lever arm with shear transmitted by shear stresses. In arch action, discussed in section 2.2.4, the shear is transmitted by the vertical component of the compression thrust. Second, the beam properties, such as $f'c$ and ρ which govern the shear strength are not properly weighted. Using the technique of dimensional analysis, the basic format of a cracking shear strength prediction equation was obtained. After using regression analysis and existing beam data from shear failure tests of simply supported reinforced prismatic concrete beams without web reinforcement, it was decided that beams with $x/d > 2.5$ should be categorized under beam action and beams with $x/d \leq 2.5$ should be categorized under arch action. Regression analysis was again used to evaluate the empirical constants of the cracking shear strength prediction equation.

$$vcz = 59 \sqrt[3]{f'c.\rho\left(\frac{d}{x}\right)} \qquad (4.6)$$

where vcz = the cracking shear stress, in psi.

Zsutty found that Eqn. 4.6 predicted accurately the cracking shear of beams with $x/d > 2.5$. These beams showed consistent and stable behaviour. For beams with $x/d \le 2.5$ loaded on the top face and supported on the bottom face, the data were highly variable and Eqn. 4.6 represents only a lower bound to the cracking shear stress. However, for beams with $x/d \le 2.5$ loaded indirectly through side flanges or brackets, the shear strength was predicted well with Eqn. 4.6.

The cracking shear stress computed using Eqn. 4.6 are shown in column 8 of Table 4.6 and the ratios of the actual to the computed cracking shear stresses are shown on column 9. Compared with the actual cracking shear stress, the computed values were consistently lower, confirming Eqn. 4.6 as a lower bound to the actual cracking shear stresses.

4.7 Ultimate Shear Stress

Shear forces, Vu, and shear stresses, vu, of the interior span at failure or ultimate loads during the original test and the retest are shown in Table 4.7. The ultimate shear forces were extrapolated using values of A* taken from the last load step in Tables 4.1 to 4.4 and Tables E.1 to E.4. In the extrapolation, the north jack load was assumed equalled to the south jack load and the north end support reaction was assumed equalled to the south end reaction. The ultimate shear forces extrapolated from A*

were found to be very close to the ultimate shear forces extrapolated from plots of jack load versus shear force.

Results from the original tests indicate that the presence of horizontal web reinforcement did not increase the ultimate shear capacity. In fact, the ultimate shear capacity of the beam with only horizontal web reinforcement (Beam No. 3) was slightly lower than the beam without web reinforcement (Beam No. 1). The slight difference in the ultimate shear capacity of the two beams was probably due to the variation of concrete strength within the beams.

Beam No. 4 showed a much higher ultimate shear stress than Beam No. 1 in the original test. This indicates that vertical web reinforcement was efficient in increasing the ultimate shear capacity. Although Beam No. 4 also contained horizontal web reinforcement, it was shown that horizontal web reinforcement had no influence on the shear capacity. Therefore, Beam No. 4 can be considered to have just vertical web reinforcement. The results showed Beam No. 4 had an ultimate shear stress of over 50% higher than Beam No. 1. Beam No. 2, with only vertical web reinforcement, also showed an ultimate shear capacity higher than Beam No. 1 in the original test. The effect of vertical web reinforcement on shear strength cannot be singled out in this case since Beam No. 2 had a much lower concrete strength much lower than Beam No. 1.

Concrete strength appeared to influence the ultimate shear capacity. A decrease in concrete strength resulted in a decrease in ultimate shear capacity. The vertical web reinforcement in Beam No. 2 should have increased its ultimate shear stress to the order of that in Beam No. 4 but the low concrete strength resulted in a lower ultimate shear stress than Beam No. 4.

Results from the retest showed that the ultimate shear stresses in the retest were always higher than the stresses from the original test. This is expected since the weaker of the two interior spans should fail first. Except for Beam No. 1, the ultimate shear stresses of Beams No. 2, 3 and 4 in the retest were only slightly higher than those in the original test. The increases in ultimate shear stresses in the latter three beams were very close and averaged approximately 14% higher of the ultimate shear stresses in the original test. Beam No. 1 had an ultimate shear stress in the retest of 55% higher than the ultimate shear stress in the original test. These increases in the retest values over the original test values give an indication of how variable the strength component resulting from concrete strength was.

From section 4.4.2, it was shown that when extrapolated to failure loads, the strains in the vertical stirrups that crossed a critical inclined crack were very close to if not beyond the yield point strain. Therefore, it can be generalized that all the vertical stirrups developed full yield stress. A higher ultimate shear stress can therefore be expected for beams with vertical web reinforcement.

Additional loads are required to yield the stirrups after the formation of inclined cracks.

The increase in shear stress at ultimate from Beam No. 1 to Beam No. 4 was 1.14 MPa. The shear corresponding to yield of all the vertical stirrups crossing the diagonal of the interior shear span was 1.50 MPa. This suggests that although the vertical web reinforcement was fully effective at failure, the shear carried by other mechanisms was smaller than in Beam No. 1. Thus, V_u was less than $V_c + V_s$.

The strains in the horizontal stirrups that crossed a critical crack, when extrapolated to failure load, showed that all these stirrups yielded (see section 4.4.3). This resulted from the widening of the critical inclined crack. Horizontal stirrups transmit shear through their contribution to interface shear transfer. Shear stresses to be transfered by interface shear transfer would be reduced by the widening of the cracks. The contribution of the shear transferred by dowel action of the stirrups is believed to be very small compared to the total shear transferred. Therefore, horizontal stirrups can be expected not to increase the ultimate shear capacity in this case.

The actual ultimate shear stresses from the original tests, v_u, are compared with the ultimate shear stresses computed from several sources and are shown in Table 4.8

The first comparision was made with the ACI 318-77 (1977) equations for the total shear capacity, V_n, given in

Eqns. 2.8 and 2.9. The shear carried by the concrete, Vc, given in Eqn. 2.8, contains the $Vu.d/Mu$ ratio. As has been pointed out, for the interior spans of a continuous beam loaded with concentrated loads, for a critical section chosen at $0.5x$ from the face of the support, Mu approaches zero. Therefore, $Vu.d/Mu$ is a very large value and $Mu/(Vu.d)$ is a very small value. As such, the first term in paranthesis in Eqn. 2.8 will assume the limiting value of 2.5. Since Vc is not to be taken greater than $6\sqrt{f'c}.b.d$, the limiting value of $6\sqrt{f'c}.b.d$ applies. This resulted in very unconservative values of Vc when compared with the actual case. These are listed in column 3 of Table 4.8 and compared to the actual ultimate shears in column 4.

If the $Vu.d/Mu$ ratio was substituted by an equivalent d/x ratio as in Eqn. 4.5, and the shear force converted to shear stress, the modified equation for the shear stress carried by the concrete, vc, can be shown as:

$$vc = [3.5 - 2.5(\frac{0.25Lc+0.5x+0.25Ls}{d})][\text{Eqn. } 4.5] \quad (4.7)$$
$$\le 6\sqrt{f'c}$$

Similarly as in Eqn. 4.5, $(0.25Lc+0.5x+0.25Ls)$ should not be taken more than $(1.15/2)x$. The total shear stress, vn, can now be computed by the addition of vc from Eqn. 4.7 and $vs = Vs/(b.d)$ where Vs is the computed shear force carried by the web reinforcement (Eqn. 2.9). The results are shown in column 5 of Table 4.8. Ratios of the actual to the computed ultimate shear stresses are shown in column 6. Except for Beam No. 3, very conservative results were obtained.

The shear stresses carried by the horizontal and vertical stirrups, as computed by Eqn. 2.9, were 0.54 MPa and 0.40 MPa respectively. The actual results show that the horizontal stirrups did not contribute to the ultimate shear stress. In this sense, the ACI equation for the shear carried by the horizontal stirrups is unconservative. On the other hand, the shear stress contribution of the vertical stirrups, assuming all the stirrups yielded, was 1.50 MPa which suggests that the ACI equation for the shear carried by the vertical stirrups is very conservative.

On the whole, the total shear force, according to the original ACI equations (Eqns. 2.8 and 2.9), is very unconservative. If the $V_u.d/M_u$ ratio was substituted by an equivalent d/x ratio, the results are very conservative. The shear carried by the horizontal web reinforcement is unconservative and the shear carried by the vertical web reinforcement is very conservative.

Column 7 of Table 4.8 shows the total shear stress computed according to the ACI-ASCE Committee 426 (1977). The equations for the shear stress, developed by the ACI-ASCE Committee 426, were presented and discussed in section 2.4.5. Ratios of the actual to the computed ultimate shear stresses are shown in column 8. The results show that the computed shear stresses are very low compared to the actual shear stresses. This is especially so in Beams No. 1 and 3. The computed shear force carried by the horizontal stirrups, V_h, was found to equal zero. This is consistent with the actual results. The computed shear force carried by the vertical stirrups, V_v, was found to produce a shear stress of 1.10 MPa. This value is lower than the actual shear stress of 1.50 MPa in the vertical stirrups, assuming all the stirrups yielded but is very close to the observed increase in shear strength between Beams No. 1 and 4. The computed shear stress carried by the concrete, v_c, was generally lower than the actual shear stress carried by the concrete after the full contribution of the web reinforcement had been subtracted. Therefore, the conservatism of the ACI-ASCE Committee 426 method for predicting the ultimate shear stress in this case lies in the shear stresses carried by the concrete and the vertical reinforcement.

The equation derived by Zsutty (1968,1971) to predict the cracking shear stress, shown as Eqn. 4.6, can be modified to predict the ultimate shear stress in deep beams. The modified equation is shown as Eqn. 4.8.

$$v'_{cz} = \left(\frac{2.5}{x/d}\right)(\text{Eqn. } 4.6) \qquad (4.8)$$

where v'_{cz} = the ultimate shear stress carried by the concrete for beams with $x/d \le 2.5$ loaded on the top face and supported on the bottom face.

The first term in paranthesis in Eqn. 4.8 represents an increase in strength of deep beams over slender beams. It represents an arch action factor; the factor 2.5 is the limiting value for slender beam action.

For beams with vertical stirrups, the ultimate shear stress, v_{uz}, is based on the superposition of the shear stress carried by the concrete and the shear stress carried by the fully yielded stirrups. Horizontal stirrups are not mentioned by Zsutty. Compared with existing deep beam data, reasonable agreement was obtained. The results were 10 to 15 percent lower for beams with concrete strength near 14 MPa and were 10 to 15 percent higher for beams with concrete strength above 40 MPa.

The results of Eqn. 4.8 are shown in column 9 of Table 4.8. Ratios of the actual to the computed ultimate shear stresses are shown in column 10. For Beams No. 2 and 4, the full yield strength of 1.50 MPa of the vertical stirrups were added to v'_{cz}. High values were obtained. The predicted shear stress carried by the concrete overestimated the actual shear stress in the concrete.

Table 4.1 Cracking and Ultimate Loads

Beam No.	Flex. Crack. Load (KN)			First Incl. Crack. Load (KN)				Ultimate Load (KN)	
	N-P	N-M	S-P	N-E	N-I	S-I	S-E	N-I	S-I
1	116	177	116	299	239	330	239	571.8	362.1
2	90	180	90	180	240	180	240	472.1	405.3
3	150	179	150	299	239	239	299	327.3	377.1
4	158	178	158	396	266	320	369	605.6	546.4

N-P = north positive moment span

N-M = negative moment span

S-P = south positive moment span

N-E = north exterior shear span

N-I = north interior shear span

S-I = south interior shear span

S-E = south exterior shear span

Table 4.2 Jack Loads and Support Reactions of Beam No. 1

LOAD STEP	*P*1 (KN)	*P*2 (KN)	*R*1 (KN)	*R*2 (KN)	*R*3 (KN)	*A*∗	*V*[N] (KN)	*V*[S] (KN)
0	0.0	0.0	0.0	0.0	0.0	-	0.0	0.0
1	31.8	30.5	17.3	28.3	16.7	0.45	14.5	13.8
2	60.8	60.0	29.5	62.4	29.1	0.52	31.4	31.0
3	90.9	89.7	40.3	100.5	39.7	0.56	50.6	50.0
4	116.7	115.1	50.8	131.0	50.0	0.57	65.9	65.1
5	150.6	149.5	57.4	185.9	56.9	0.62	93.2	92.7
6	178.7	176.2	65.3	225.5	64.0	0.64	113.4	112.2
7	208.5	203.8	74.0	266.8	71.6	0.65	134.5	132.3
8	240.2	237.8	83.4	312.5	82.1	0.65	156.8	155.7
9	271.2	268.4	93.8	353.4	92.3	0.65	177.4	176.0
10	300.4	298.0	108.3	383.1	107.0	0.64	192.1	191.0
11	331.1	328.3	125.4	410.1	124.0	0.62	205.7	204.4

Notes:

A∗ = *R*2/(*P*1 + *P*2)

*P*1 and *R*1 = north load and reaction

*P*2 and *R*3 = south load and reaction

*R*2 = interior reaction

V[N] = shear in the north interior shear span

V[S] = shear in the south interior shear span

Table 4.3 Jack Loads and Support Reactions of Beam No. 2

LOAD STEP	P1 (KN)	P2 (KN)	R1 (KN)	R2 (KN)	R3 (KN)	A*	V[N] (KN)	V[S] (KN)
0	0.0	0.0	0.0	0.0	0.0	-	0.0	0.0
1	33.8	35.1	15.7	36.8	16.4	0.54	18.1	18.7
2	62.1	63.1	25.6	73.4	26.1	0.59	36.5	37.0
3	91.6	90.3	35.8	110.9	35.1	0.61	55.8	55.1
4	123.7	121.0	47.3	151.4	45.9	0.62	76.3	75.1
5	152.1	149.9	58.4	186.4	57.2	0.62	93.7	92.7
6	181.8	179.3	70.0	222.4	68.7	0.62	111.8	110.6
7	209.3	206.3	78.7	259.7	77.2	0.63	130.6	129.2
8	241.5	238.0	93.3	294.8	91.5	0.62	148.2	146.5
9	269.5	266.6	103.6	330.4	102.1	0.62	165.8	164.5
10	299.8	296.5	115.7	366.5	114.0	0.62	184.0	182.4
11	325.9	321.3	127.2	395.2	124.8	0.61	198.7	196.5
12	357.9	352.9	137.4	438.7	134.8	0.62	220.5	218.1
13	389.8	385.2	152.4	472.6	150.0	0.61	237.4	235.2

(See notes in Table 4.2)

Table 4.4 Jack Loads and Support Reactions of Beam No. 3

LOAD STEP	P1 (KN)	P2 (KN)	R1 (KN)	R2 (KN)	R3 (KN)	A*	V[N] (KN)	V[S] (KN)
0	0.0	0.0	0.0	0.0	0.0	-	0.0	0.0
1	30.3	31.8	12.6	36.1	13.4	0.58	17.7	18.4
2	60.5	62.5	23.2	75.5	24.3	0.61	37.3	38.2
3	91.1	89.8	33.6	114.3	33.0	0.63	57.5	56.8
4	120.1	118.4	42.7	154.0	41.8	0.65	77.4	76.6
5	149.2	146.1	52.4	192.1	50.8	0.65	96.8	95.3
6	180.3	177.8	62.0	235.6	60.6	0.66	118.4	117.2
7	214.4	211.4	73.3	280.6	71.8	0.66	141.0	139.6
8	240.8	237.4	84.2	311.5	82.4	0.65	156.5	154.9
9	270.5	266.7	99.6	340.1	97.6	0.63	170.9	169.1
10	300.4	297.1	107.5	384.2	105.8	0.64	192.9	191.3
11	324.5	320.8	117.1	412.9	115.2	0.64	207.3	205.6

(See notes in Table 4.2)

Table 4.5 Jack Loads and Support Reactions of Beam No. 4

LOAD STEP	*P*1 (KN)	*P*2 (KN)	*R*1 (KN)	*R*2 (KN)	*R*3 (KN)	*A**	*V*[N] (KN)	*V*[S] (KN)
0	0.0	0.0	0.0	0.0	0.0	-	0.0	0.0
1	29.0	26.7	12.9	31.3	11.7	0.56	16.2	15.1
2	58.9	57.1	23.6	69.7	22.7	0.60	35.3	34.4
3	87.3	85.1	33.9	105.7	32.7	0.61	53.4	52.4
4	120.2	117.6	44.8	149.6	43.4	0.63	75.4	74.2
5	147.1	144.1	54.4	184.0	52.9	0.63	92.7	91.3
6	179.5	176.0	64.6	228.3	62.7	0.64	115.0	113.3
7	209.2	206.2	75.6	265.8	74.0	0.64	133.6	132.2
8	239.6	236.3	84.9	307.8	83.2	0.65	154.7	153.1
9	267.7	263.9	94.5	344.7	92.5	0.65	173.2	171.4
10	297.0	293.8	103.0	386.5	101.3	0.65	194.0	192.5
11	322.3	318.7	112.6	417.7	110.7	0.65	209.7	208.0
12	346.8	343.8	121.8	448.7	120.2	0.65	225.0	223.6
13	370.7	367.4	130.5	478.9	128.7	0.65	240.3	238.7
14	398.0	394.2	144.3	505.8	142.3	0.64	253.8	252.0
15	421.3	417.2	153.9	532.9	151.7	0.64	267.4	265.5
16	447.1	443.6	163.9	564.7	162.1	0.63	283.2	281.5
17	472.2	467.4	173.7	594.8	171.2	0.63	298.5	296.2
18	496.5	491.3	182.9	624.7	180.2	0.63	313.6	311.1

(See notes in Table 4.2)

Table 4.6 Comparision of Actual and Computed Shear Stresses at Inclined Cracking

Beam No.	$\sqrt{f'c}$ (MPa)	Vcr * (MPa)	Vx ** (MPa)	$\frac{Vcr}{Vx}$	Vc + (MPa)	$\frac{Vcr}{Vc}$	Vcz ++ (MPa)	$\frac{Vcr}{Vcz}$
1	5.51	1.49	1.41	1.06	1.11	1.34	1.33	1.12
2	3.81	1.06	1.11	0.96	0.84	1.26	1.04	1.02
3	5.70	1.48	1.44	1.03	1.14	1.30	1.36	1.09
4	6.10	1.64	1.52	1.08	1.20	1.37	1.43	1.15

* : actual shear stresses

** : shear stresses computed by modified de Cossio and Siess equation (Eqn. 4.3)

+ : shear stresses computed by modified ACI equation (Eqn. 4.5)

++ : shear stresses computed by Zsutty's equation (Eqn. 4.6)

Table 4.7 Actual Ultimate Shear Stresses in the Original Test and Retest

Beam No.	ORIGINAL TEST				RETEST		
	Failure span	Pu[N] * (KN)	Vu ** (KN)	vu (MPa)	Pu[N] * (KN)	Vu ** (KN)	vu (MPa)
1	S-I	362.1	224.5	2.14	571.8	348.8	3.32
2	S-I	405.3	247.2	2.36	472.1	288.0	2.74
3	N-I	327.3	209.5	2.00	377.1	237.6	2.26
4	S-I	546.4	344.2	3.28	605.6	387.6	3.69

* : north jack load at failure

** : shear force extrapolated using value of A* from loads prior to failure

N-I = north interior span

S-I = south interior span

$vu = Vu/(b.d)$

Table 4.8 Comparision of Actual Ultimate Shear Stresses from the Original Test With Computed Ultimate Shear Stresses

Beam No.	vu * (MPa)	vn ** (MPa)	$\frac{vu}{vn}$	v"n # (MPa)	$\frac{vu}{v''n}$	v'n + (MPa)	$\frac{vu}{v'n}$	vuz ++ (MPa)	$\frac{vu}{vuz}$
1	2.14	2.75	0.78	1.61	1.33	1.21	1.77	2.33	0.92
2	2.36	2.30	1.03	1.62	1.46	1.89	1.25	3.32	0.71
3	2.00	3.38	0.59	2.19	0.91	1.25	1.60	2.38	0.84
4	3.28	3.98	0.82	2.68	1.22	2.39	1.37	4.00	0.82

* : actual shear stresses

** : shear stresses computed by original ACI equation (Eqn. 2.8 and 2.9)

# : shear stresses computed by modified ACI equation (Eqn. 4.7 and 2.9)

+ : shear stresses computed by ACI-ASCE equation (Eqns. 2.10 to 2.14)

++ : shear stresses computed by Zsutty's equation (Eqn. 4.8)

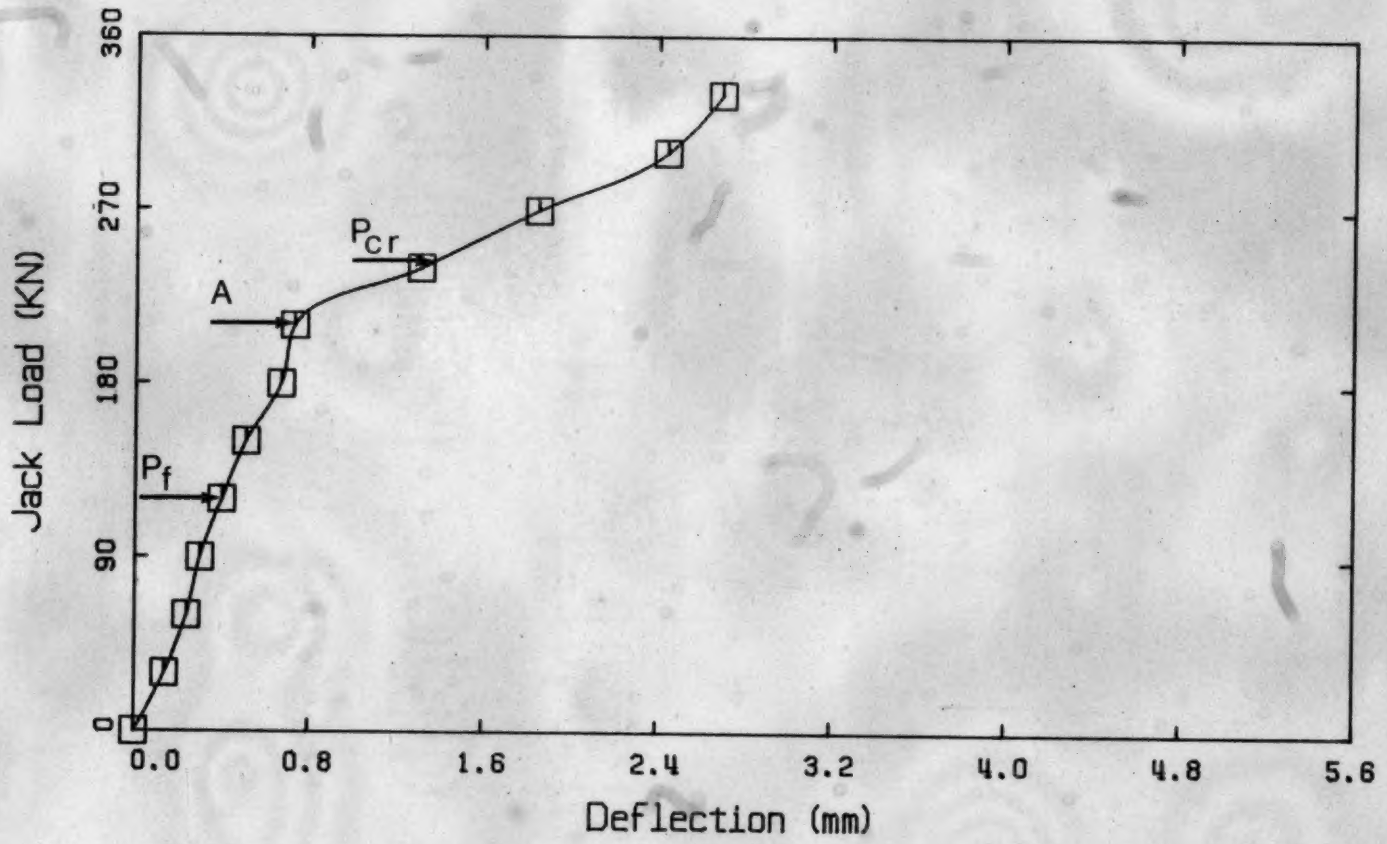

Figure 4.1 Plot of Jack Load Versus North Midspan Deflection of Beam No. 1

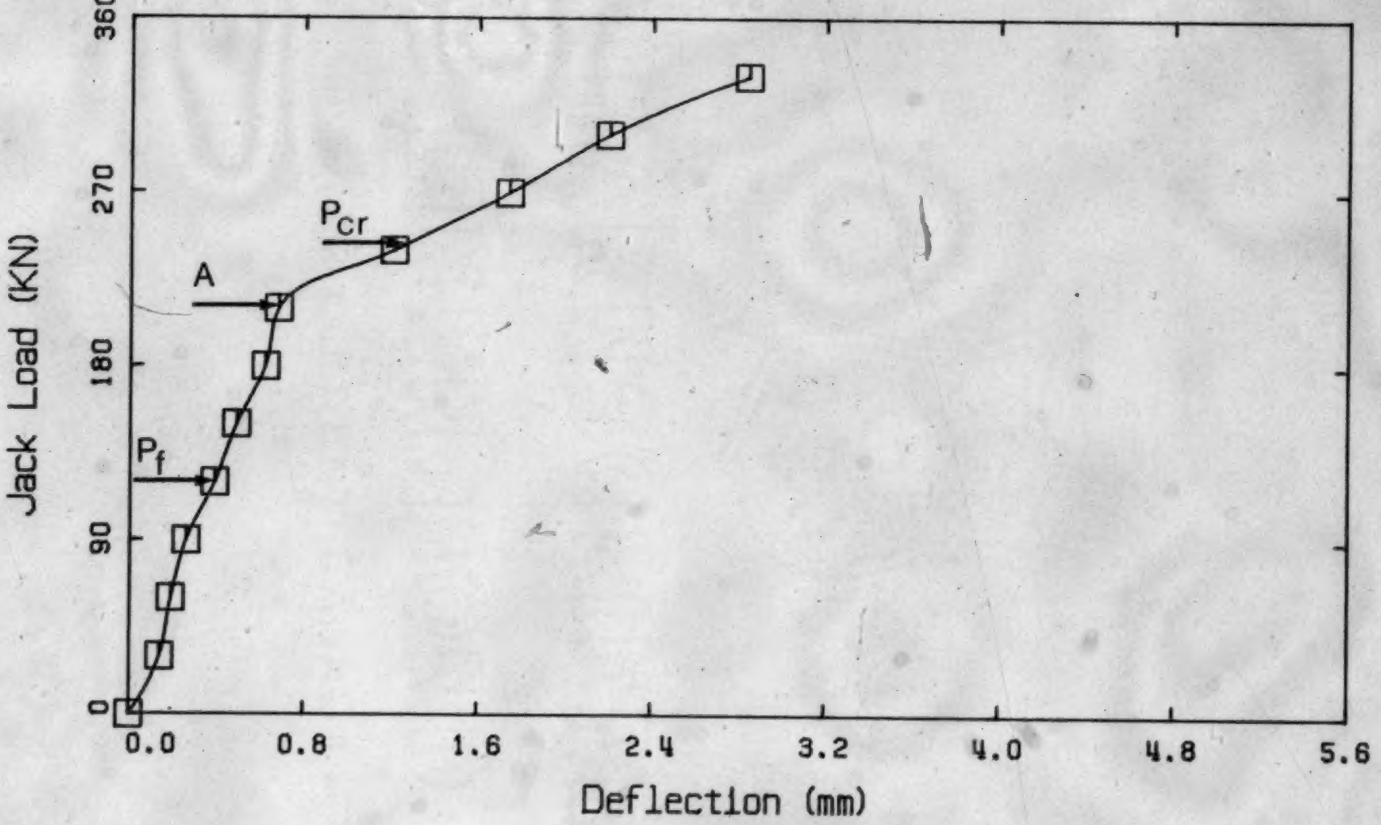

Figure 4.2 Plot of Jack Load Versus South Midspan Deflection of Beam No. 1

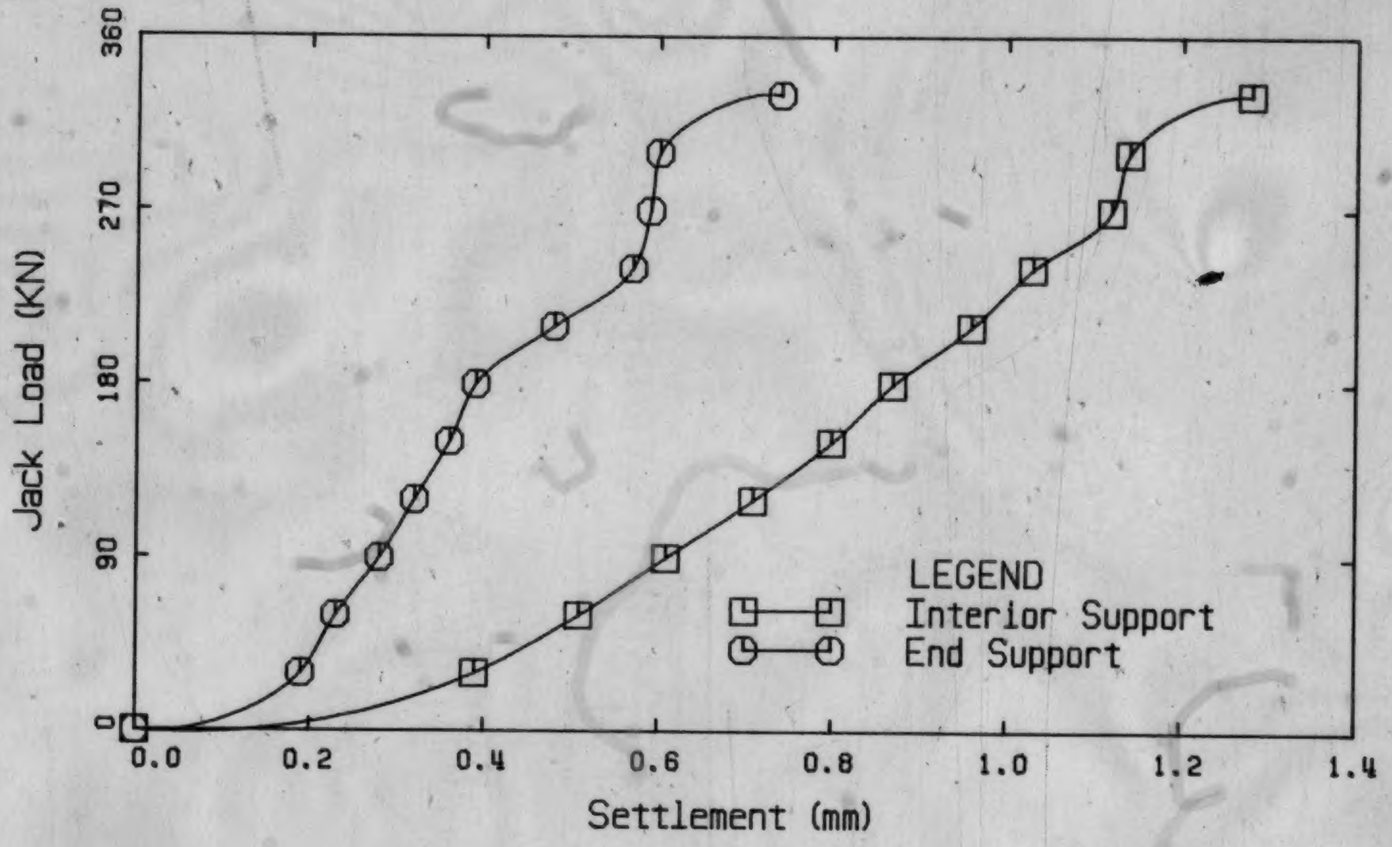

Figure 4.3 Plot of Jack Load Versus Support Settlement of Beam No. 1

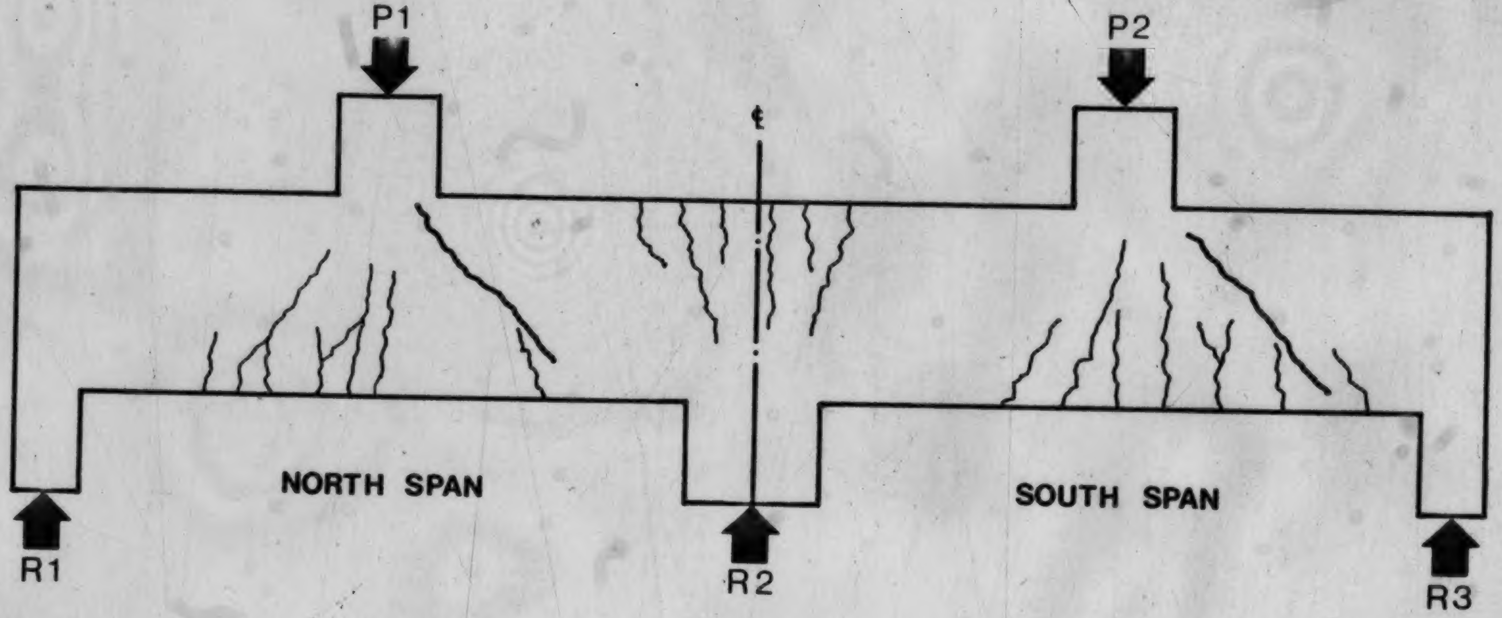
P1
P2
℄
NORTH SPAN
SOUTH SPAN
R1
R2
R3

Figure 4.4 First Inclined Cracking Pattern of Beam No. 1
(Load Step 8)

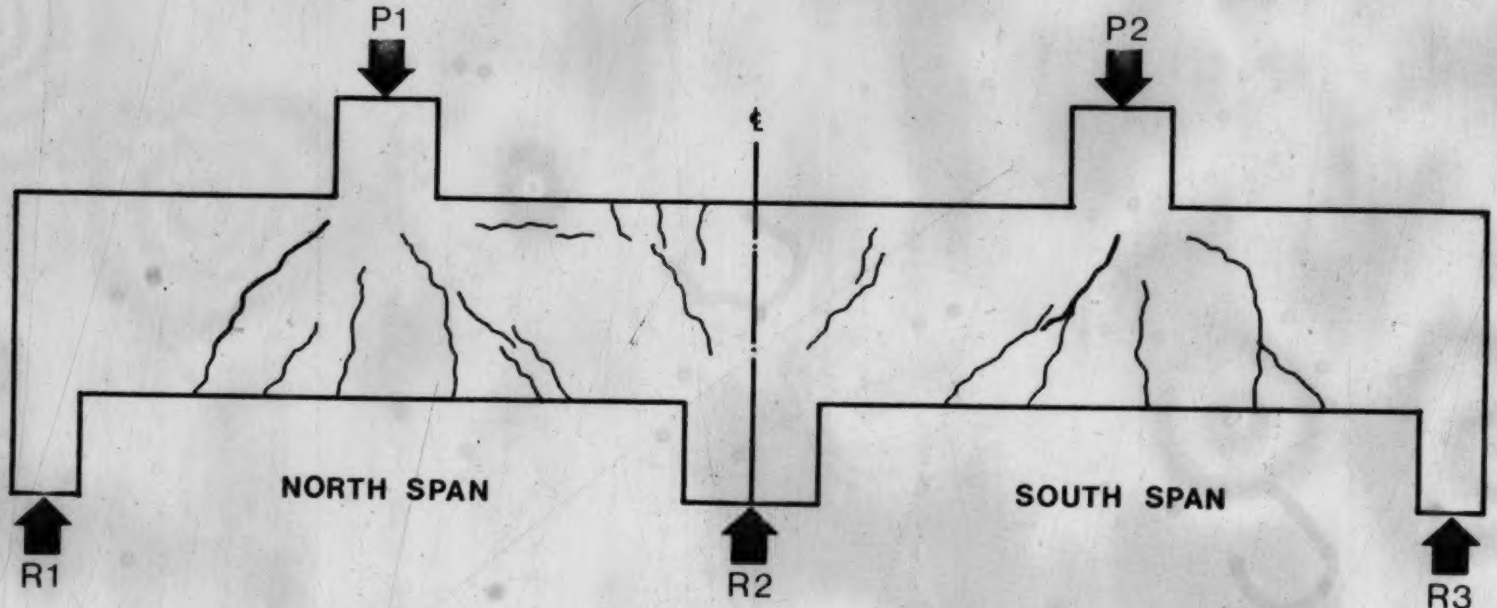
P1
P2
℄
NORTH SPAN
SOUTH SPAN
R1
R2
R3

Figure 4.5 First Inclined Cracking Pattern of Beam No. 2

(Load Step 6)

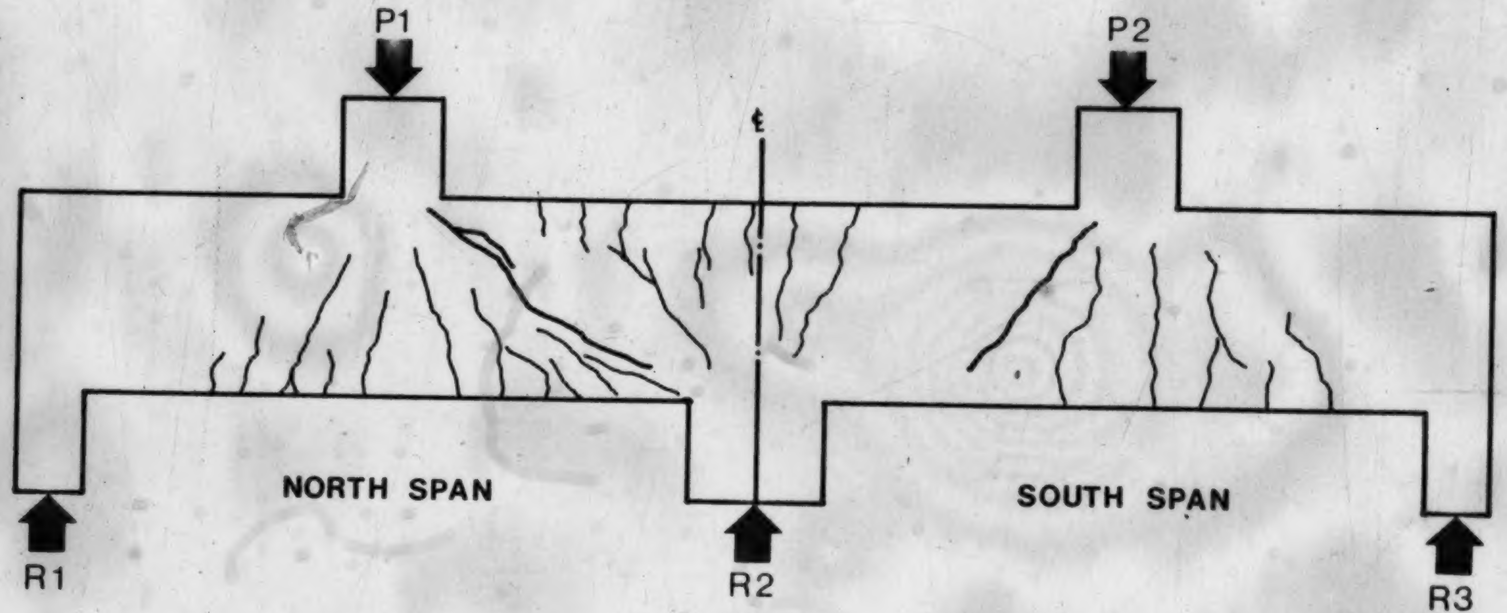
P1
P2
℄
NORTH SPAN
SOUTH SPAN
R1
R2
R3

Figure 4.6 First Inclined Cracking Pattern of Beam No. 3

(Load Step 8)

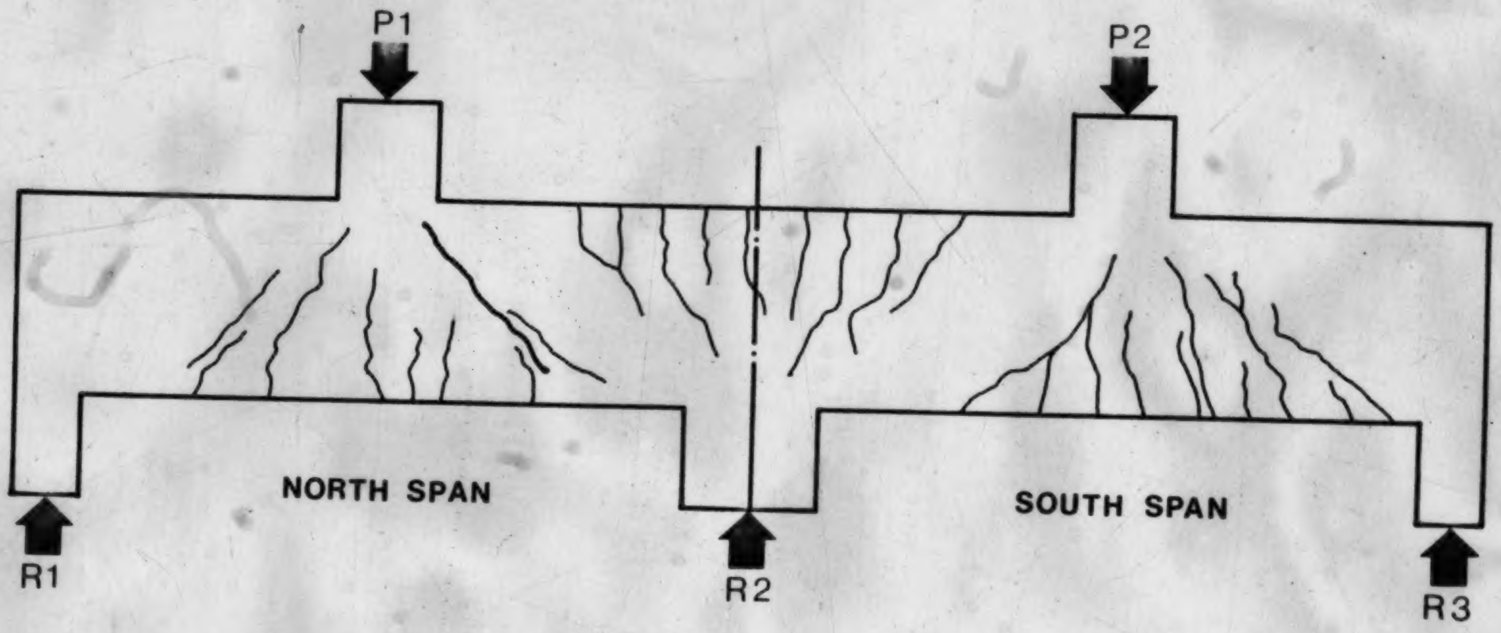
P1
P2
NORTH SPAN
SOUTH SPAN
R1
R2
R3

Figure 4.7 First Inclined Cracking Pattern of Beam No. 4

(Load Step 9)

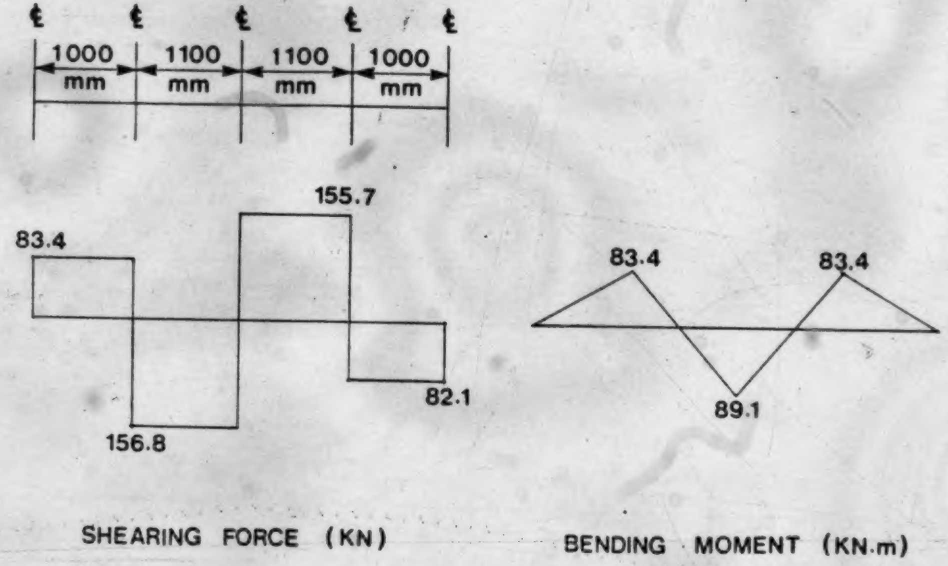
℄
℄
℄
℄
℄
1000 mm
1100 mm
1100 mm
1000 mm
83.4
155.7
156.8
82.1
83.4
83.4
89.1
SHEARING FORCE (KN)
BENDING MOMENT (KN.m)

a) ACTUAL SHEARING FORCE AND BENDING MOMENT DIAGRAMS

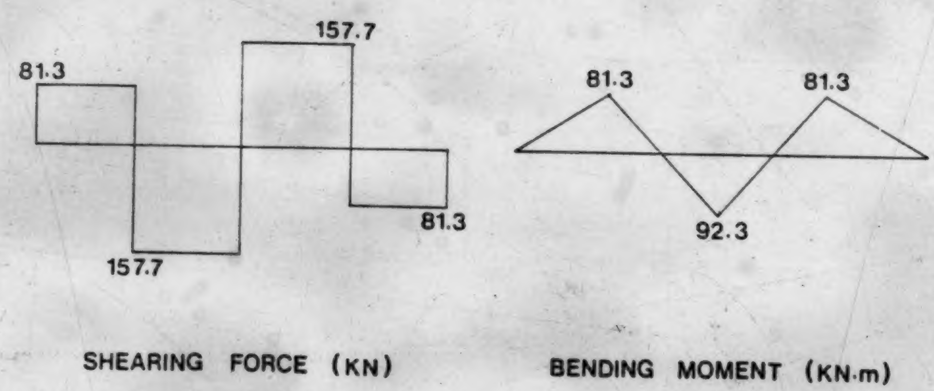
81.3
157.7
157.7
81.3
81.3
81.3
92.3
SHEARING FORCE (KN)
BENDING MOMENT (KN.m)

b) ELASTIC SHEARING FORCE AND BENDING MOMENT DIAGRAMS

Figure 4.8 Comparision of Actual and Elastic Shearing Force and Bending Moment Diagrams of Beam No. 1 at First Inclined Cracking (Load Step 8)

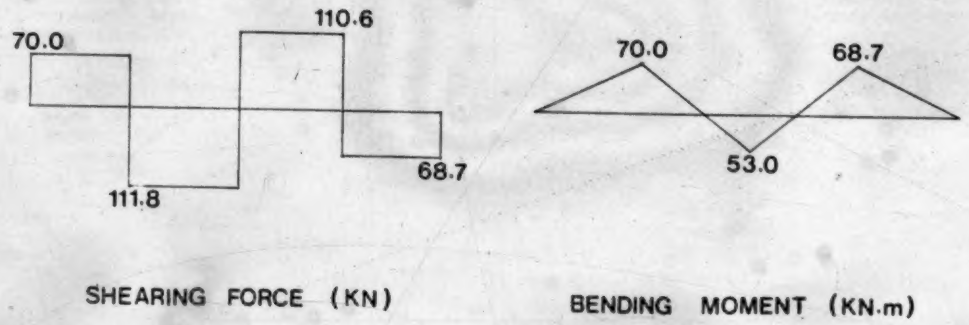
70.0
111.8
110.6
68.7
70.0
53.0
68.7
SHEARING FORCE (KN)
BENDING MOMENT (KN.m)

a) ACTUAL SHEARING FORCE AND BENDING MOMENT DIAGRAMS

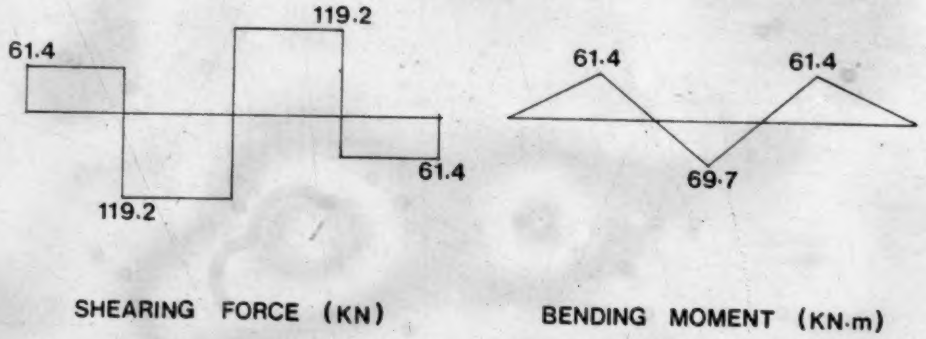
61.4
119.2
119.2
61.4
61.4
69.7
61.4
SHEARING FORCE (KN)
BENDING MOMENT (KN.m)

b) ELASTIC SHEARING FORCE AND BENDING MOMENT DIAGRAMS

Figure 4.9 Comparision of Actual and Elastic Shearing Force and Bending Moment Diagrams of Beam No. 2 at First Inclined Cracking (Load Step 6)

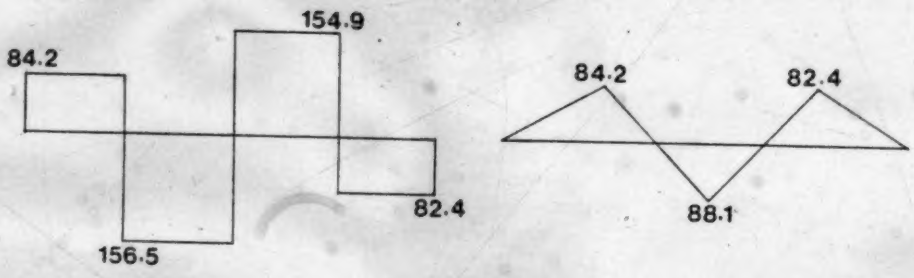
84.2
154.9
156.5
82.4
84.2
82.4
88.1

SHEARING FORCE (KN) BENDING MOMENT (KN.m)

a) ACTUAL SHEARING FORCE AND BENDING MOMENT DIAGRAMS

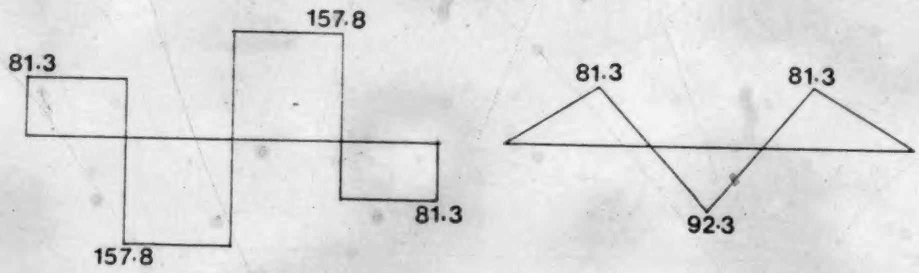
81.3
157.8
157.8
81.3
81.3
81.3
92.3

SHEARING FORCE (KN) BENDING MOMENT (KN.m)

b) ELASTIC SHEARING FORCE AND BENDING MOMENT DIAGRAMS

Figure 4.10 Comparision of Actual and Elastic Shearing Force and Bending Moment Diagrams of Beam No. 3 at First Inclined Cracking (Load Step 8)

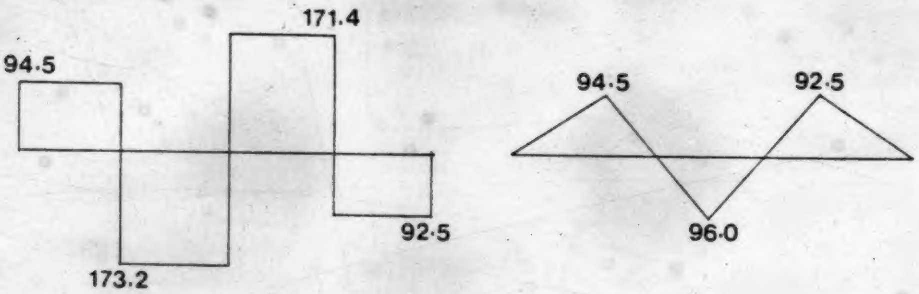
171.4
94·5
173.2
92·5
94·5
92·5
96·0

SHEARING FORCE (KN)

BENDING MOMENT (KN·m)

a) ACTUAL SHEARING FORCE AND BENDING MOMENT DIAGRAMS

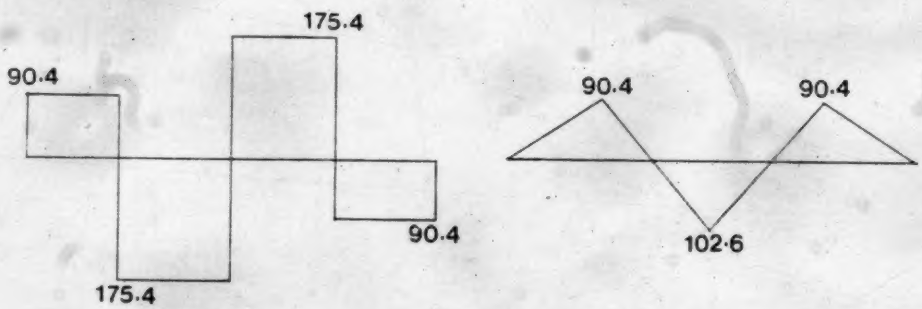
175.4
90·4
175·4
90·4
90·4
90·4
102·6

SHEARING FORCE (KN)

BENDING MOMENT (KN·m)

b) ELASTIC SHEARING FORCE AND BENDING MOMENT DIAGRAMS

Figure 4.11 Comparision of Actual and Elastic Shearing Force and Bending Moment Diagrams of Beam No. 4 at First Inclined Cracking (Load Step 9)

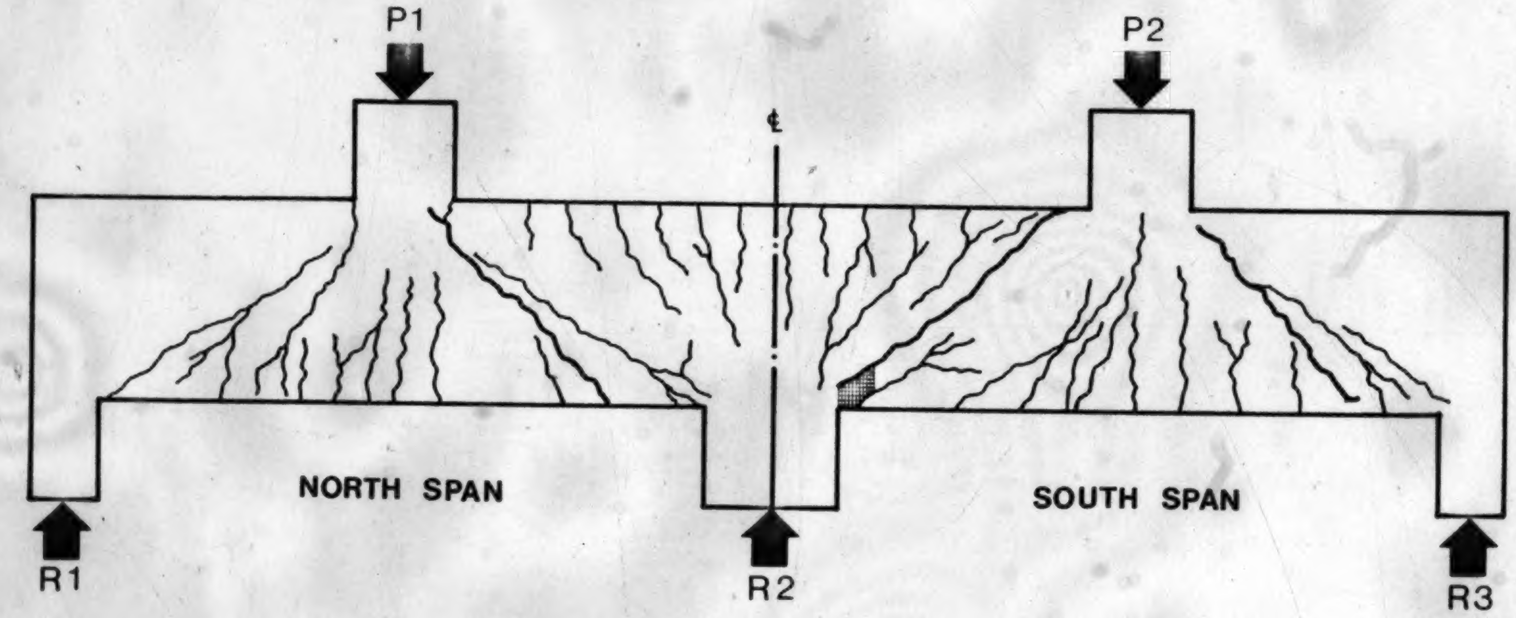
P1
P2
℄
NORTH SPAN
SOUTH SPAN
R1
R2
R3

Figure 4.12 Failure Cracking Pattern of Beam No. 1

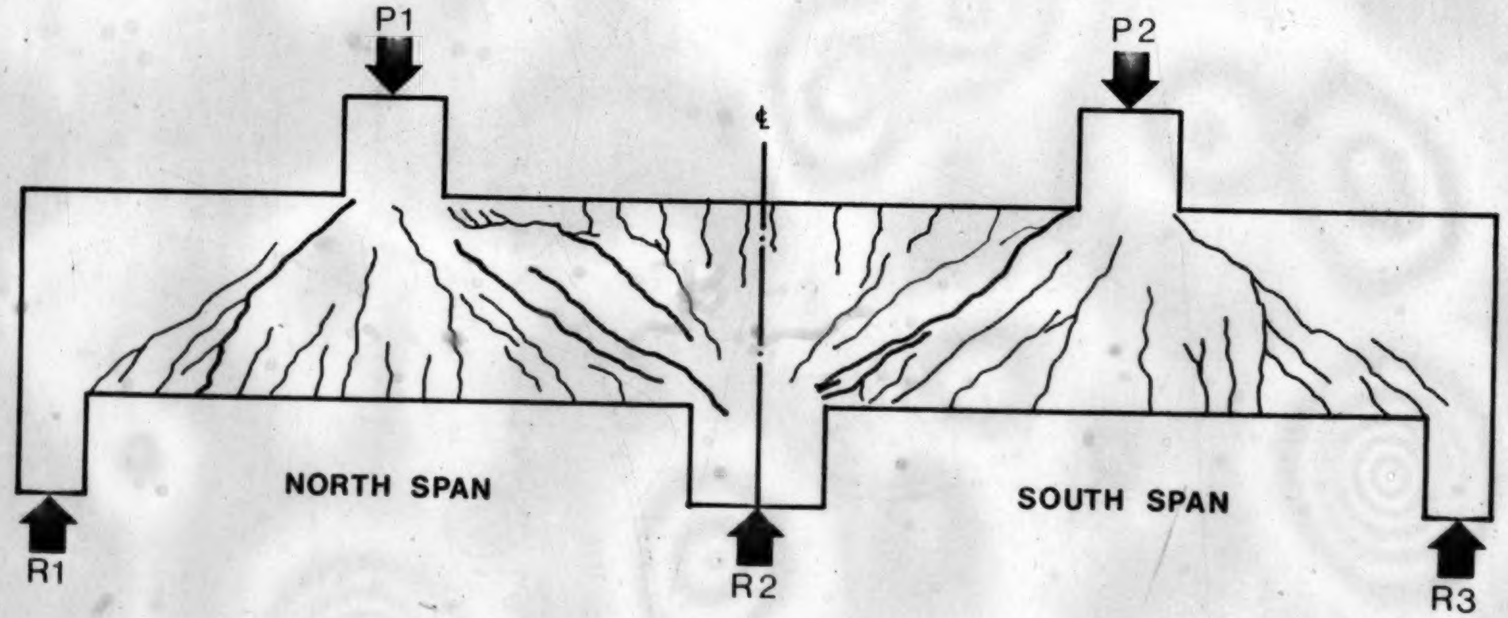
P1
P2
℄
NORTH SPAN
SOUTH SPAN
R1
R2
R3

Figure 4.13 Failure Cracking Pattern of Beam No. 2

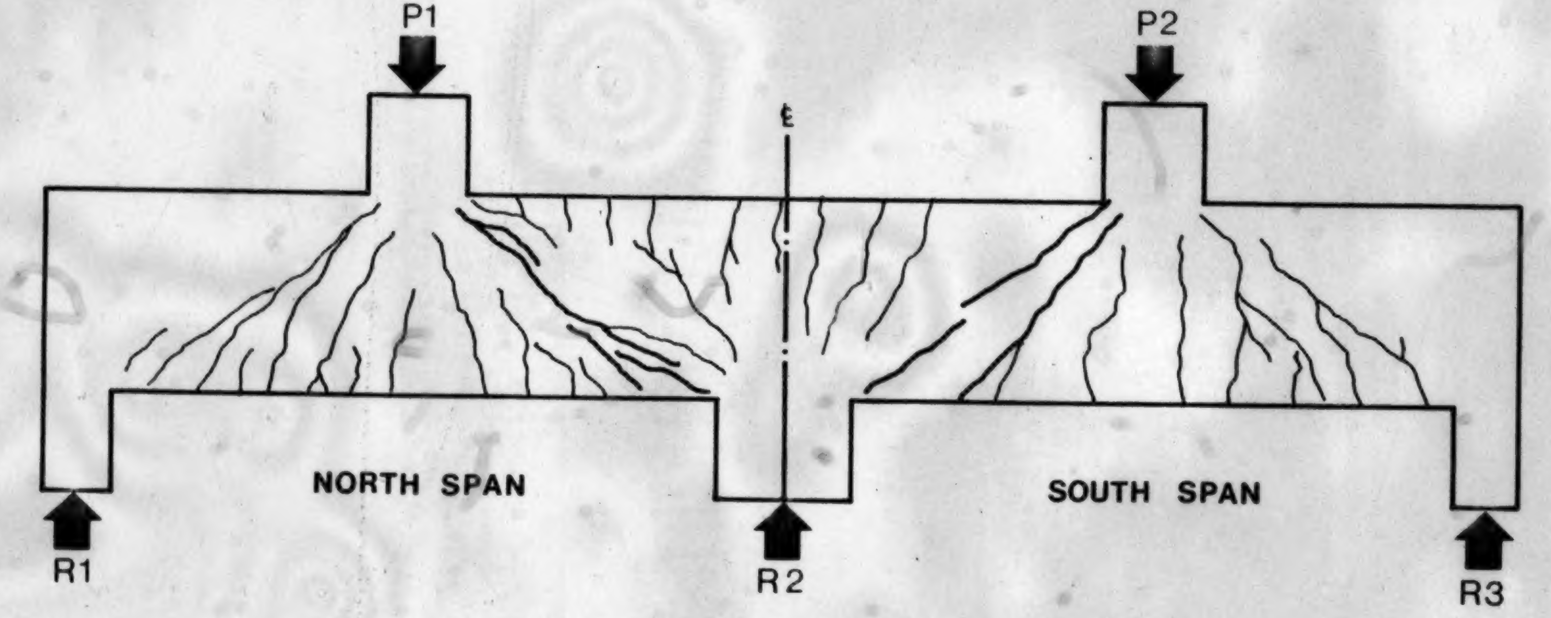
P1
P2
℄
NORTH SPAN
SOUTH SPAN
R1
R2
R3

Figure 4.14 Failure Cracking Pattern of Beam No. 3

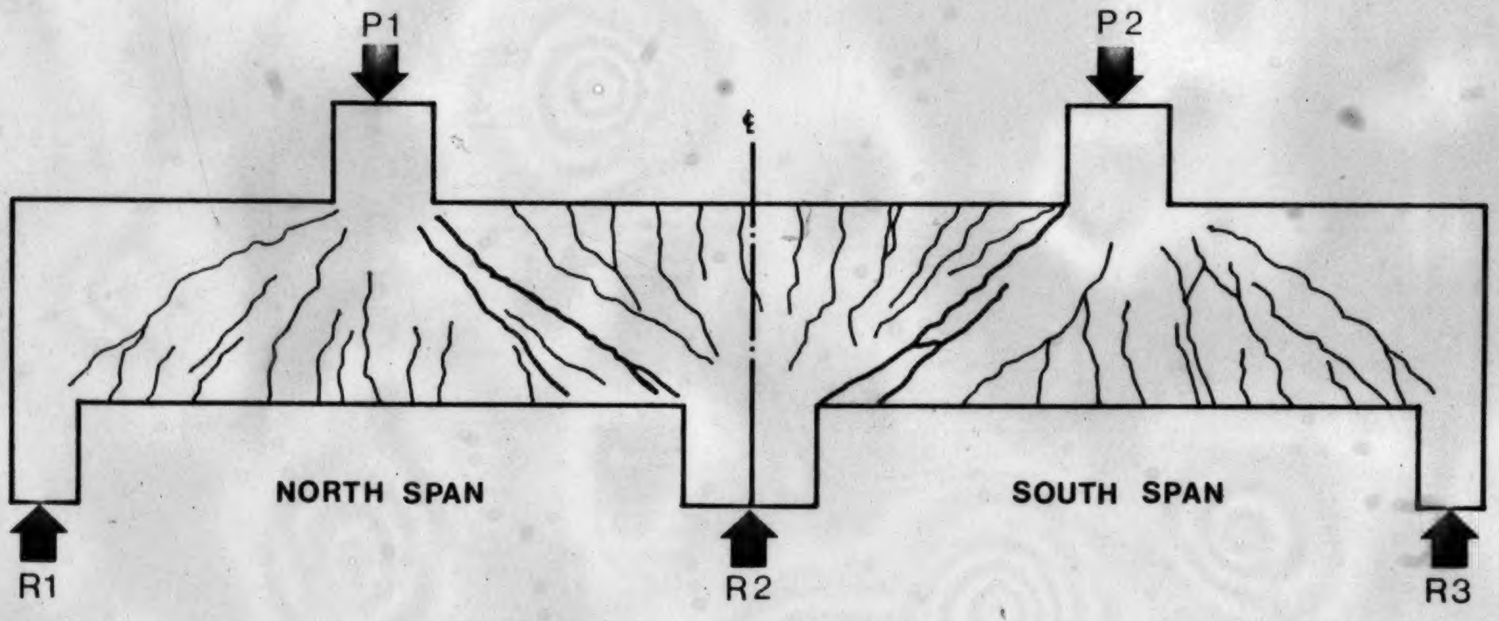
P1
P2
℄
NORTH SPAN
SOUTH SPAN
R1
R2
R3

Figure 4.15 Failure Cracking Pattern of Beam No. 4

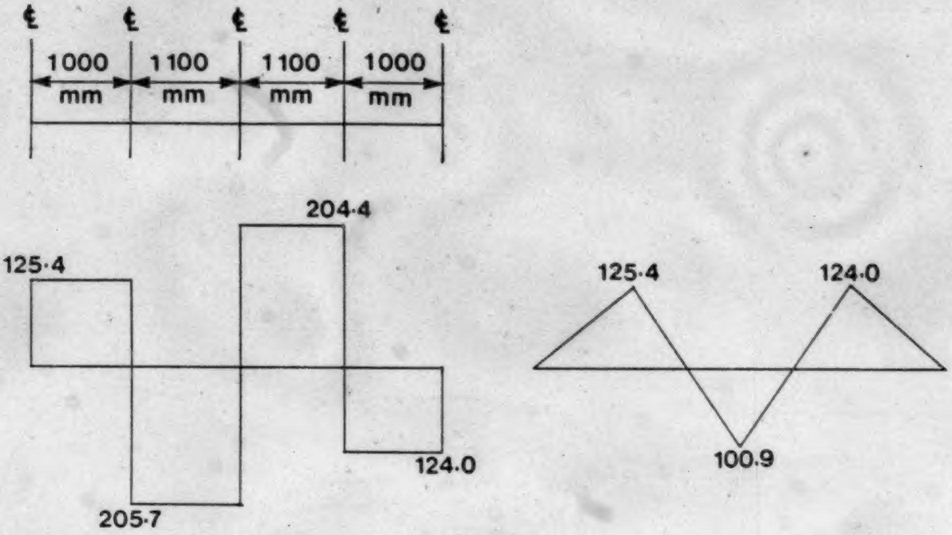
℄
℄
℄
℄
℄
1000 mm
1100 mm
1100 mm
1000 mm
204·4
125·4
205·7
124·0
125·4
124·0
100·9

SHEARING FORCE (KN) BENDING MOMENT (KN·m)

a) ACTUAL SHEARING FORCE AND BENDING MOMENT DIAGRAMS

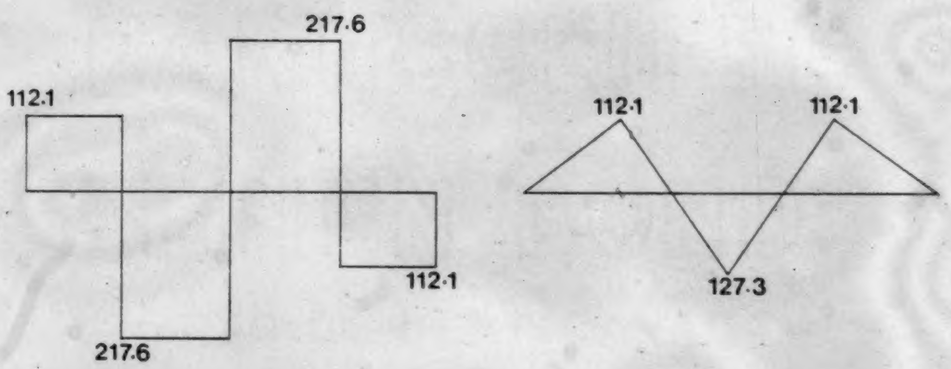
217·6
112·1
217·6
112·1
112·1
112·1
127·3

SHEARING FORCE (KN) BENDING MOMENT (KN·m)

b) ELASTIC SHEARING FORCE AND BENDING MOMENT DIAGRAMS

Figure 4.16 Comparision of Actual and Elastic Shearing Force and Bending Moment Diagrams of Beam No. 1 at Last Load Step Prior to Failure (Load Step 11)

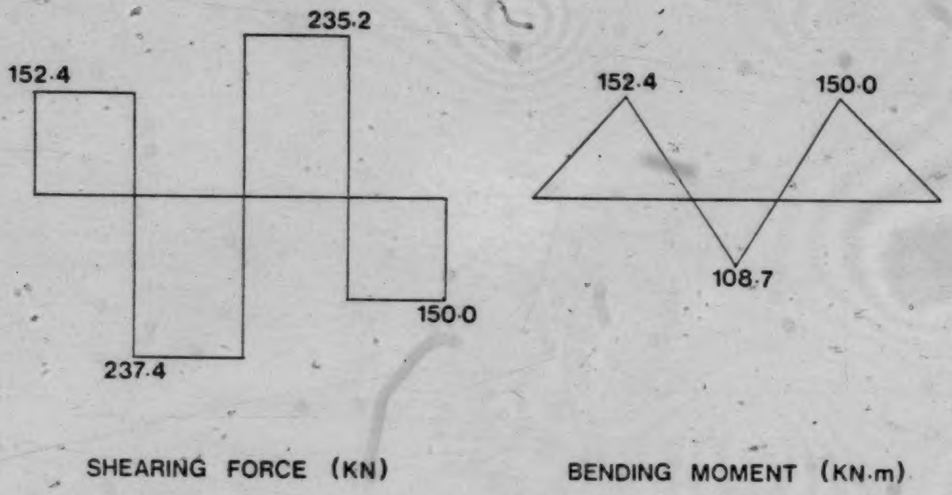
235.2
152.4
150.0
237.4
SHEARING FORCE (KN)
152.4
150.0
108.7
BENDING MOMENT (KN.m)

a) ACTUAL SHEARING FORCE AND BENDING MOMENT DIAGRAMS

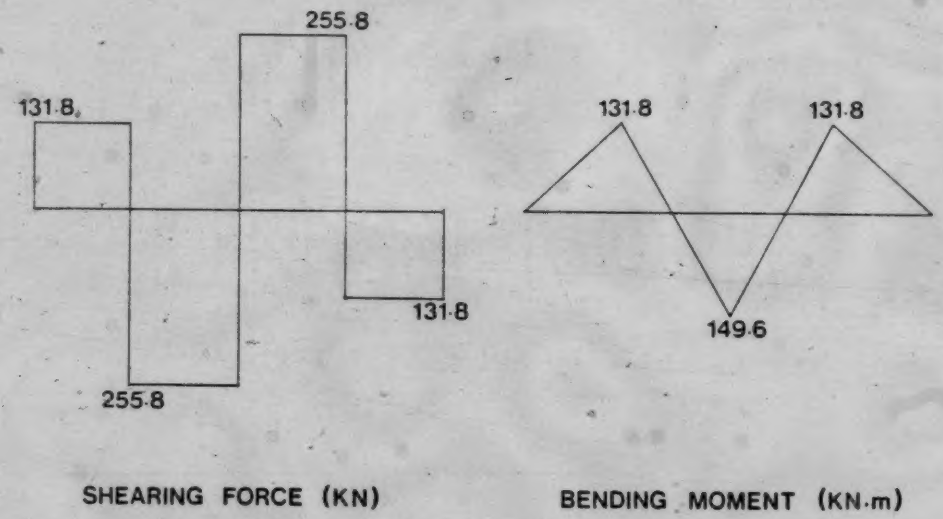
255.8
131.8
131.8
255.8
SHEARING FORCE (KN)
131.8
131.8
149.6
BENDING MOMENT (KN.m)

b) ELASTIC SHEARING FORCE AND BENDING MOMENT DIAGRAMS

Figure 4.17 Comparision of Actual and Elastic Shearing Force and Bending Moment Diagrams of Beam No. 2 at Last Load Step Prior to Failure (Load Step 13)

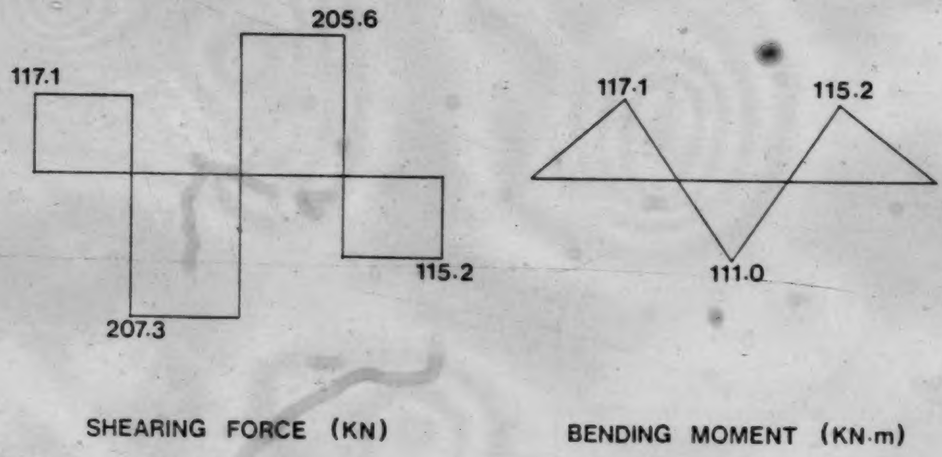
205.6
117.1
207.3
115.2
117·1
115.2
111.0
SHEARING FORCE (KN)
BENDING MOMENT (KN.m)

a) ACTUAL SHEARING FORCE AND BENDING MOMENT DIAGRAMS

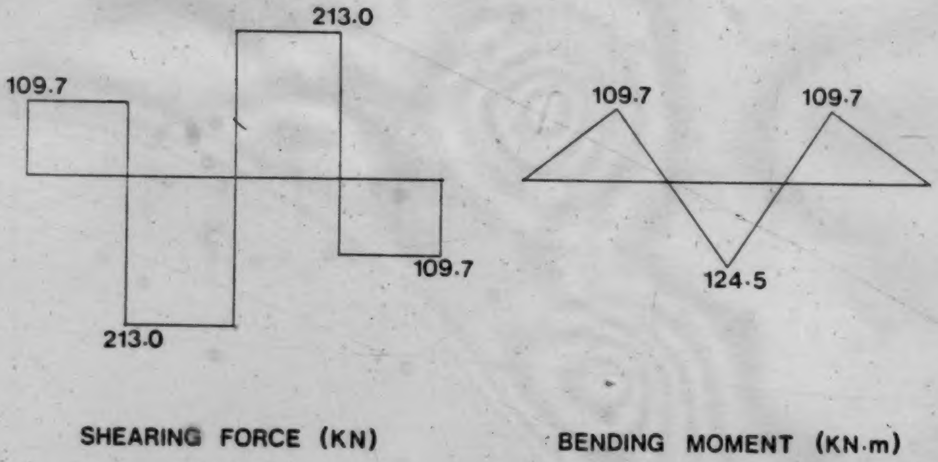
213.0
109.7
213.0
109.7
109.7
109·7
124·5
SHEARING FORCE (KN)
BENDING MOMENT (KN.m)

b) ELASTIC SHEARING FORCE AND BENDING MOMENT DIAGRAMS

Figure 4.18 Comparision of Actual and Elastic Shearing Force and Bending Moment Diagrams of Beam No. 3 at Last Load Step Prior to Failure (Load Step 11)

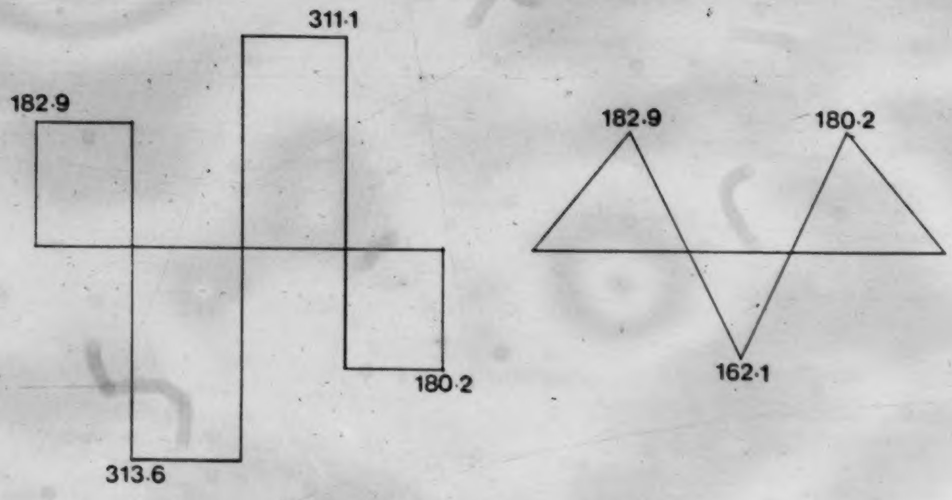
311·1
182·9
180·2
313·6
182·9
180·2
162·1

SHEARING FORCE (KN) BENDING MOMENT (KN·m)

a) ACTUAL SHEARING FORCE AND BENDING MOMENT DIAGRAMS

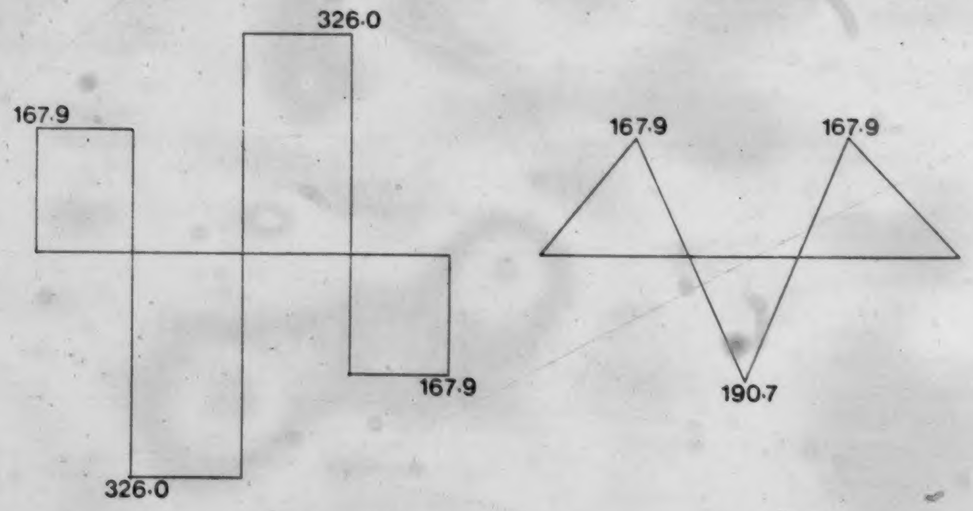
326·0
167·9
167·9
326·0
167·9
167·9
190·7

SHEARING FORCE (KN) BENDING MOMENT (KN·m)

b) ELASTIC SHEARING FORCE AND BENDING MOMENT DIAGRAMS

Figure 4.19 Comparision of Actual and Elastic Shearing Force and Bending Moment Diagrams of Beam No. 4 at Last Load Step Prior to Failure (Load Step 18)

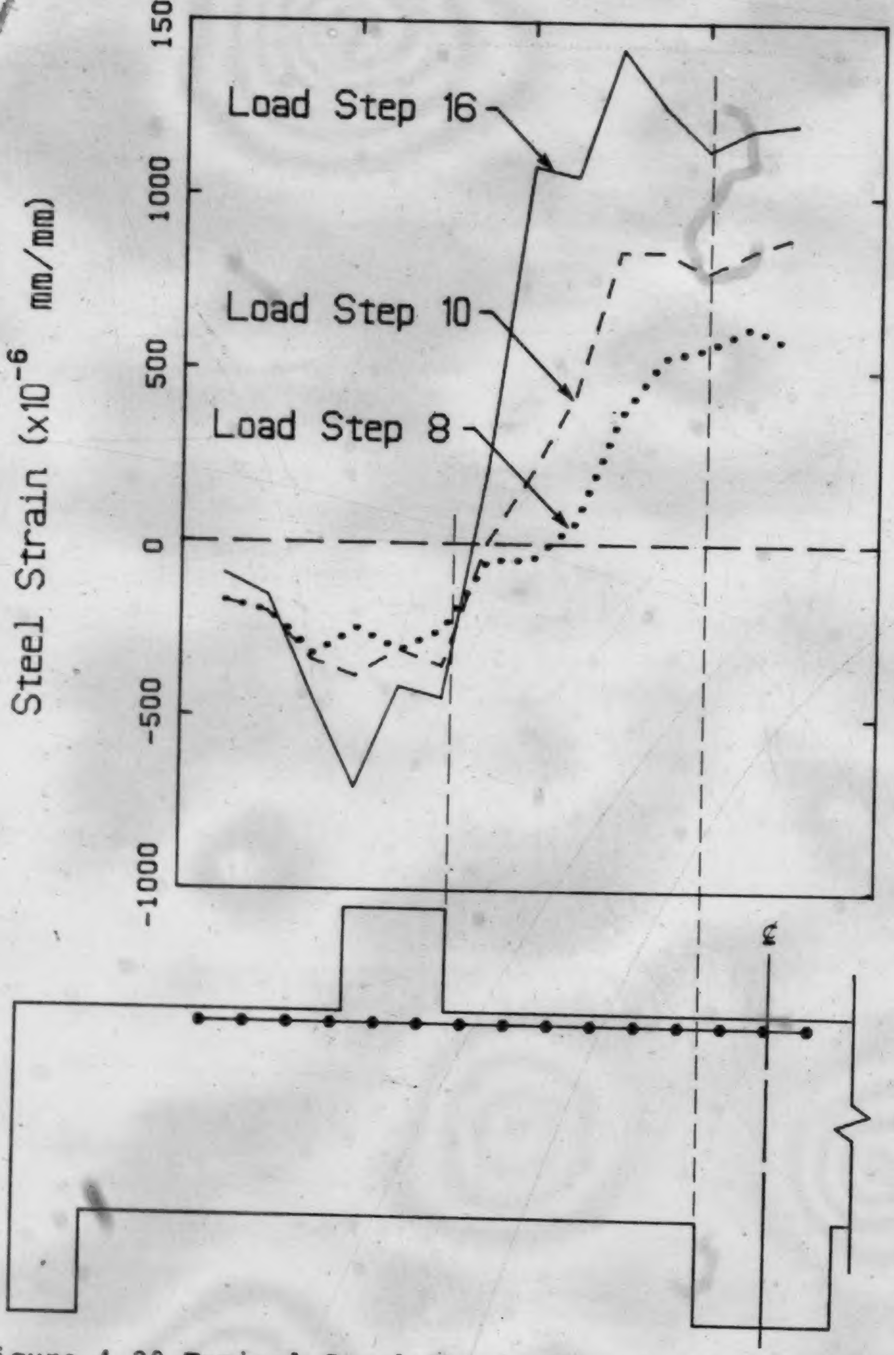

Figure 4.20 Typical Steel Strain Distribution in the Negative Moment Flexural Reinforcement, North Span of Beam No. 4

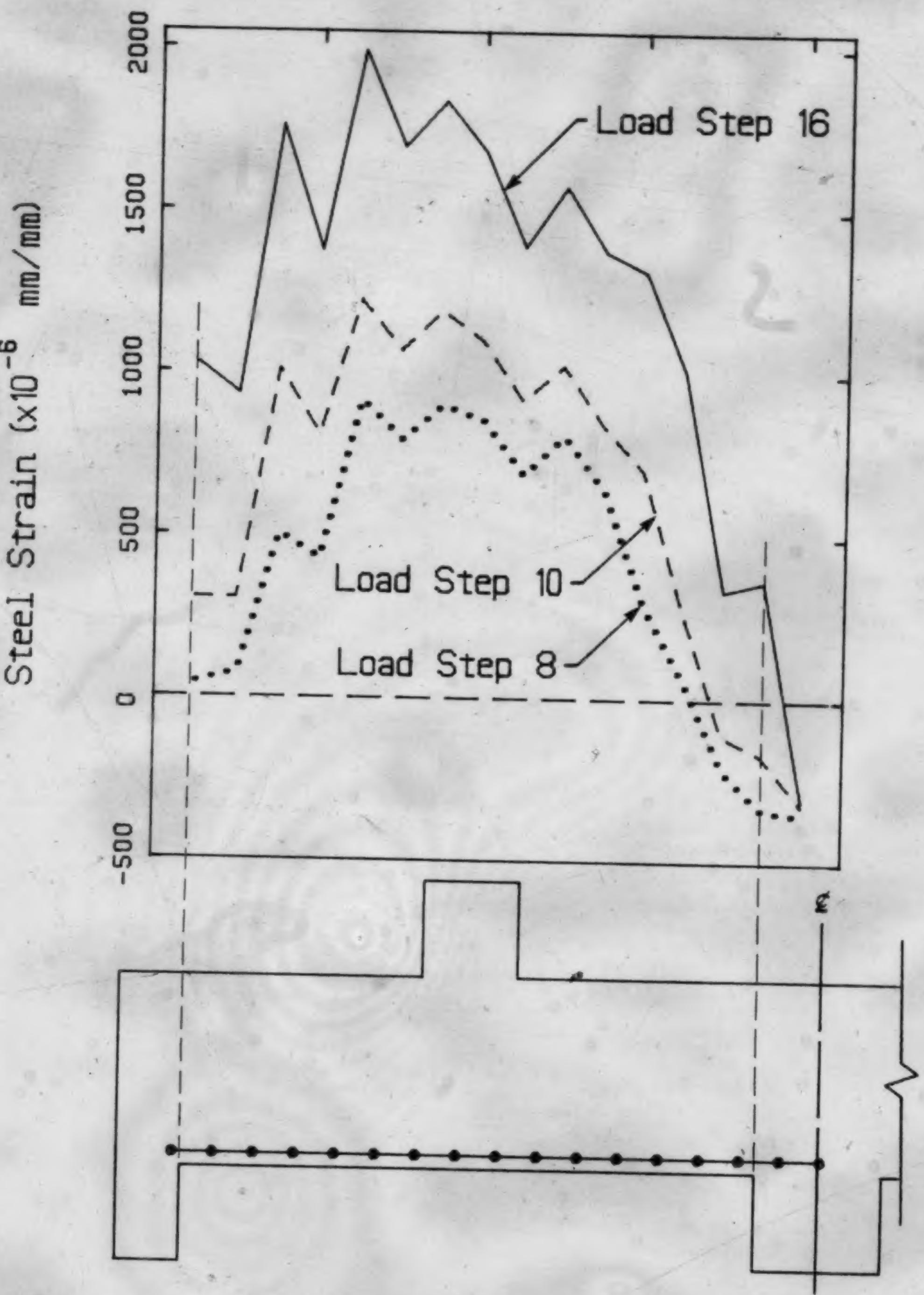

Figure 4.21 Typical Steel Strain Distribution in the Positive Moment Flexural Reinforcement, North Span of Beam No. 4

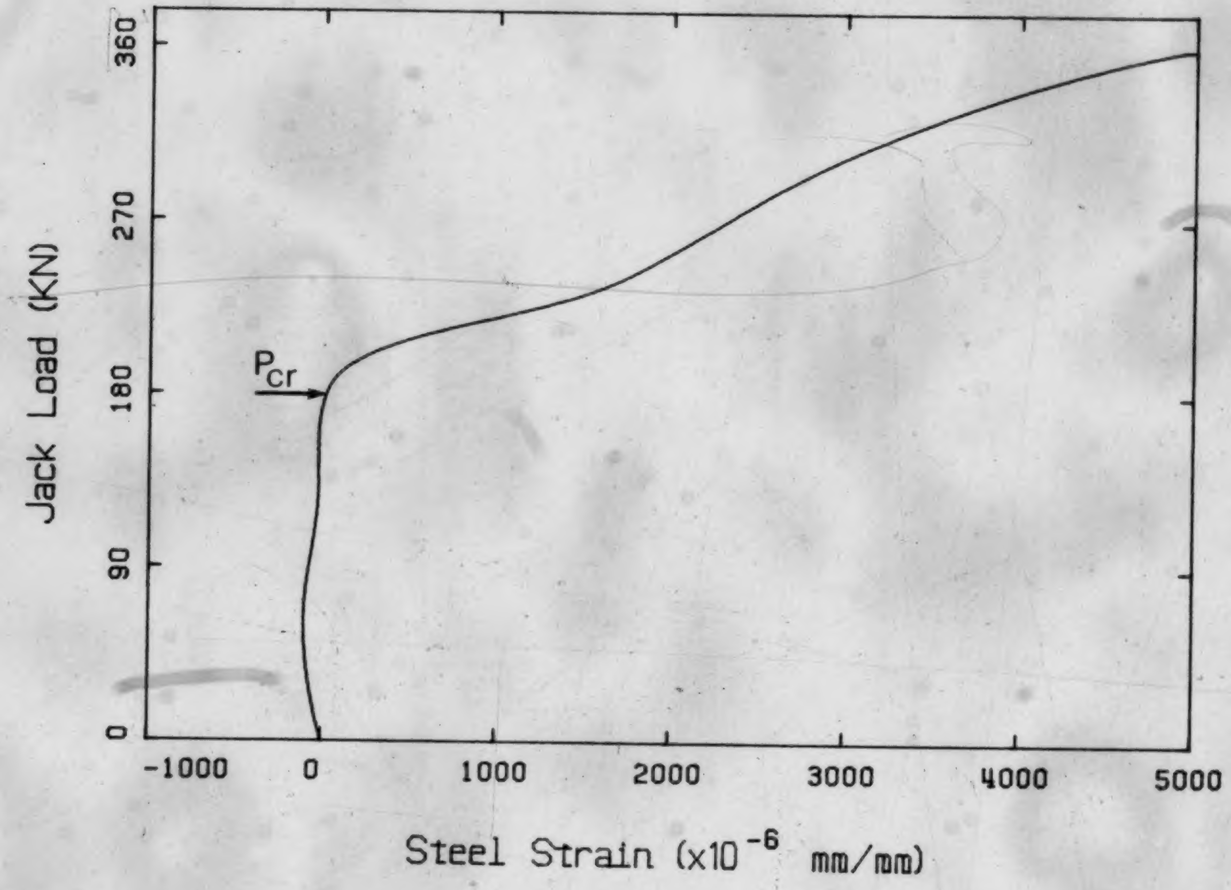

Figure 4.22 Typical Plot of Jack Load versus Steel Strain in a Vertical Stirrup

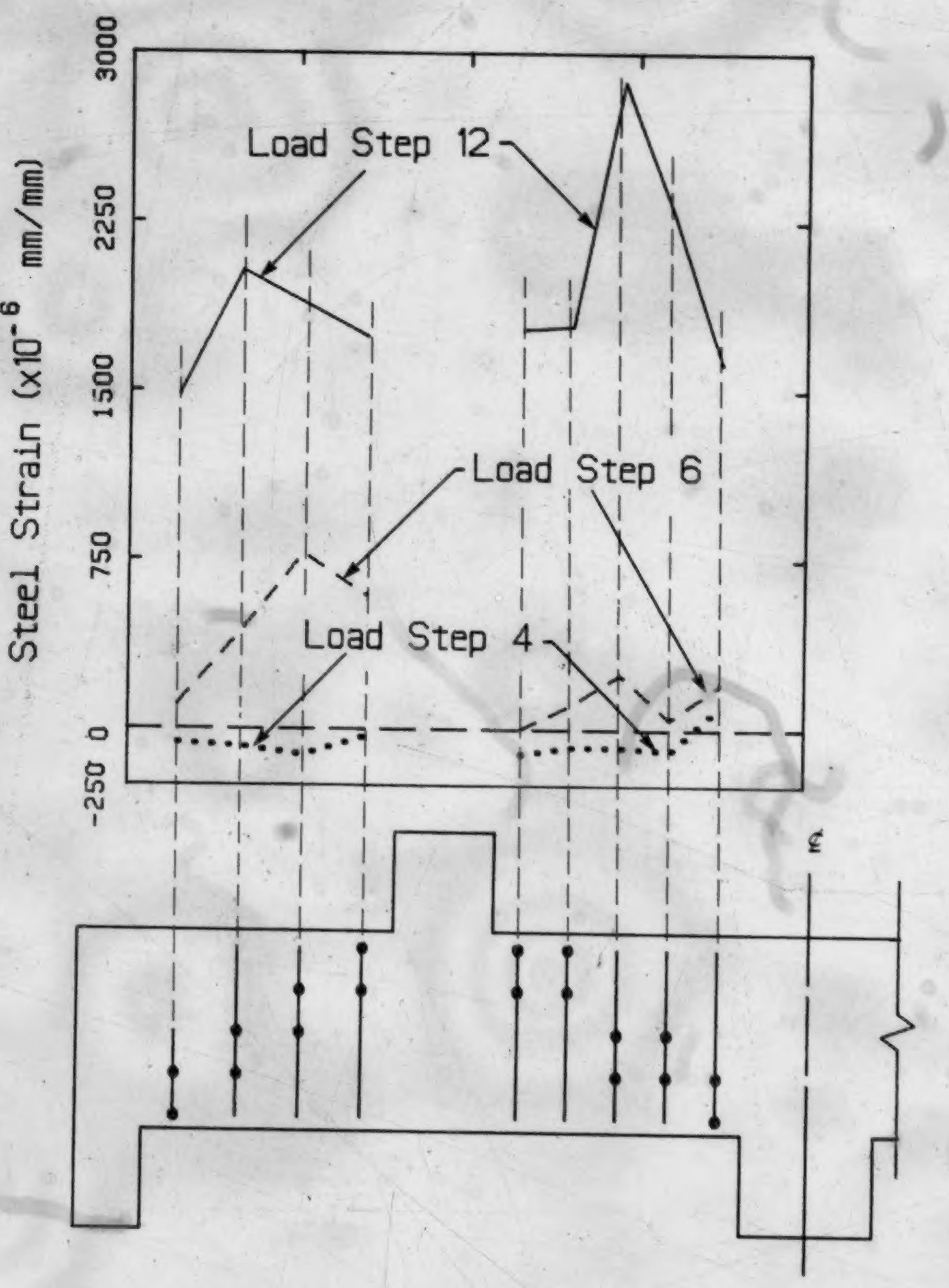

Figure 4.23 Steel Strain Distribution of Vertical Stirrups Crossing Major Inclined Cracks in Beam No. 2

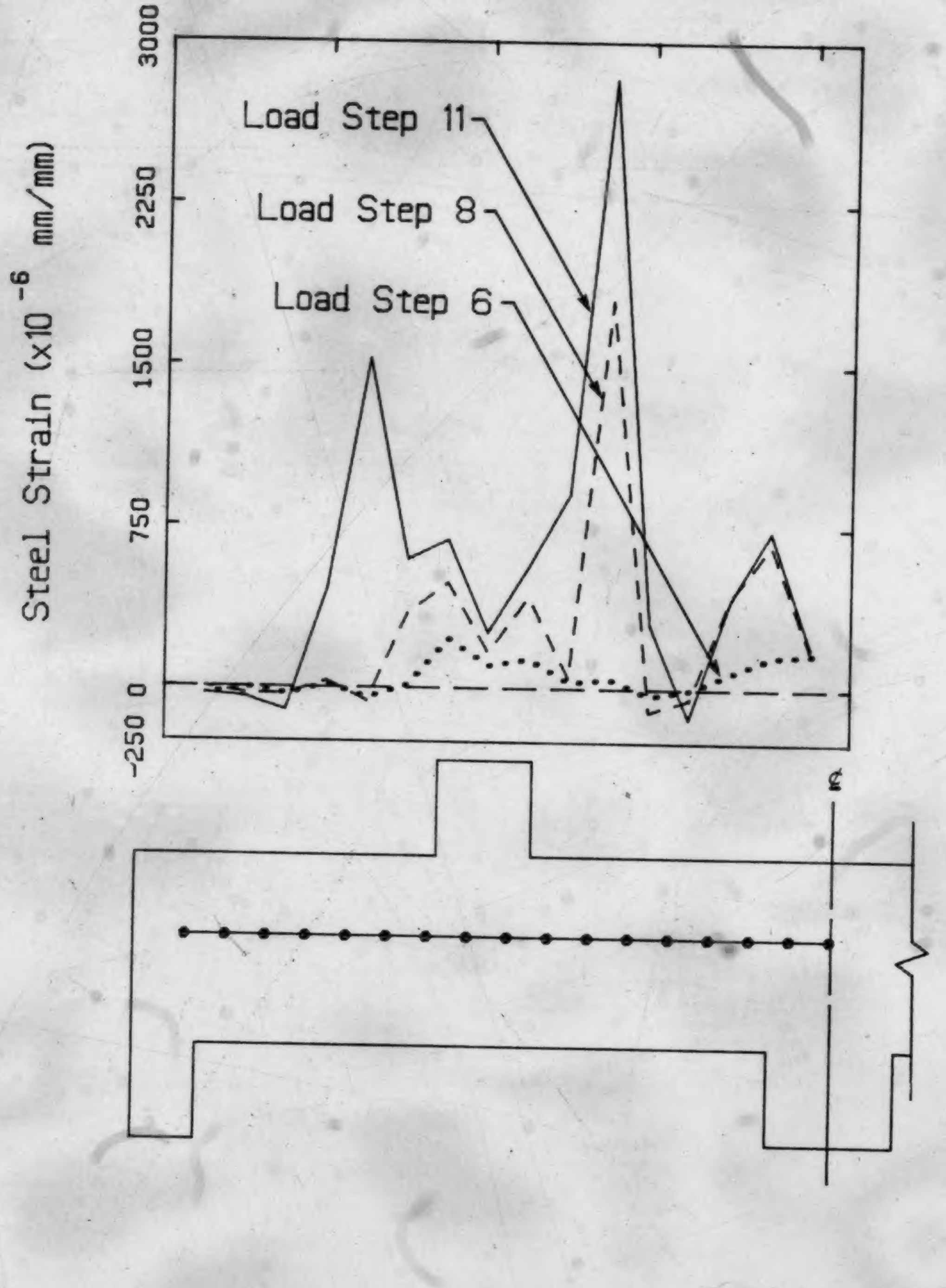

Figure 4.24 Typical Steel Strain Distribution in a Horizontal Stirrup

5. SUMMARY AND CONCLUSIONS

5.1 Behaviour

1) For the beams tested, the initiation of an inclined crack was not from the top or bottom face of the beam but from a region near the mid-depth. The first inclined cracks formed were not fully developed inclined cracks. The critical inclined cracks formed followed the thrust line joining the load point to the support.
2) Strains in the flexural reinforcement before first inclined cracking were consistent with the elastic bending moment. After inclined cracking, the point of zero strain in the negative moment flexural reinforcement in the interior shear spans moved towards the loading columns and the point of zero strain in the positive moment flexural reinforcement moved towards the interior supporting column. At the failure load, the entire length of the positive moment reinforcement is expected to be in tension. Strains in the positive moment reinforcement near the end supports increased much higher than zero, approaching the magnitude of the strain at the midspan. This result indicated that a high amount of arch action had occurred. When extrapolated to the failure load, the strains in the flexural reinforcement were generally below the yield

point strain.

3) Before inclined cracking, the vertical web reinforcement experienced very little or no deformation. Large deformation occurred immediately after inclined cracking. Strains in the vertical web reinforcement that crossed a critical inclined crack, when extrapolated to failure load, were generally greater than the yield point strain. The vertical web reinforcement can be considered to have reached its full yield strength.
4) Strains in the horizontal web reinforcement that crossed a critical inclined crack, when extrapolated to failure load, were beyond the yield point strain. Full yield strength was realized by the horizontal web reinforcement.
5) Strains in the concrete indicated a compression strut existed between the loading and supporting columns with very high compressive strains at the regions near the faces of the loading and supporting columns. The magnitude of the strain was sufficient to cause crushing of the concrete. In the middle of the shear span, at mid-depth, compressive strains were in both principal directions. No tensile strain existed at that region. The direction of the principal compressive strain indicated a widening of the compressive strut at the middle of the shear span.
6) All the beams were able to sustain higher loads than the first inclined cracking load before final failure.

Sliding along the inclined crack was the major cause of failure of the beams.

7) The shearing force and bending moment diagrams of the beams at first inclined cracking load were predicted accurately using the elastic beam theory provided that the differential settlement of the interior support with respect to the end supports was not excessive. At loads near the failure load, the interior support reaction was less than anticipated from elastic theory and the elastic beam theory could not be used to compute moments and shears. The behaviour of the beams was inelastic at loads near the failure load.
8) The presence of web reinforcement had the effect of reducing the midspan deflection. Orthogonal web reinforcement appeared to be more effective than horizontal web reinforcement alone in deflection control. Low concrete strength resulted in high midspan deflection.
9) The anchorage and bearing details of the beams proved to be adequate during the test.

5.2 Strength

1) Horizontal web reinforcement had no apparent influence on the first inclined cracking and ultimate shear capacities of deep beams with an x/d ratio of 1.43.

2) Vertical web reinforcement was effective in increasing the first inclined cracking and ultimate shear capacities of deep beams with an *x/d* ratio of 1.43.

3) A reduction in concrete strength resulted in the reduction of the first inclined cracking and ultimate shear capacities.

4) The first inclined cracking shear capacity of the interior shear spans was predicted fairly accurately by the de Cossio and Siess formula provided that the *V.d/M* ratio was replaced by an equivalent *d/a* ratio for the span and the constant 4600 replaced by 11500.

5) The deep beam provisions of the ACI 318-77 for the ultimate shear capacity were very unconservative with respect to the actual ultimate shear capacity of the interior shear span. After the *Vu.d/Mu* ratio was replaced by an equivalent *d/x* ratio for the span, very conservative results were obtained. The shear carried by the horizontal and vertical web reinforcements according to the ACI Code was unconservative and very conservative, respectively.

BIBLIOGRAPHY

ACI-ASCE Committee 326, "Shear and Diagonal Tension," American Concrete Institute Journal, *Proceedings*, Vol. 59, Feb., 1962, pp. 277 - 334.

ACI-ASCE Committee 426, "The Strength of Reinforced Concrete Members," *Journal of the Structural Division*, ASCE, Vol. 99, No. ST6, June, 1973, pp. 1091 - 1187.

ACI Committee 318, "Building Code Requirements for Reinforced Concrete (ACI 318-77)," American Concrete Institute, Detriot, Mich., 1977.

ACI Committee 318, "Commentary on Building Code Requirements for Reinforced Concrete (ACI 318-77)," American Concrete Institute, Detroit, Mich., 1977.

ACI-ASCE Committee 426, "Suggested Revisions to Shear Provisions for Building Code," American Concrete Institute Journal, *Proceedings*, Vol. 74, No. 9, Sept., 1977, pp. 458 - 468.

Bresler, B., and MacGregor, J.G., "Review of Concrete Beams Failing in Shear," *Journal of the Structural Division*, ASCE, Vol. 93, No. ST1, Proc. Paper 5106, Feb., 1967, pp. 343 - 372.

Baumann, T., "Experiments to Study the Dowelling Action of Flexural Tensile Reinforcement in a Reinforced Concrete Beam," *Bericht Nr. 77*, Munich Technischen Hochschule, 1968 (English Translation by Portland Cement Association).

Comité Europeén du Béton, "International Recommendations for the Design and Construction of Deep Beams," *Information Bulletin No. 73*, Paris, France, June, 1970, pp. 19 - 24.

Crist, R.A., "Static and Dynamic Shear Behaviour of Uniformly Loaded Reinforced Concrete Beams," thesis presented to The University of New Mexico at Albuquerque, New Mexico, in partial fulfilment of the requirements for the degree of Doctor of Philosophy, May, 1971.

CSA Standard CAN3-A23.3-M77, "Code for the Design of Concrete Structures for Buildings," Canadian Standards Association, Rexdale, Ontario, 1977.

de Paiva, H.A.R., and Siess, C.P., "Strength and Behaviour of Deep Beams in Shear," *Journal of the Structural Division*, ASCE, Vol. 91, No. ST5, Proc. Paper 4496, Oct., 1965, pp. 19 - 41.

Diaz de Cossio, R., and Siess, C. P., "Behaviour and Strength in Shear of Beams and Frames Without Web Reinforcement," American Concrete Institute Journal, *Proceedings*, Vol. 56, No. 2, Feb., 1960, pp. 695 - 735.

Dulacska, H., "Dowel Action of Reinforcement Crossing Cracks in Concrete," American Concrete Institute Journal, *Proceedings*, Vol. 69, No. 12, Dec., 1972, pp. 754 - 757.

Fenwick, R.C., and Paulay, T., "Mechanisms of Shear Resistance of Concrete Beams," *Journal of the Structural Division*, ASCE, Vol. 94, No. ST10, Proc. Paper 6167, Oct., 1968, pp. 2325 - 2350.

Hofbeck, J.A., Ibrahim, I.O., and Mattock, A.H., "Shear Transfer in Reinforced Concrete," American Concrete Institute Journal, *Proceedings*, Vol. 66, No. 2, Feb., 1969, pp. 119 - 128.

Kong, F.K., Robins, P.J., and Cole, D.F., "Web Reinforcement Effects on Deep Beams," American Concrete Institute Journal, *Proceedings*, Vol. 67, No. 12, Dec., 1970, pp. 1010 - 1017.

Kong, F.K., and Robins, P.J., "Web Reinforcement Effects on Lightweight Concrete Deep Beams," American Concrete Institute Journal, *Proceedings*, Vol. 68, No. 7, July, 1971, pp. 514 - 520.

Kong, F.K., Robins, P.J., Kirby, D.P., and Short, D.R., "Deep Beams With Inclined Web Reinforcement," American Concrete Institute Journal, *Proceedings*, Vol. 69, No. 3, March, 1972, pp. 172 - 176.

Kong, F.K., and Singh, A., "Diagonal Cracking and Ultimate Loads of Lightweight Deep Beams," American Concrete Institute Journal, *Proceedings*, Vol. 69, No. 8, Aug., 1972, pp. 512 - 521.

Kong, F.K., Robins, P.J., Singh, A., and Sharp, G.R., "Shear Analysis and Design of Reinforced Concrete Deep Beams," *The Structural Engineer*, Vol. 50, No. 10, Oct., 1972 pp. 405 - 409.

Kong, F.K., Robins, P.J., and Sharp, G.R., "The Design of Reinforced Concrete Deep Beams in Current Practice," *The Structural Engineer*, Vol. 53, No. 4, April, 1975, pp. 173 - 180.

Krefeld, W.J., and Thurston, C.W., "Contribution of Longitudinal Steel to Shear Resistance of Reinforced Concrete Beams," American Concrete Institute Journal, *Proceedings*, Vol. 63, No. 3, March, 1966, pp. 325 - 344.

Leonhardt, F., Discussion of "Strength and Behaviour of Deep Beams in Shear" by de Paiva, H.A.R. and Siess, C.P., *Journal of the Structural Division*, ASCE, Vol. 92, No. ST2, April, 1966, pp. 427 - 432.

Luapa, A., Siess, C.P., and Newmark, N.M., "Strength in Shear of Reinforced Concrete Beams," *Bulletin No. 428*, Engineering Experiment Station, University of Illinois, Urbana, Ill., March, 1959.

MacGregor, J.G., "The Design of Reinforced Concrete Beams for Shear," *Shear in Reinforced Concrete*, SP-42, American Concrete Institute, Vol. 2, Detroit, Mich., 1974, pp. 503 - 537.

MacGregor, J.G., and Gergely, P., "Suggested Revisions to ACI Building Code Clauses Dealing With Shear in Beams," American Concrete Institute Journal, *Proceedings*, Vol. 74, No. 10, Oct., 1977, pp. 493 - 500.

MacGregor, J.G., and Hawkins, N.M., "Suggested Revisions to ACI Building Code Clauses Dealing With Shear Friction and Shear in Deep Beams and Corbels," American Concrete Institute Journal, *Proceedings*, Vol. 74, No. 11, Nov., 1977, pp. 537 - 545.

Manuel, R.F., Slight, B.W., and Suter, G.T., "Deep Beam Behaviour Affected by Length and Shear Span Variations," American Concrete Institute Journal, *Proceedings*, Vol. 68, No. 12, Dec., 1971, pp. 954 - 958.

Manuel, R.F., "Failure of Deep Beams," *Shear in Reinforced Concrete*, SP-42, American Concrete Institute, Vol. 2, Detroit, Mich., 1974, pp. 425 - 440.

Mattock, A.H., and Hawkins, N.M., "Shear Transfer in Reinforced Concrete - Recent Research," *Prestressed Concrete Institute Journal*, Vol. 17, No. 2, March-April, 1972, pp. 55 - 75.

Mattock, A.H., "Shear Transfer in Concrete Having Reinforcement at an Angle to the Shear Plane," *Shear in Reinforced Concrete*, SP-42, American Concrete Institute, Vol. 1, Detroit, Mich., 1974, pp. 17 - 42.

Park, R. and Paulay, T., *"Reinforced Concrete Structures,"* John Wiley and Sons, New York, 1975, pp. 637 - 662 and 700 - 716.

Paulay, T., "Coupling Beams of Reinforced Concrete Shear Walls," *Journal of the Structural Division*, ASCE, Vol. 97, No. ST3, Proc. Paper 7984, March, 1971, pp. 843 - 862.

Paulay, T., "Simulated Seismic Loading of Spandrel Beams," *Journal of the Structural Division*, ASCE, Vol. 97, No. ST9, Proc. Paper 8365, Sept., 1971, pp. 2407 - 2419.

Paulay, T., and Binney, J.R., "Diagonally Reinforced Coupling Beams of Shear Walls," *Shear in Reinforced Concrete*, SP-42, American Concrete Institute, Vol. 2, Detroit, Mich., 1974, pp. 579 - 598.

Ramakrisnan, V., and Ananthanarayana, Y., "Ultimate Strength of Deep Beams in Shear," American Concrete Institute Journal, *Proceedings*, Vol. 65, No. 2, Feb., 1968, pp. 87 - 98.

Smith, K.N., and Ferigh, S.M., "Effect of Loading and Supporting Conditions on the Shear Strength of Deep Beams," *Shear in Reinforced Concrete*, SP-42, American Concrete Institute, Vol. 2, Detroit, Mich., 1974, pp. 441 - 460.

Suarez, J.J., and Nilson, A.H., "Deep Reinforced Concrete Members: State of the Art," Report of the Department of Structural Engineering, Cornell University, Ithaca, N.Y., Aug., 1974.

Suarez, J.J., "Unified Shear Design Theory for Reinforced Concrete Deep Members," thesis presented to Cornell University at Ithaca, N.Y., in partial fulfilment of the requirements for the degree of Doctor of Philosophy, Aug., 1977.

Swamy, R.N., and Andripoulos, A.D., "Contribution of Aggregate Interlock and Dowel Forces to the Shear Resistance of Reinforced Beams With Web Reinforcement," *Shear in Reinforced Concrete*, SP-42, American Concrete Institute, Vol. 1, Detroit, Mich., 1974, pp. 129 - 166.

Taylor, H.P.J., "Shear Stress in Reinforced Concrete Beams Without Web Reinforcement," *Technical Report TRA 407*, Cement and Concrete Association, London, England, Feb., 1968, 23 pp.

Taylor, H.P.J., "Investigation of the Dowel Shear Forces Carried by the Tensile Steel in Reinforced Concrete Beams," *Technical Report TRA 431*, Cement and Concrete Association, London, England, Nov., 1969, 24 pp.

Taylor, H.P.J., "Investigation of the Forces Carried Across Cracks in Reinforced Concrete Beams in Shear by Interlock of Aggregates," *Technical Report 42.477*, Cement and Concrete Association, London, England, Nov., 1970, 22 pp.

Taylor, H.P.J., "The Fundamental Behaviour of Reinforced Concrete Beams in Bending and Shear," *Shear in Reinforced Concrete*, SP-42, American Concrete Institute, Vol. 1, Detroit, Mich., 1974, pp. 43 - 77.

Taylor, H.P.J., "Web Crushing - A Review of Research," *Technical Report 42.509*, Cement and Concrete Association, London, England, Aug., 1975, 16 pp.

Zsutty, T., "Beam Shear Strength Prediction by Analysis of Existing Data," American Concrete Institute Journal, *Proceedings*, Vol. 65, No. 11, Nov., 1968, pp. 943 - 951.

Zsutty, T., "Shear Strength Prediction for Separate Categories of Simple Beam Tests," American Concrete Institute Journal, *Proceedings*, Vol. 68, No. 2, Feb., 1971, pp. 138 - 143.

APPENDIX A

Plots of Jack Load versus Midspan Deflection of Beams No. 2, 3 and 4

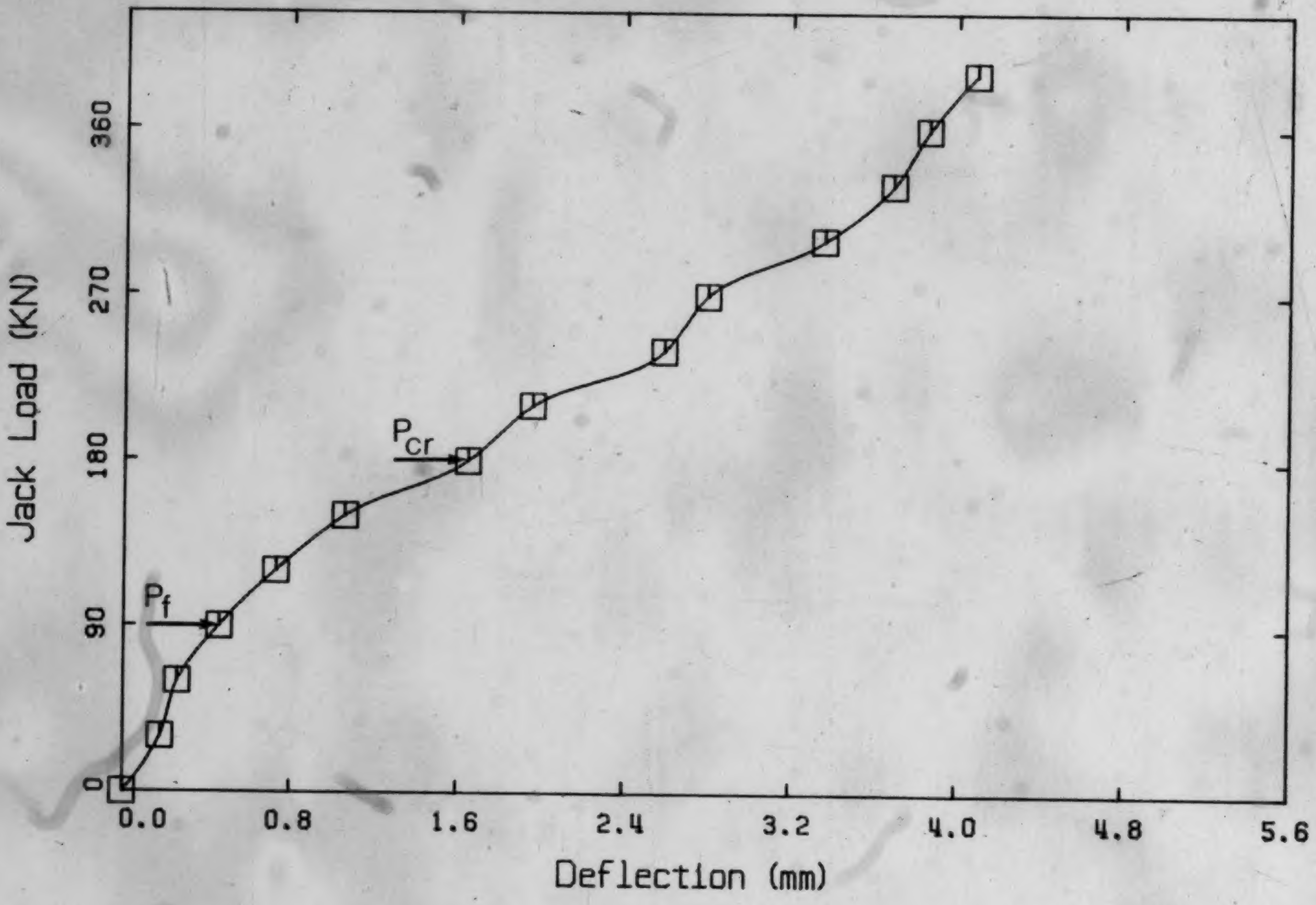

Figure A.1 Plot of Jack Load Versus North Midspan Deflection of Beam No. 2

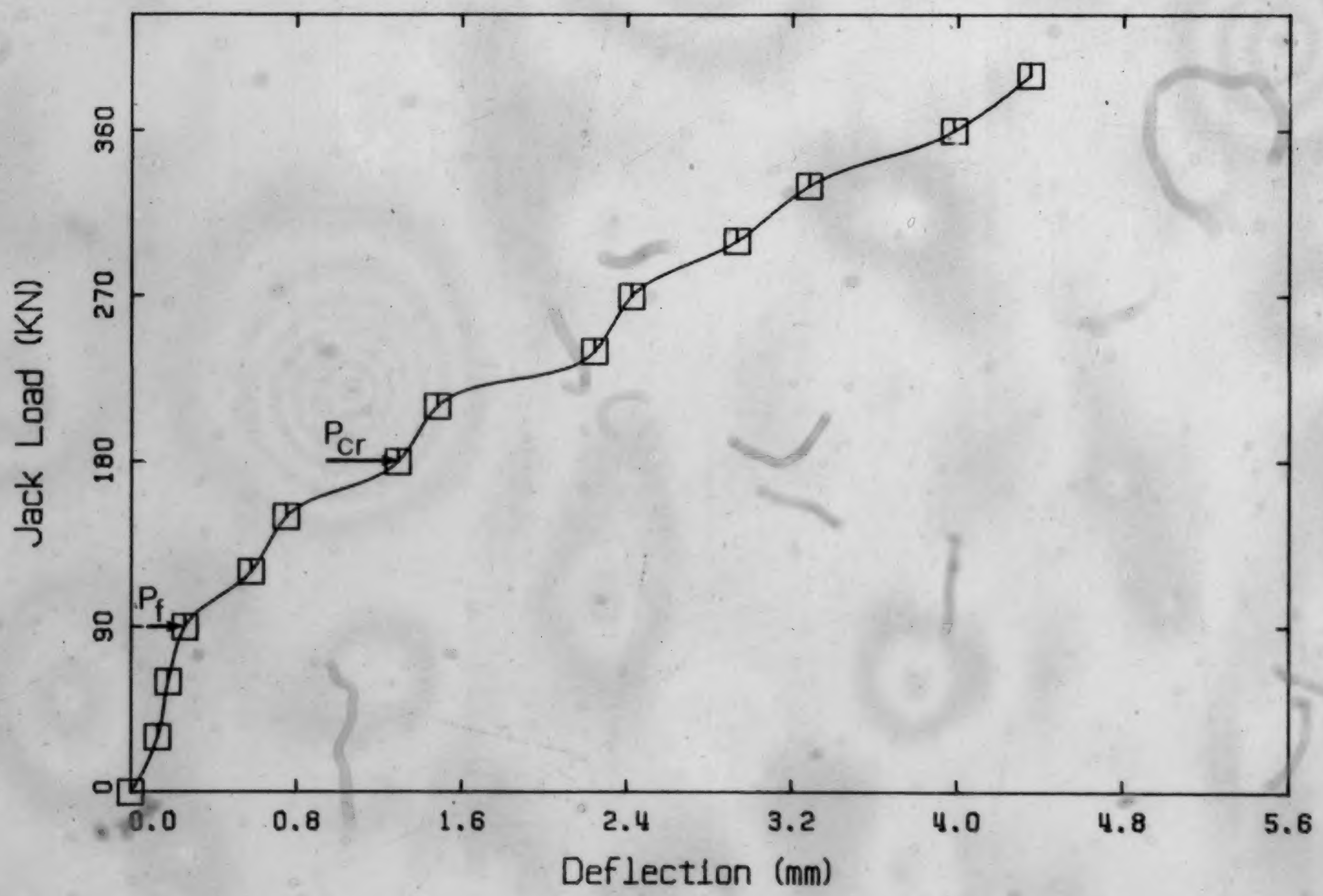

Figure A.2 Plot of Jack Load Versus South Midspan Deflection of Beam No. 2

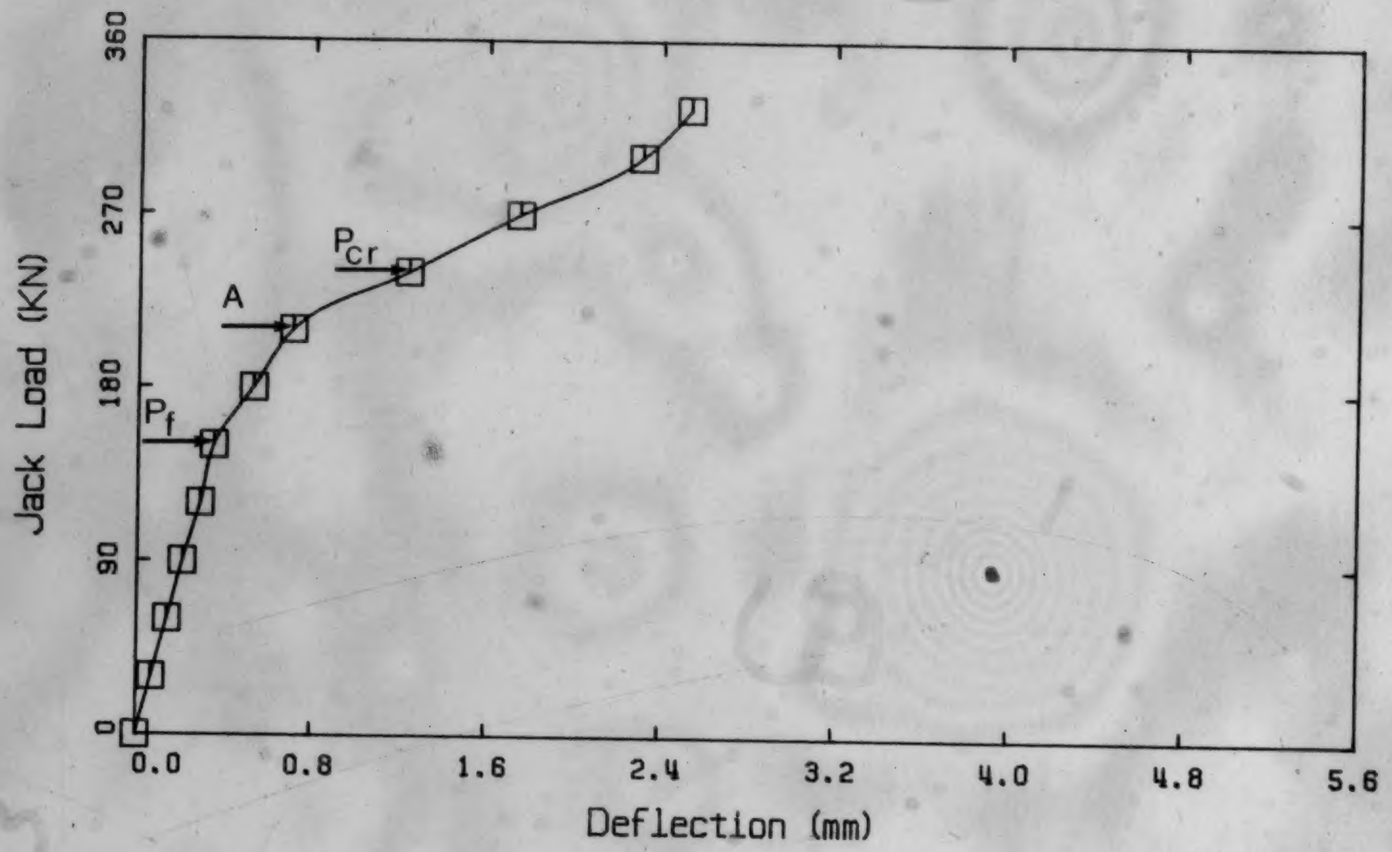

Figure A.3 Plot of Jack Load Versus North Midspan Deflection of Beam No. 3

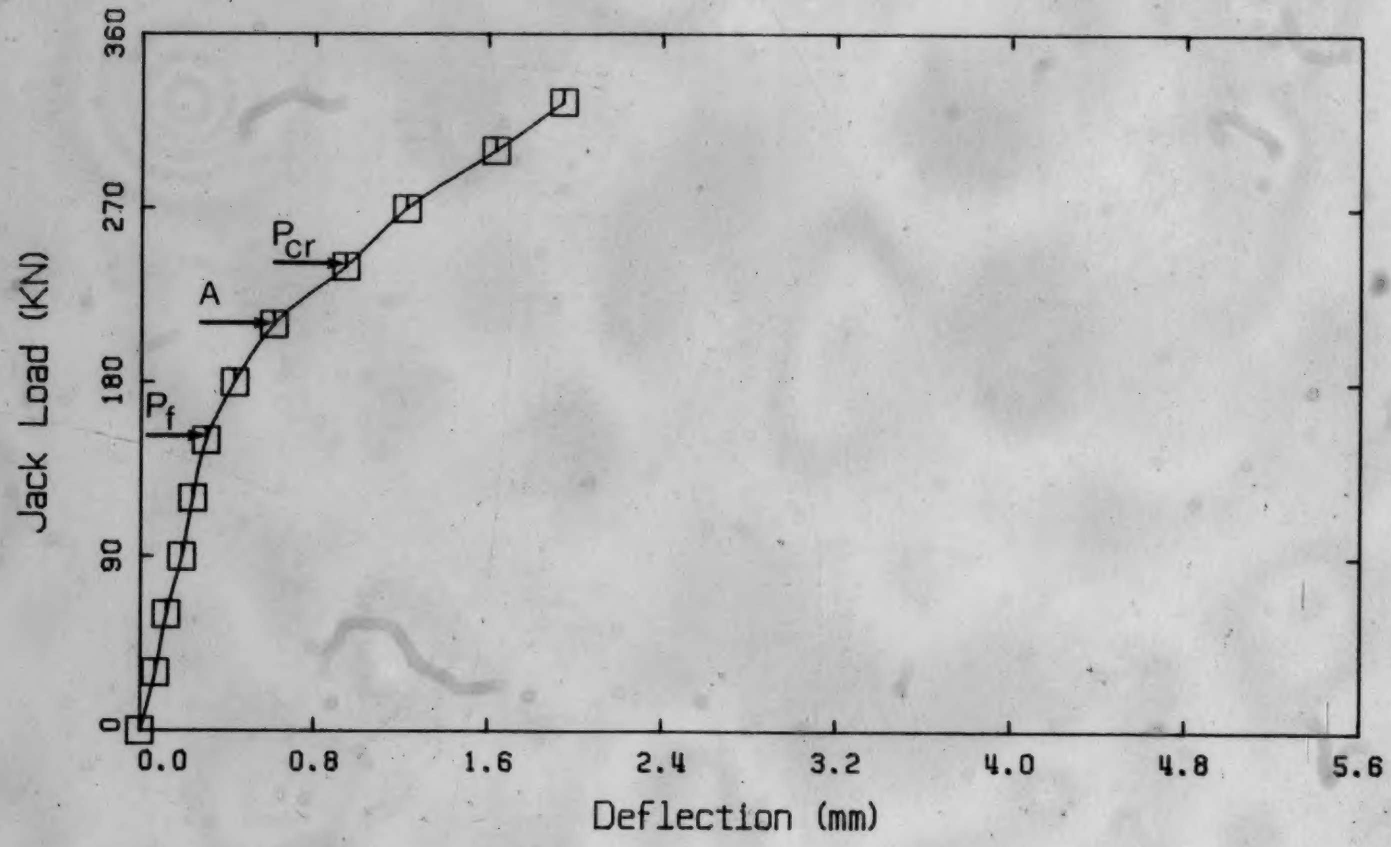

Figure A.4 Plot of Jack Load Versus South Midspan Deflection of Beam No. 3

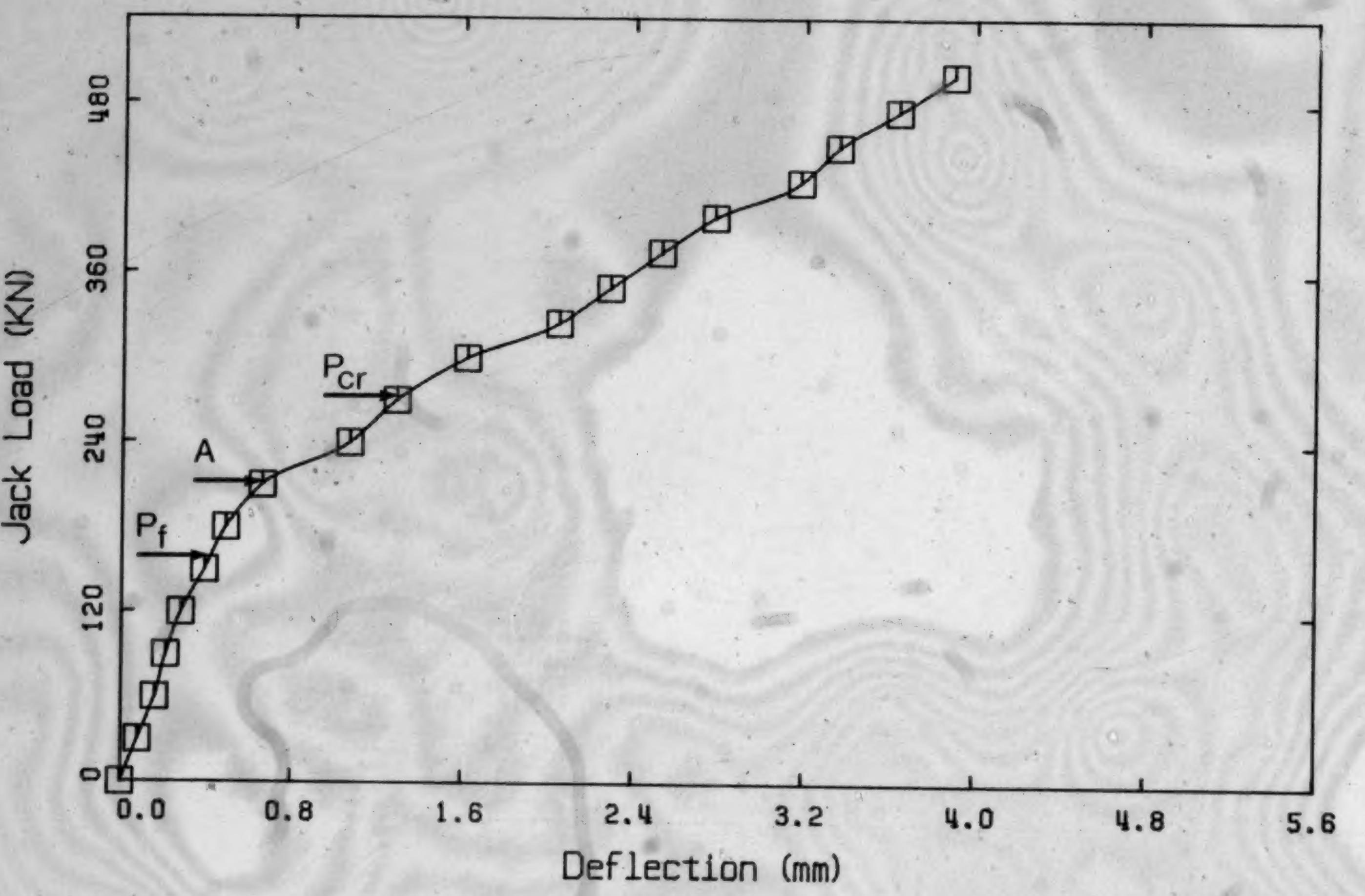

Figure A.5 Plot of Jack Load Versus North Midspan Deflection of Beam No. 4

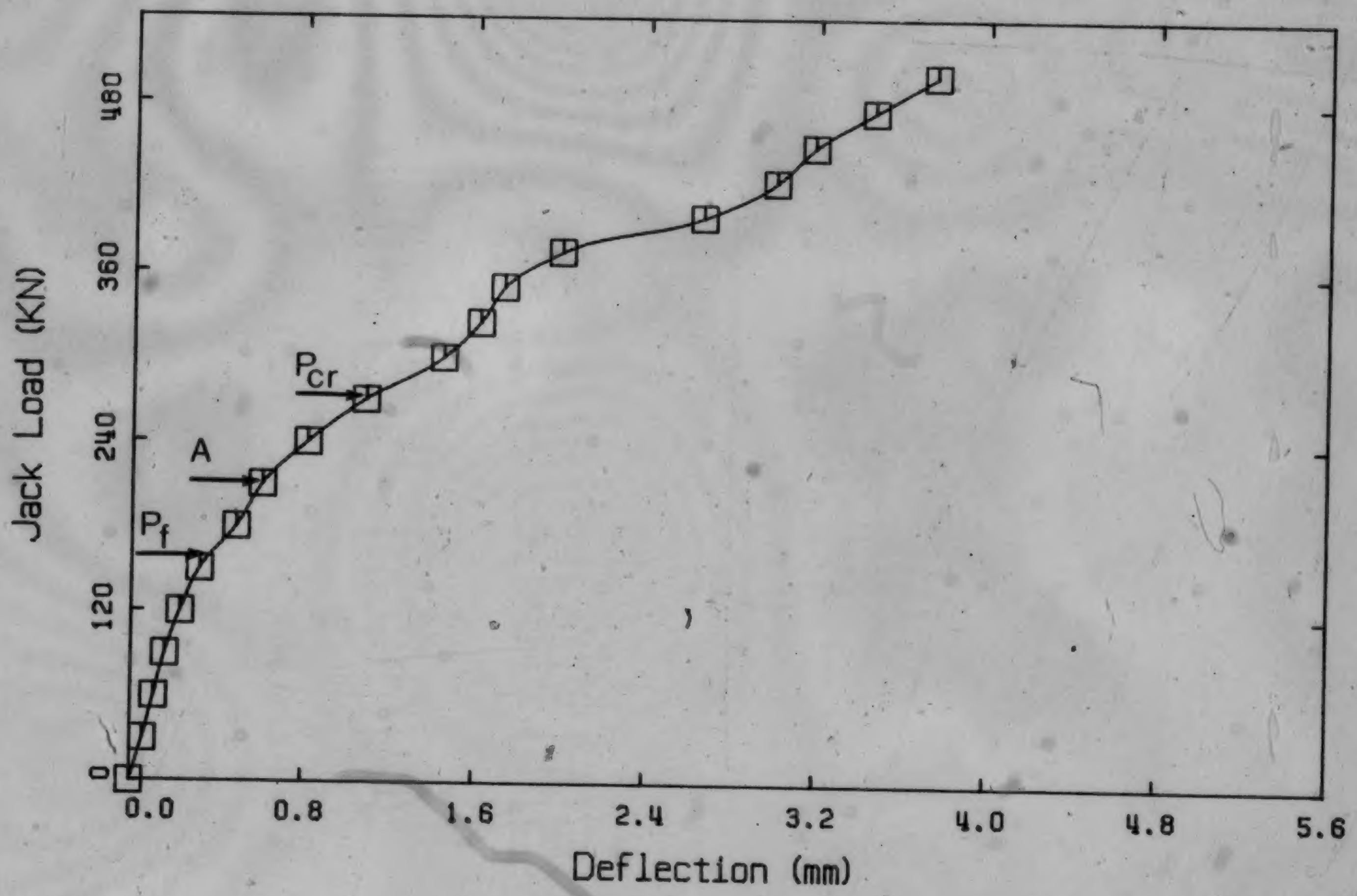

Figure A.6 Plot of Jack Load Versus South Midspan Deflection of Beam No. 4

APPENDIX B

Plots of Jack Load versus Support Settlement of Beams No. 2, 3 and 4

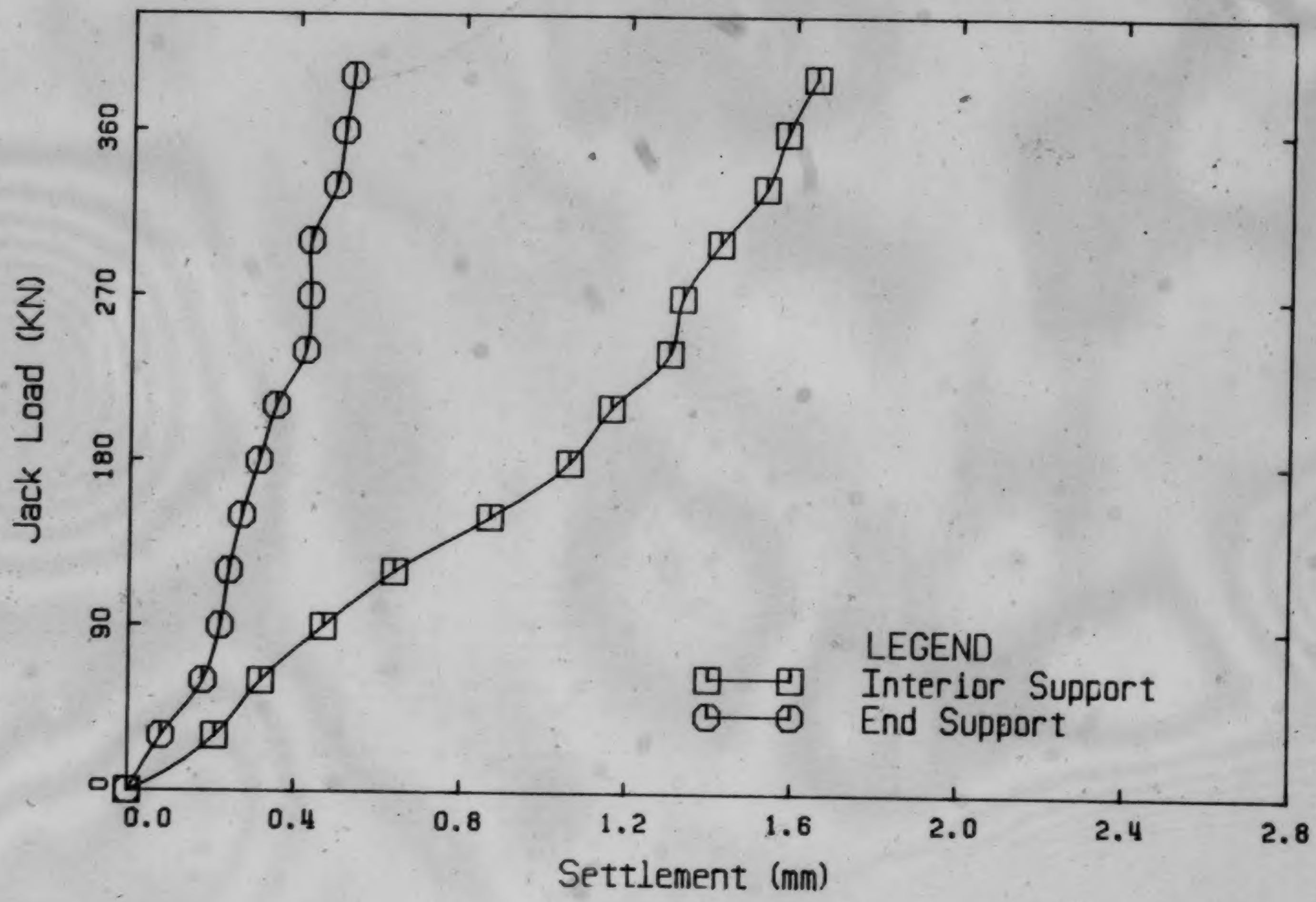

Figure B.1 Plot of Jack Load Versus Support Settlement of Beam No. 2

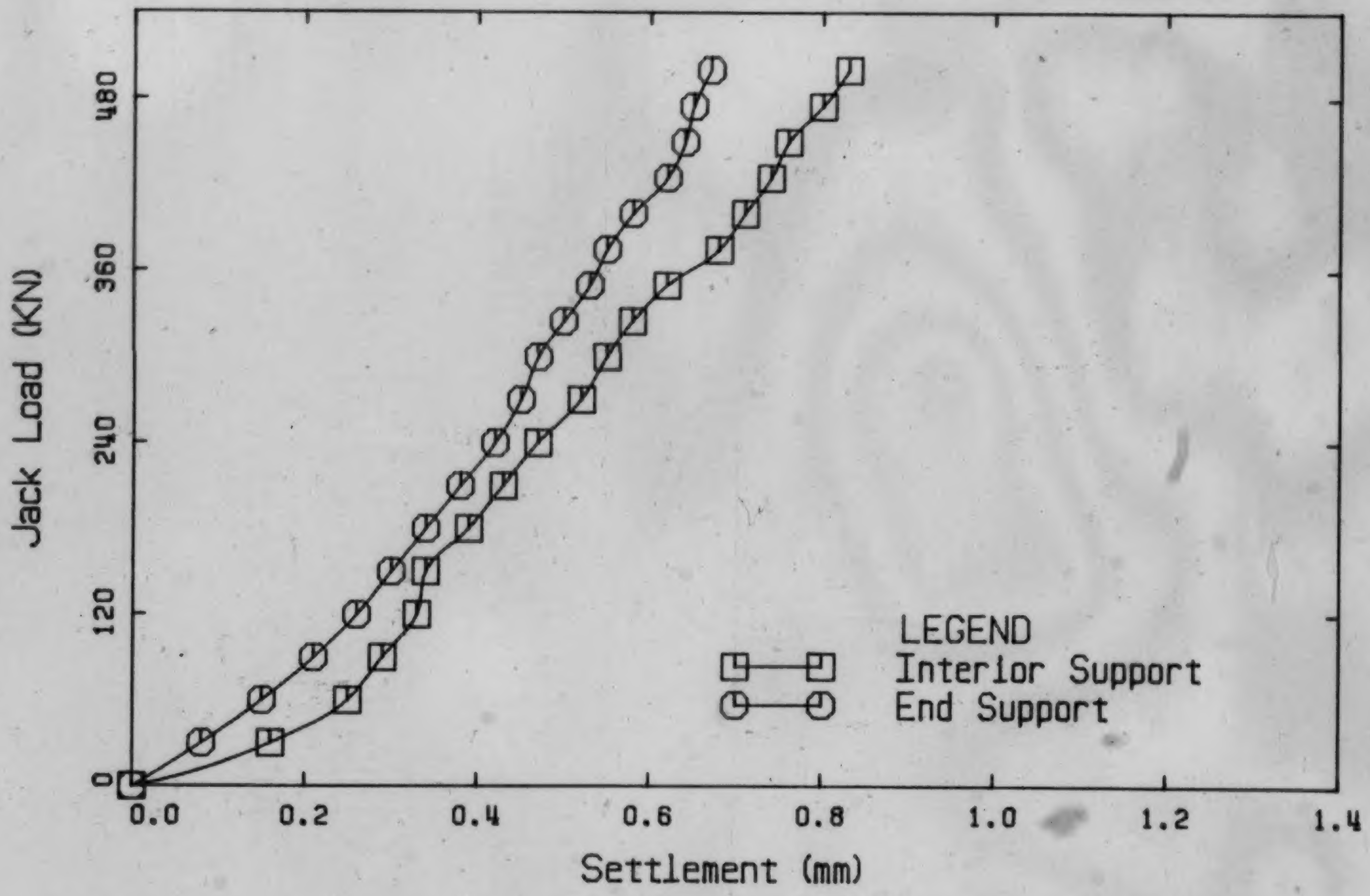

Figure B.2 Plot of Jack Load Versus Support Settlement of Beam No. 3

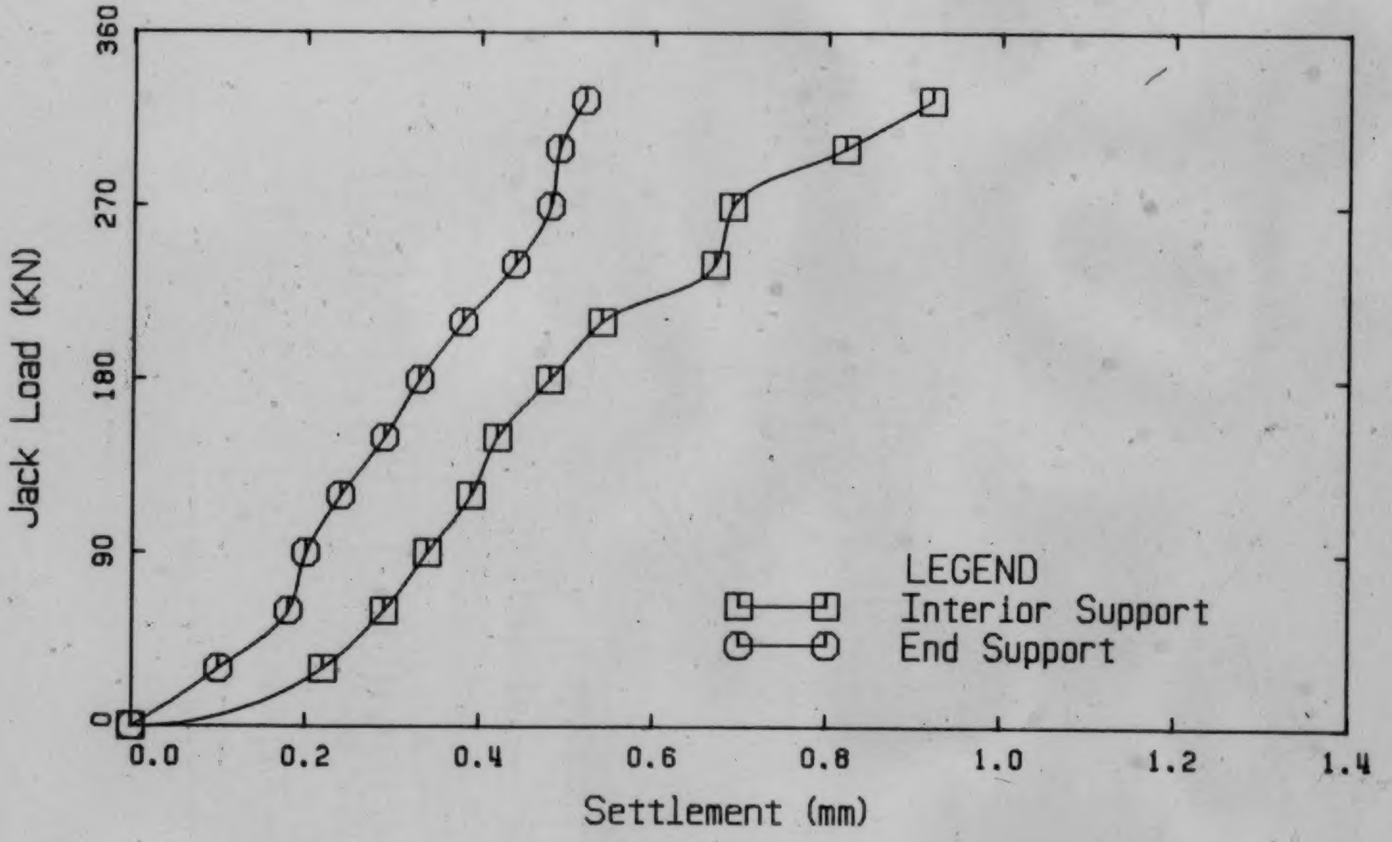

Figure B.3 Plot of Jack Load Versus Support Settlement of Beam No. 4

APPENDIX C

Plots of Jack Load versus Midspan Deflection of Beams No. 1, 2, 3 and 4 from the Retest

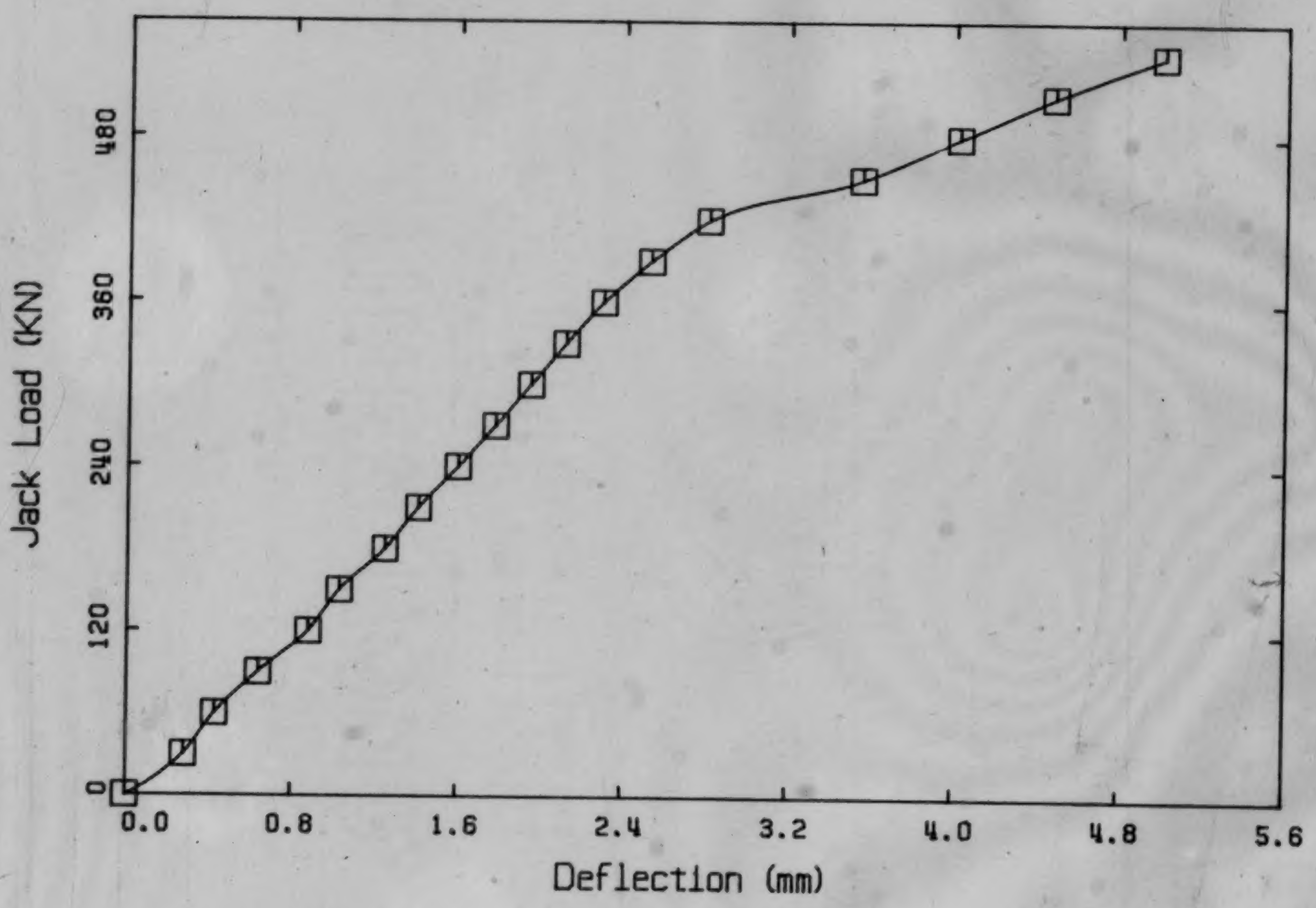

Figure C.1 Plot of Jack Load Versus North Midspan Deflection from the Retest of Beam No. 1

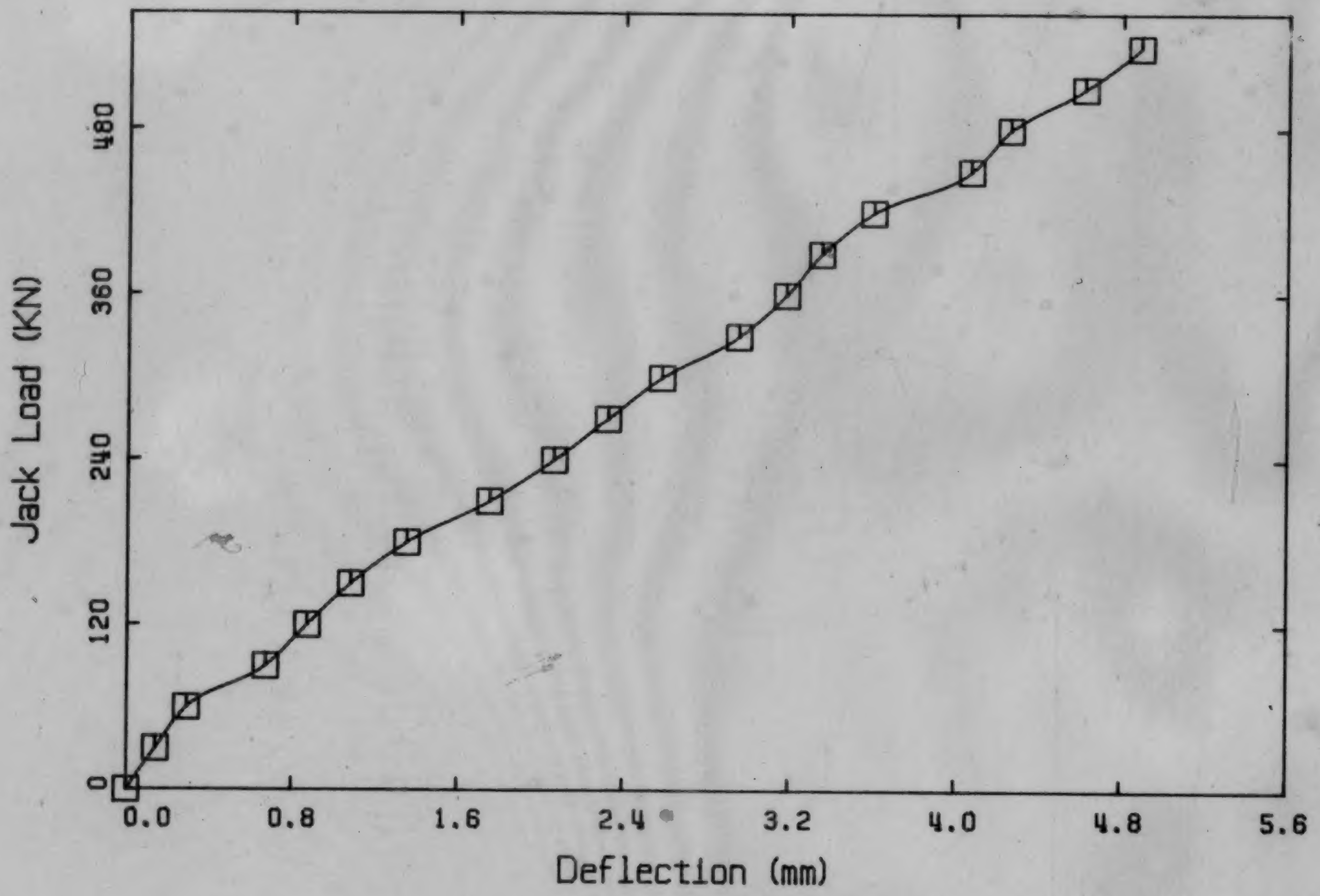

Figure C.2 Plot of Jack Load Versus South Midspan Deflection from the Retest of Beam No. 1

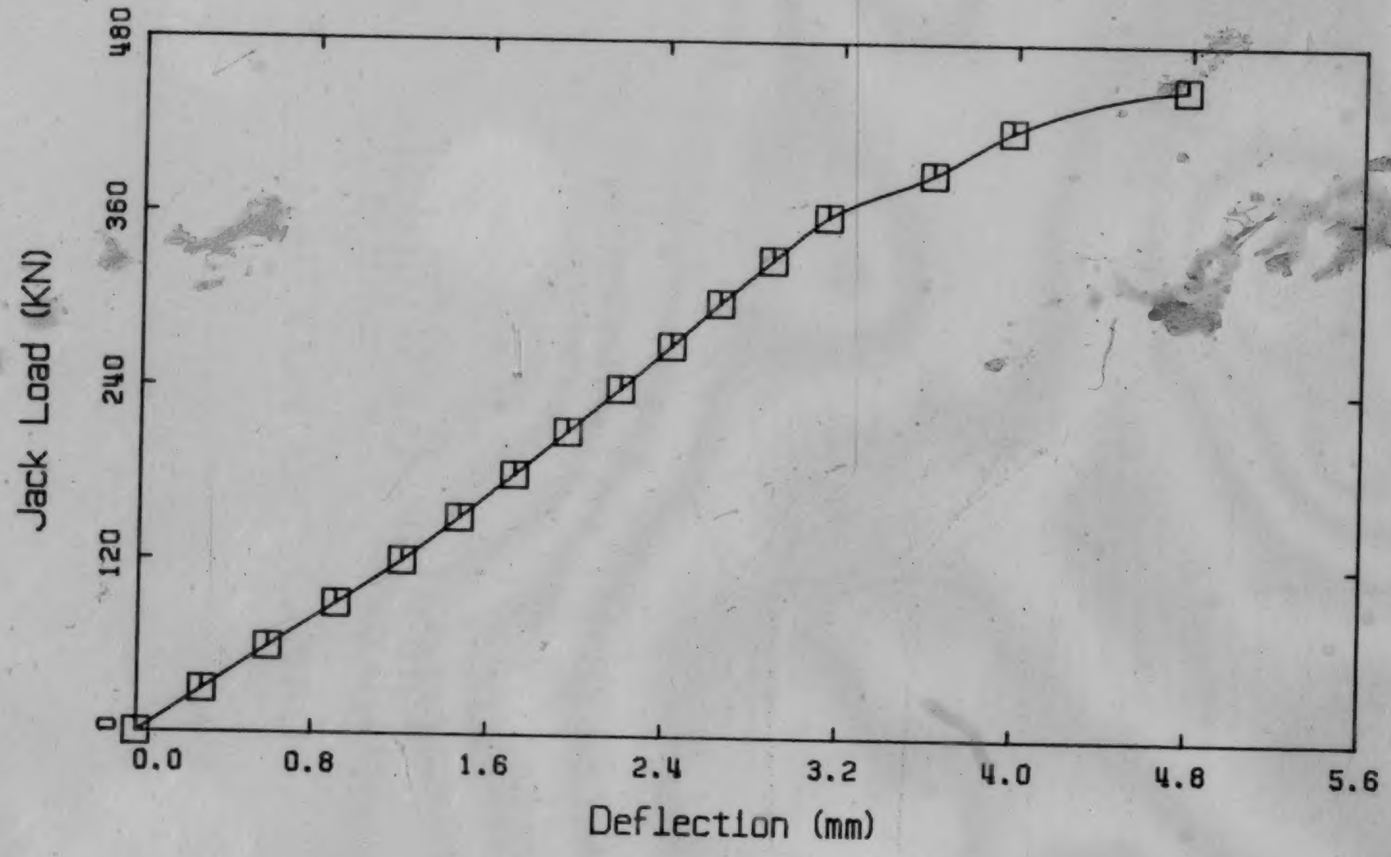

Figure C.3 Plot of Jack Load Versus North Midspan Deflection from the Retest of Beam No. 2

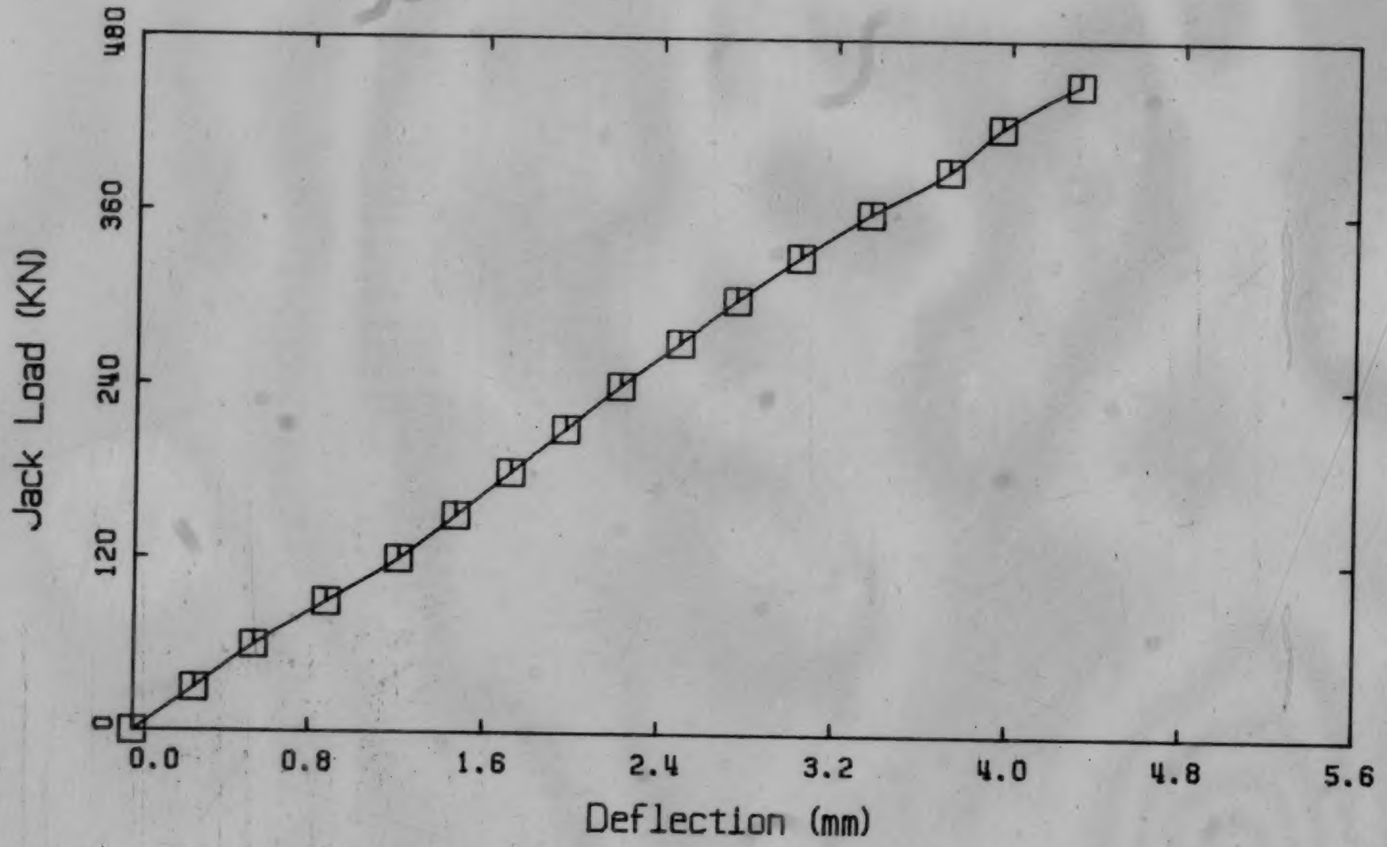

Figure C.4 Plot of Jack Load Versus South Midspan Deflection from the Retest of Beam No. 2

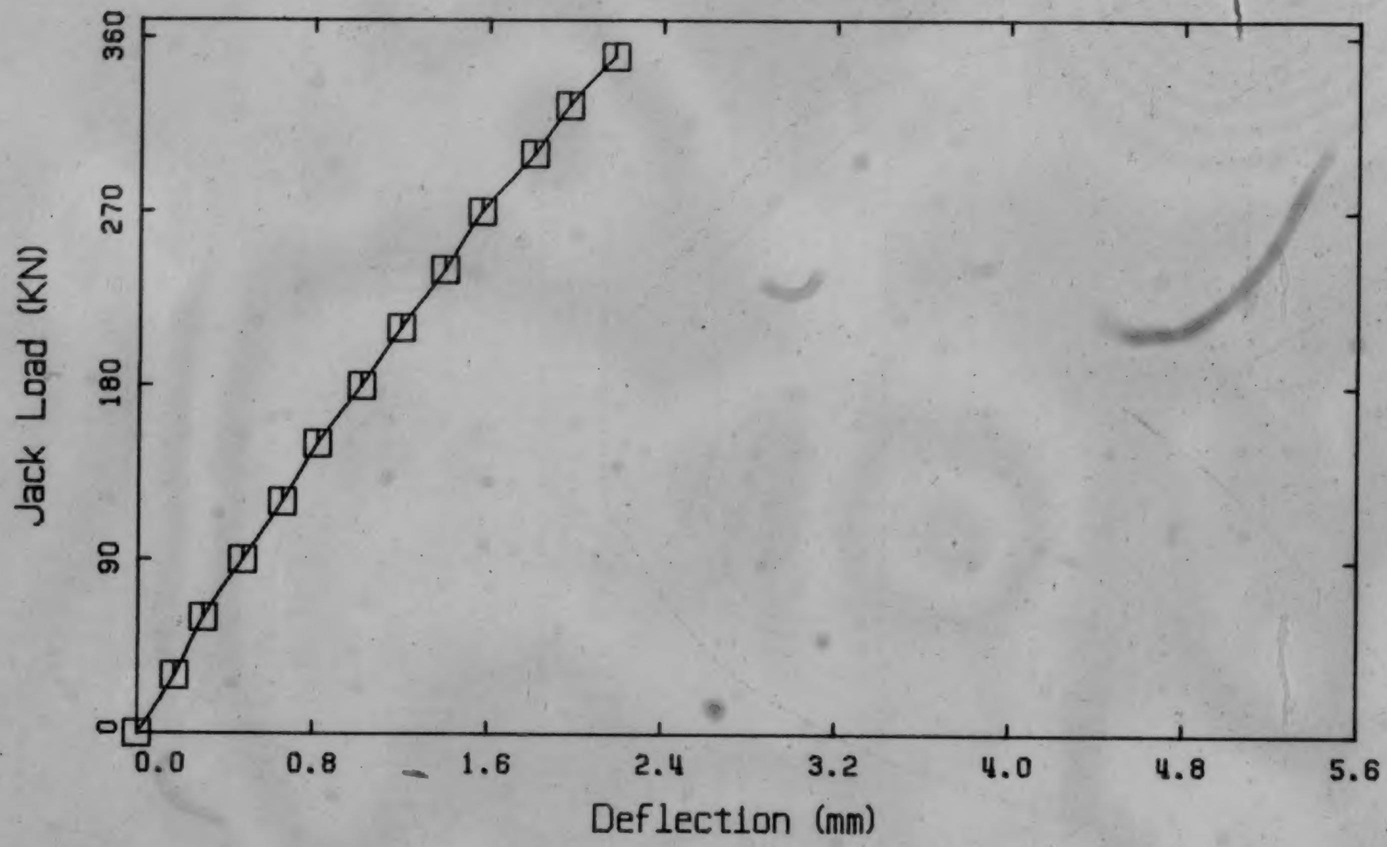

Figure C.5 Plot of Jack Load Versus North Midspan Deflection from the Retest of Beam No. 3

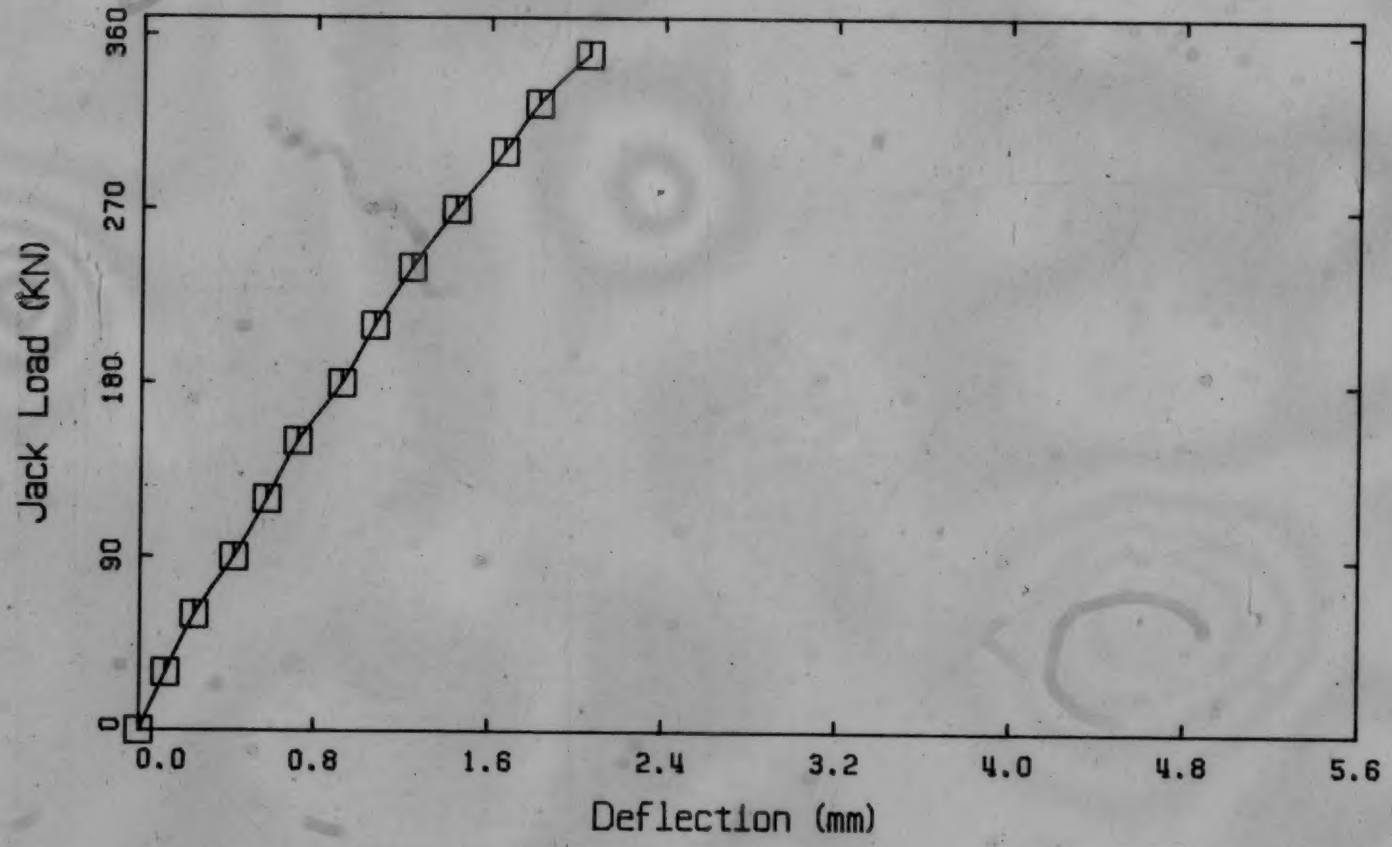

Figure C.6 Plot of Jack Load Versus South Midspan Deflection from the Retest of Beam No. 3

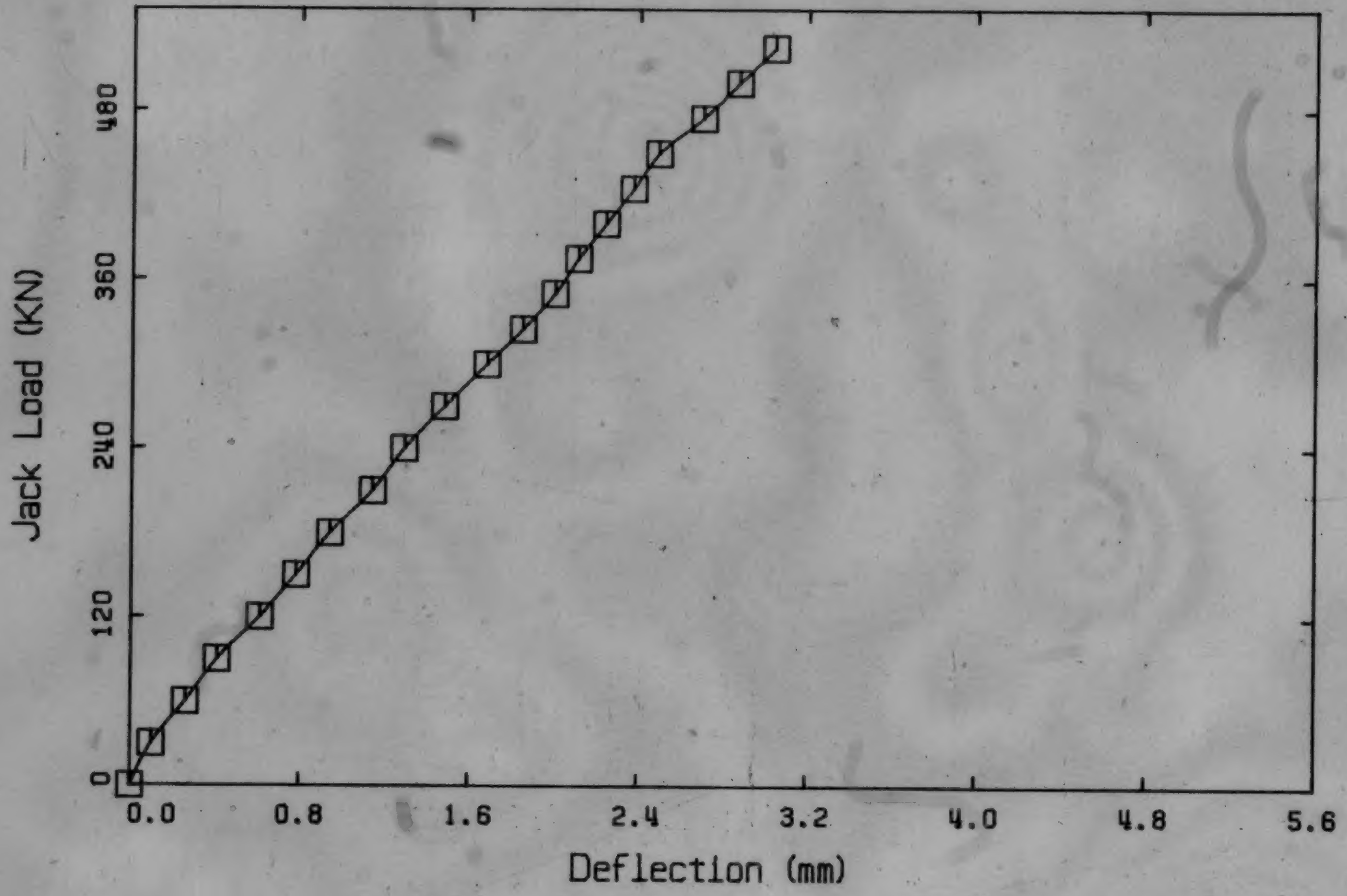

Figure C.7 Plot of Jack Load Versus North Midspan Deflection from the Retest of Beam No. 4

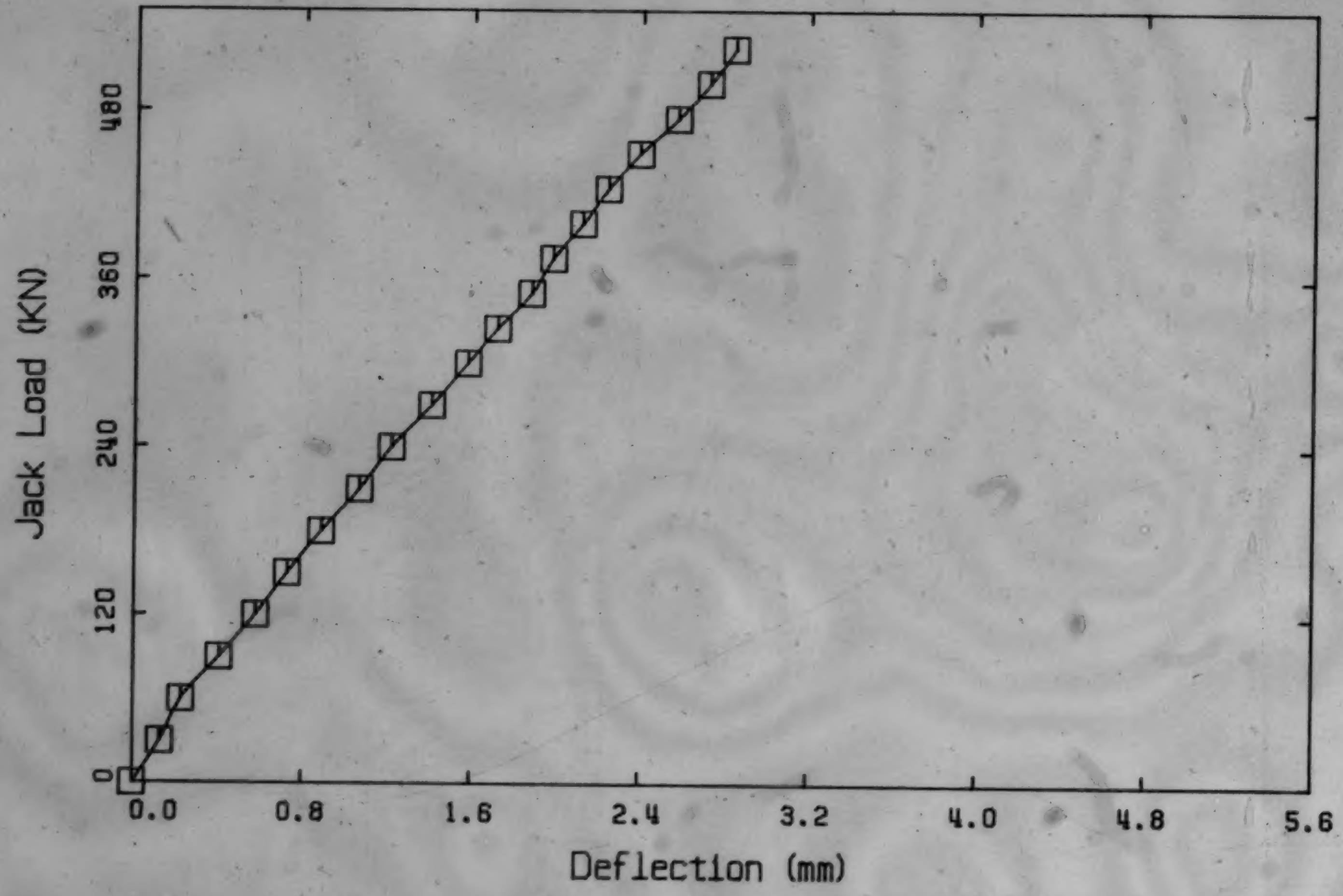

Figure C.8 Plot of Jack Load Versus North Midspan Deflection from the Retest of Beam No. 4

APPENDIX D

Plots of Jack Load versus Support Settlement of Beams No. 1, 2, 3 and 4 from the Retest

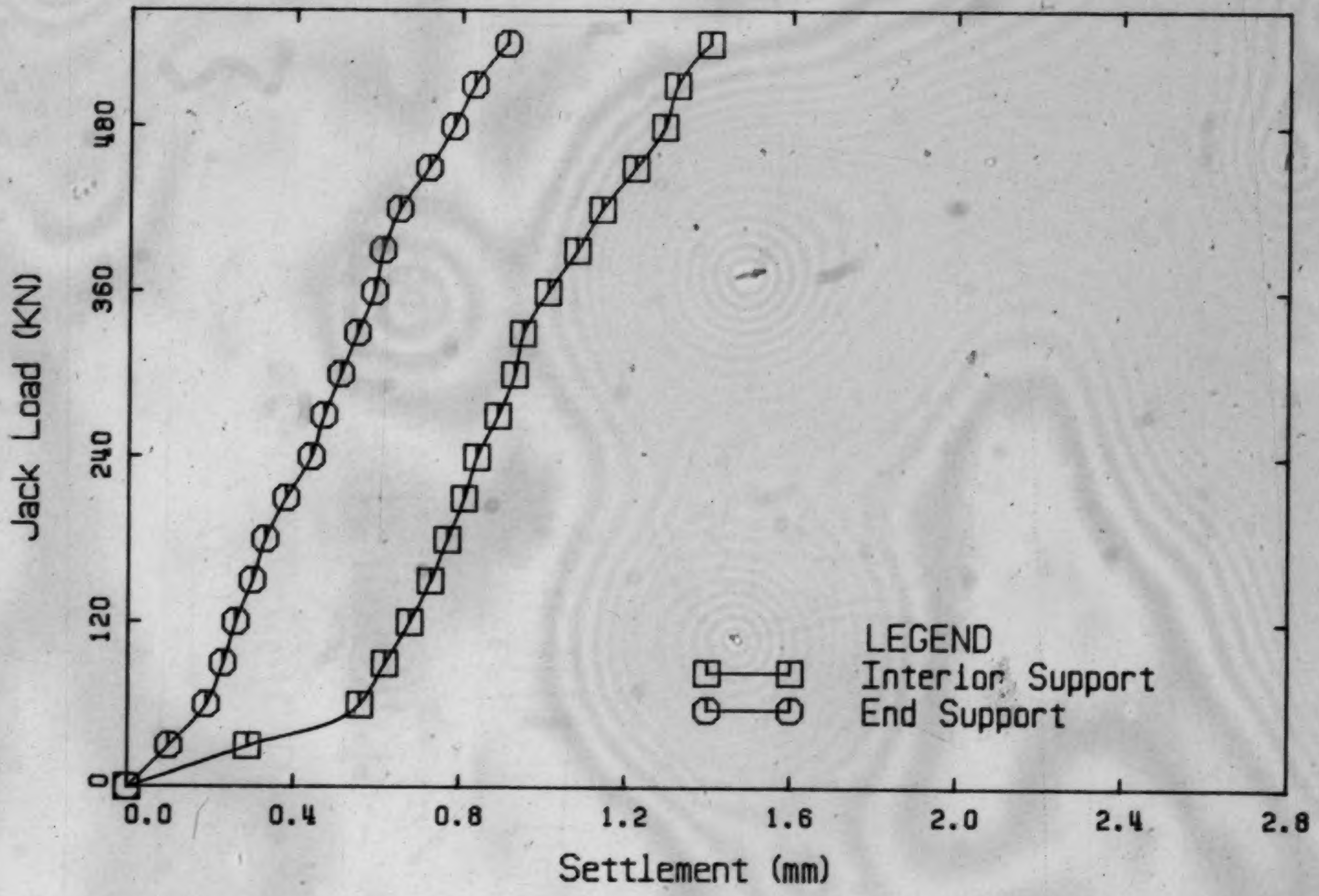

Figure D.1 Plot of Jack Load Versus Support Settlement from the Retest of Beam No. 1

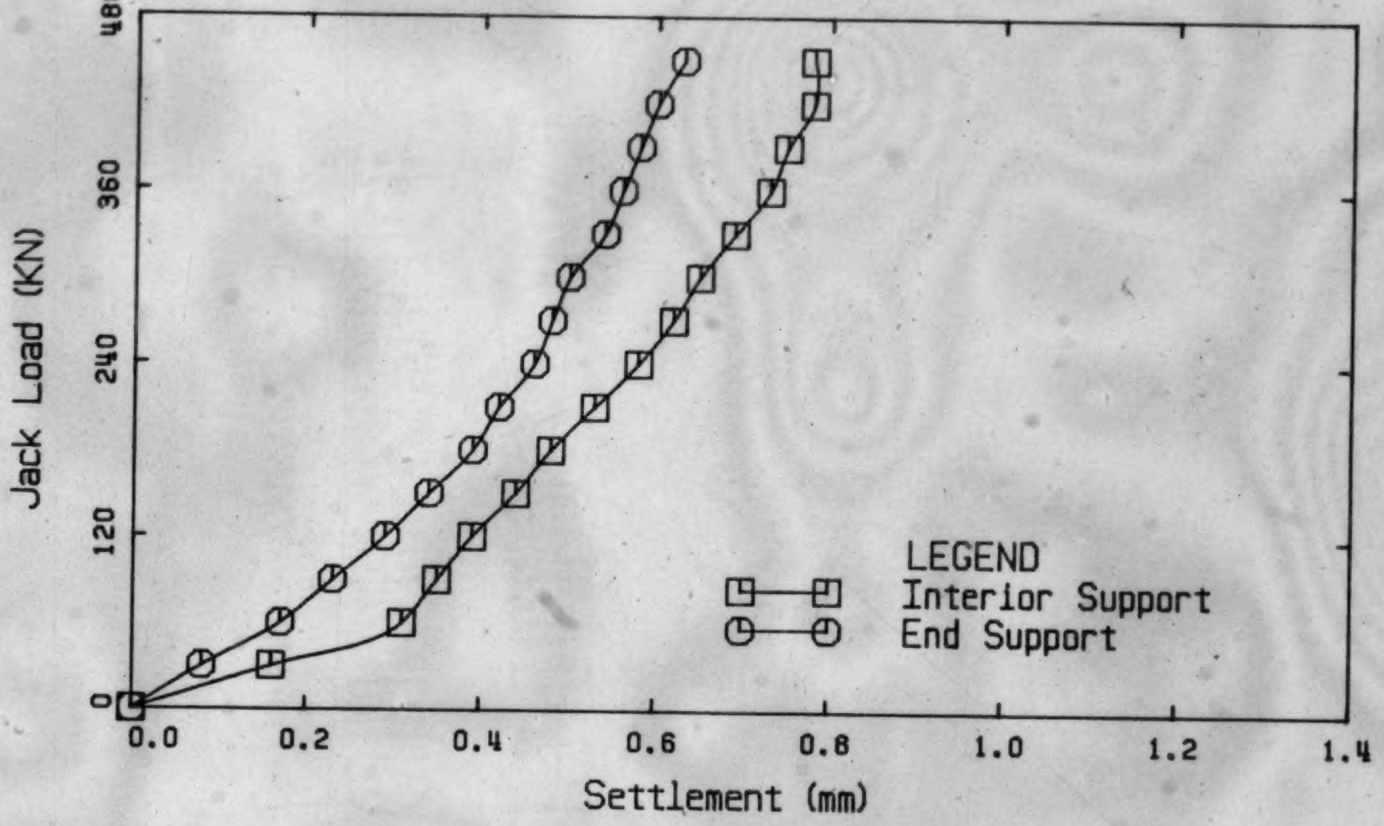

Figure D.2 Plot of Jack Load Versus Support Settlement from the Retest of Beam No. 2

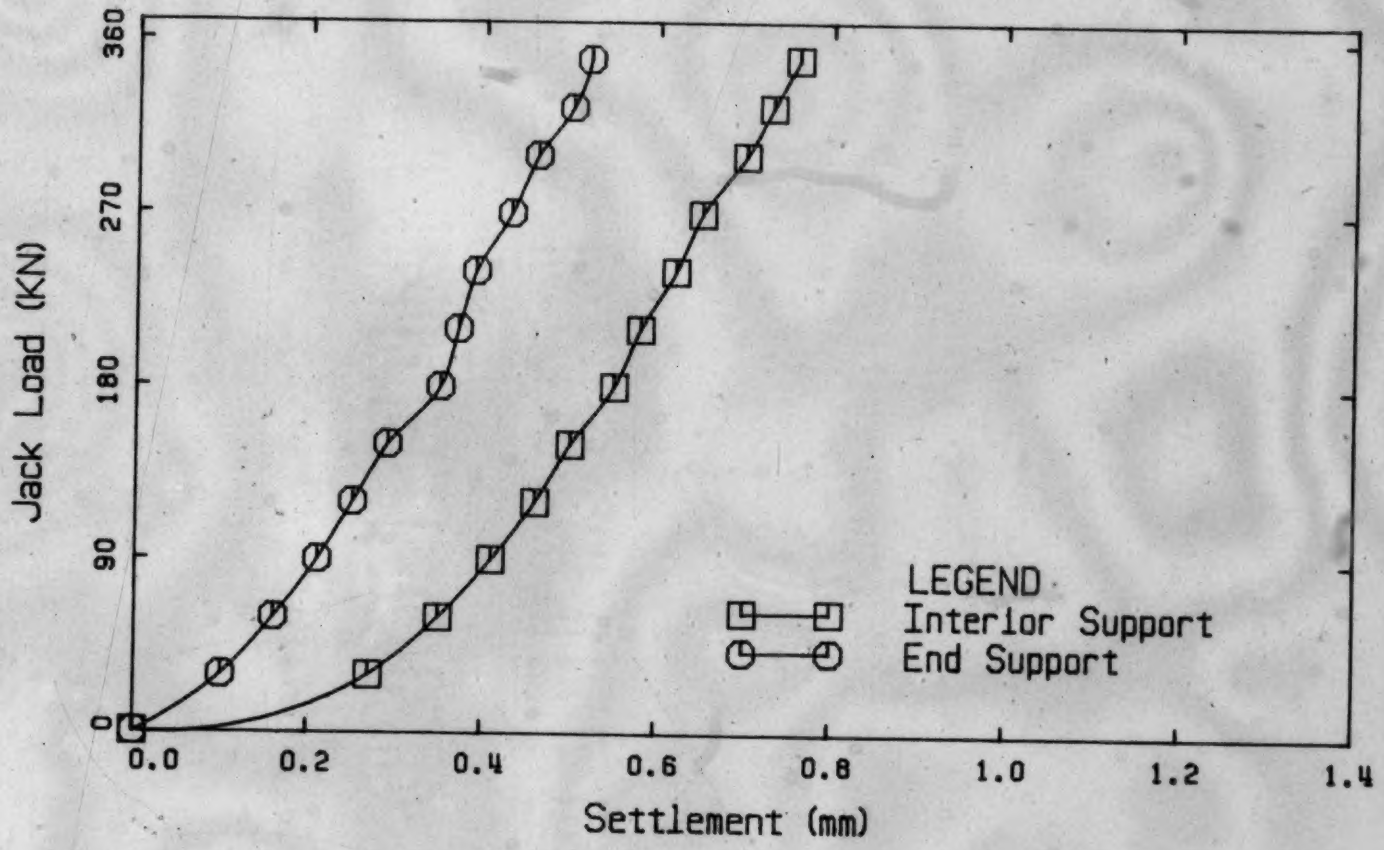

Figure D.3 Plot of Jack Load Versus Support Settlement from the Retest of Beam No. 3

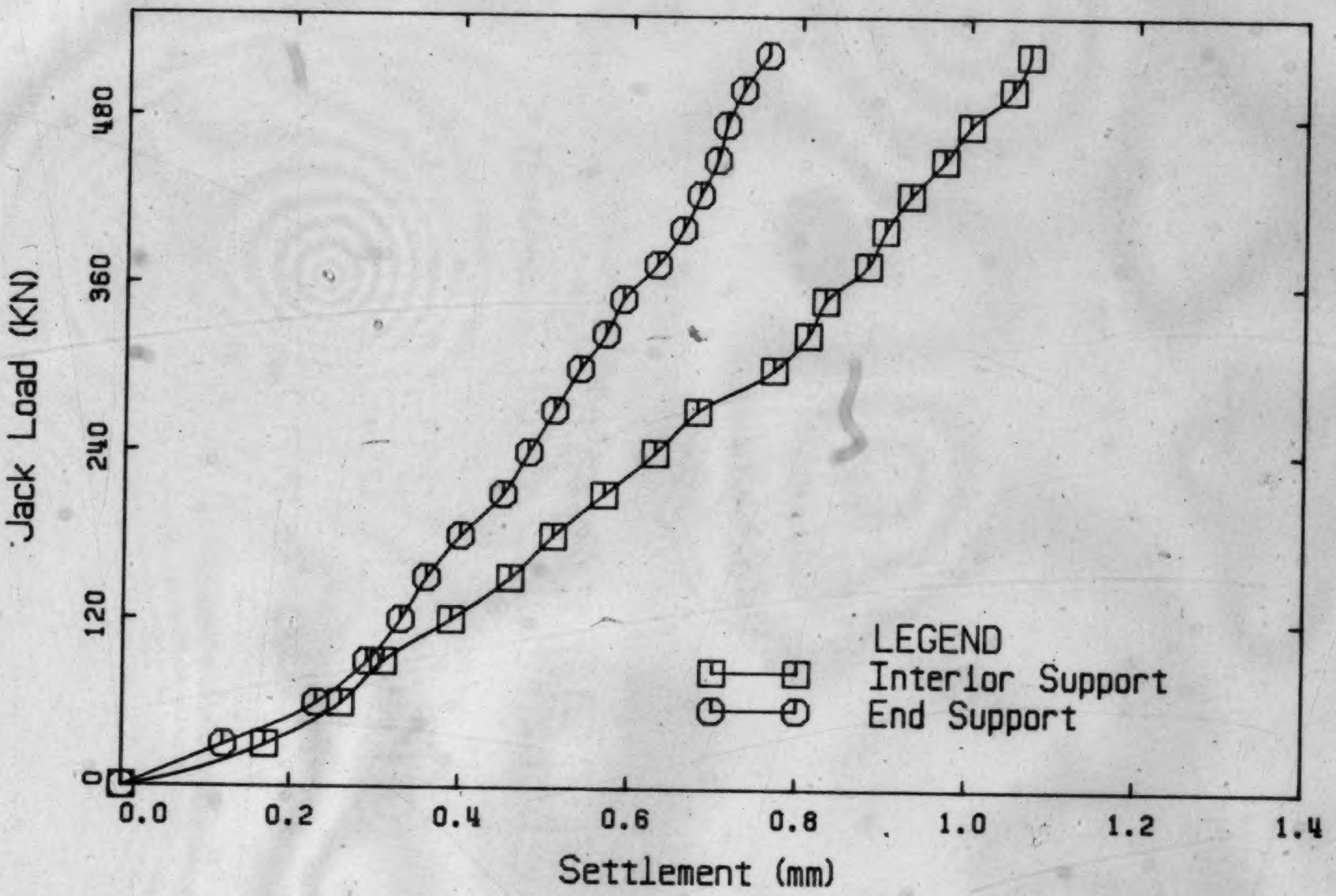

Figure D.4 Plot of Jack Load Versus Support Settlement from the Retest of Beam No. 4

APPENDIX E

Jack Loads and Support Reactions of Beams No. 1, 2, 3 and 4 from the Retest

Table E.1 Jack Loads and Support Reactions from the Retest of Beam No. 1

LOAD STEP	*P1* (KN)	*P2* (KN)	*R1* (KN)	*R2* (KN)	*R3* (KN)	*A**	*V*[N] (KN)	*V*[S] (KN)
0	0.0	0.0	0.0	0.0	0.0	-	0.0	0.0
1	30.0	31.4	16.2	28.3	16.9	0.46	13.8	14.5
2	61.8	61.8	27.8	68.0	27.8	0.55	34.0	34.0
3	87.8	87.5	37.9	99.5	37.8	0.57	49.8	49.7
4	120.0	119.2	49.7	140.2	49.3	0.59	70.3	69.9
5	146.7	145.6	59.8	173.2	59.3	0.59	86.9	86.4
6	177.7	176.1	70.8	212.9	70.0	0.60	106.8	106.1
7	207.5	206.4	81.6	251.3	81.0	0.61	125.9	125.4
8	237.1	235.6	91.7	290.1	90.9	0.61	145.4	144.7
9	266.0	265.0	101.6	328.4	101.0	0.62	164.5	164.0
10	297.1	297.5	112.5	369.5	112.7	0.62	184.6	184.8
11	326.4	323.7	123.0	405.6	121.5	0.62	203.5	202.2
12	355.6	353.3	133.2	443.7	132.0	0.63	222.4	221.3
13	384.7	383.0	143.4	481.9	142.5	0.63	241.3	240.5
14	413.1	411.0	153.6	518.1	152.5	0.63	259.6	258.6
15	447.1	445.4	172.3	548.9	171.4	0.61	274.9	274.1
16	475.5	474.3	183.9	582.7	183.2	0.61	291.6	291.0
17	506.0	503.5	196.1	618.6	194.8	0.61	309.9	308.7

(See notes in Table 4.2)

Table E.2 Jack Loads and Support Reactions from the Retest of Beam No. 2

LOAD STEP	*P*1 (KN)	*P*2 (KN)	*R*1 (KN)	*R*2 (KN)	*R*3 (KN)	*A**	*V*[N] (KN)	*V*[S] (KN)
0	0.0	0.0	0.0	0.0	0.0	-	0.0	0.0
1	30.2	31.5	12.0	37.0	12.7	0.60	18.2	18.8
2	61.9	62.9	24.1	76.1	24.6	0.61	37.8	38.3
3	90.9	91.6	35.4	111.3	35.8	0.61	55.5	55.8
4	121.1	122.1	47.2	148.3	47.7	0.61	73.9	74.4
5	150.7	148.9	57.3	186.3	56.9	0.62	93.4	92.9
6	179.9	178.3	69.1	220.8	68.3	0.62	110.8	110.0
7	211.4	210.1	80.4	261.3	79.8	0.62	131.0	130.3
8	240.6	238.1	90.6	298.8	89.3	0.62	150.0	148.8
9	271.8	268.7	103.5	335.1	101.9	0.62	168.3	166.8
10	299.8	296.5	112.1	373.8	110.4	0.63	187.7	186.1
11	331.0	328.2	123.1	414.5	121.7	0.63	207.9	206.6
12	359.6	355.4	134.1	449.1	131.9	0.63	225.6	223.6
13	390.4	386.7	147.2	484.7	145.2	0.62	243.2	241.5
14	419.1	415.1	158.7	519.0	156.6	0.62	260.4	258.5
15	449.8	445.3	173.6	550.4	171.2	0.61	276.3	274.1

(See notes in Table 4.2)

Table E.3 Jack Loads and Support Reactions from the Retest of Beam No. 3

LOAD STEP	*P*1 (KN)	*P*2 (KN)	*R*1 (KN)	*R*2 (KN)	*R*3 (KN)	*A**	*V*[N] (KN)	*V*[S] (KN)
0	0.0	0.0	0.0	0.0	0.0	-	0.0	0.0
1	29.6	28.2	12.8	33.0	12.0	0.57	16.9	16.2
2	59.4	57.6	22.4	73.0	21.5	0.62	36.9	36.1
3	90.9	89.6	33.3	114.6	32.6	0.63	57.6	57.0
4	120.8	120.0	43.5	154.3	43.1	0.64	77.3	77.0
5	149.3	147.2	53.0	191.8	51.9	0.65	96.4	95.4
6	179.0	177.4	63.4	230.5	62.5	0.65	115.6	114.9
7	209.3	207.3	74.7	268.3	73.6	0.64	134.6	133.7
8	237.9	235.5	85.3	304.2	84.0	0.64	152.7	151.5
9	268.5	265.6	96.4	342.9	94.9	0.64	172.1	170.8
10	299.0	295.7	107.2	382.1	105.4	0.64	191.8	190.2
11	322.9	319.3	115.9	412.3	114.0	0.64	207.0	205.3
12	346.1	342.2	124.1	442.2	122.0	0.64	222.0	220.2
13	373.2	367.9	138.1	467.8	135.3	0.63	235.1	232.6

(See notes in Table 4.2)

Table E.4 Jack Loads and Support Reactions from the Retest of Beam No. 4

LOAD STEP	P1 (KN)	P2 (KN)	R1 (KN)	R2 (KN)	R3 (KN)	A*	V[N] (KN)	V[S] (KN)
0	0.0	0.0	0.0	0.0	0.0	-	0.0	0.0
1	28.5	28.0	10.2	36.2	10.0	0.64	18.2	18.0
2	59.2	56.5	21.3	74.7	19.8	0.64	38.0	36.7
3	88.6	85.5	31.0	113.7	29.4	0.65	57.6	56.1
4	118.4	113.9	41.3	152.2	38.9	0.65	77.1	75.0
5	148.5	143.6	52.3	190.2	49.7	0.65	96.3	94.0
6	177.1	171.8	62.0	227.7	59.2	0.65	115.1	112.6
7	208.4	203.5	73.0	268.3	70.5	0.65	135.3	133.0
8	237.1	232.8	83.4	305.5	81.1	0.65	153.8	151.7
9	267.3	262.6	93.8	344.9	91.3	0.65	173.6	171.3
10	296.1	292.0	104.9	380.5	102.8	0.65	191.2	189.3
11	321.4	316.8	114.4	411.7	112.0	0.65	206.9	204.8
12	347.0	342.1	123.9	443.9	121.3	0.64	223.1	220.8
13	371.0	366.7	132.3	475.4	130.1	0.64	238.7	236.7
14	394.4	389.8	140.8	505.1	138.4	0.64	253.6	251.4
15	422.1	416.2	154.0	533.3	150.9	0.64	268.0	265.2
16	444.6	439.2	164.1	558.4	161.3	0.63	280.5	277.9
17	470.0	465.2	168.6	600.7	166.1	0.64	301.5	299.2
18	496.0	490.8	178.7	632.2	175.9	0.64	317.3	314.9
19	520.1	514.6	187.7	662.2	184.9	0.64	332.4	329.8

(See notes in Table 4.2)